JAMES COOK UNIVERSITY

COLLEGE OF SCIENCE AND ENGINEERING

Cemented Paste Backfill Modification Using Different Types of Binders and Insight into its Mechanical, Micro-Structure, and Flow Properties

Niroshan Naguleswaran B.Sc.(Eng.) Hons., M.Sc.(Eng.)

Thesis submitted to the College of Science and Engineering in partial fulfilment of the requirements for the degree of

Doctor of Philosophy

(Geotechnical Engineering)

April 2018

Statement of access

I, the undersigned, the author of this thesis, understand that James Cook University will make it available for use within the University Library and via the Australian Digital Theses network for use elsewhere.

I understand that as an unpublished work, a thesis has significant protection under Copyright act and I do not wish to place restriction on access to this work.

05 / 04 / 2018

Niroshan Naguleswaran Date

Statement of sources

I declare that this thesis is my work and has not been submitted for another degree or diploma at any university or other institution of tertiary education. Information derived from published or unpublished work of others has been acknowledged in the text and a list of references given.

05 / 04 / 2018

Niroshan Naguleswaran Date

Statement on the contribution of others

Grants: This research work was supported by scholarship by College of Science and Engineering, James Cook University (JCU), and additional conference travel stipend was also awarded by the Graduate Research School (GRS) at JCU to present the papers at international conferences.

Supervision: Associate Professor Nagaratnam Sivakugan (JCU) was the primary advisor of this work. Additional supervision was provided by Dr. Ryan Veenstra (Senior Backfill Engineer at Newmont Tanami Operation), and Dr. Peter To (JCU).

Editorial Assistance: The editorial assistance for both thesis and journal articles was provided by Associate Professor Nagaratnam Sivakugan (JCU), Dr. Ryan Veenstra (Senior Backfill Engineer at Newmont Tanami Operation), Dr. Peter To (JCU). Dr. Ling Yin (JCU) provided the editorial assistance for a journal article, which is included in chapter 6 of thesis.

SEM Technical Assistance: Dr Shane Askew from Advance Analytical Centre (AAC-JCU)

Acknowledgements

Firstly, I would like to acknowledge the support of my wonderful family and relatives throughout the period of my studies. Especially, to my father, who understood my intentions to pursue for PhD and supported back from home, I am forever grateful his support and the understanding throughout this long journey.

To my primary advisor Associate Professor Nagaratnam Sivakugan, indeed a professor in the way he interprets the complex aspects in Geotechnical Engineering and Geomechanics with fundamental knowledge. Thank you Professor Siva, for being a real mentor and providing continuous support from the beginning until the end of my thesis. My co-advisors, Dr. Ryan Veenstra (Senior Backfill Engineer at Newmont Tanami Operation), and Dr. Peter To, whose guidance were very helpful throughout. Dr. Ling Yin, whose guidance for the study on the structure-property interrelationship was very useful. Thanks to all academic and technical staffs in College of Science and Engineering, especially to former senior engineering laboratory technician Mr. Warren O'Donnell and current engineering laboratory technician Mr. Shaun Robinson and Mr Troy Poole for their ongoing patience with my style of test design and testing within the laboratories. Thanks to Ms. Kellie Johns at Teaching and Learning development for the discussions provided on my research proposal and to the graduate research school and Dr. Liz Tynan on organising academic writing workshops.

In addition, my university colleagues (Sathees, Thushara, Geeth, Elsa, Korah, Mitchel, Dushyantha, Micheal, Dilip and Nasif) and the school support staffs, especially Melissa, provided support as well as company during my candidature. Also, the friends and families at Townsville (the home away from home) should be thanked for their love, company and laughs during my stay. I feel very fortunate to spend with you guys during my stay in Townsville.

I wish to acknowledge the College of Science and Engineering (JCU) scholarship, which provided a living allowance during my studies as well as the financial support received

from my school (Student Support Allocation) and the Graduate Research Scheme funds to support my academic and conference travel expenses.

Finally, I also wish to express my sincere love and gratitude to my beloved wife, Sangeertha, for her understanding and endless love throughout the duration of my studies. Thank you for being a great companion on this wonderful journey.

This work is dedicated to my family and teachers

Abstract

Cemented paste backfill (CPB) is widely used in backfilling underground mine voids. It consists of fine grained mine tailings with a small dosage of binder (~ 3–10%). Cement is the common binder, which is currently being used in most of the mines in North Queensland, Australia. In an effort to control backfilling costs, investigations are being currently carried out for the use of some alternative binders, that is, pozzolanic binder such as blended cement (BC) containing slag or fly ash in CPB. A thorough study to quantify the effects of additives, such as blast furnace slag and fly ash with ordinary Portland cement, in certain percentages on CPB could save large sums of money for Australian mining companies, if the required cement percentage is reduced in binder for CPB. In an attempt to dispose more tailings underground, the mines prefer increasing the solid content to the maximum possible limit, as dense CPB needs less binder to achieve a target strength. On the other hand, a high solid content slurry has both increased yield stress and viscosity, which increase the likelihood of blocking the reticulation pipeline.

In this research, the possibilities of partial replacement of cement binder in CPB were studied through detailed laboratory investigations on influence of binder types as well as dosages in both mechanical and flow properties. Also, five different curing methods for CPB samples were studied to propose proper method. UCS test on 25 identical samples from three different CPB mixes were conducted for the detailed statistical analysis to assess the variability of mechanical properties of CPB samples and to validate the proposed curing method. Furthermore, the possibility of using a relatively smaller cylinder (110 mm height and 110 mm diameter) in slump test is assessed via extensive slump test along with standard slump cone on different CPB mixes. Moreover, series of scanning electron microscopy (SEM) analyses were performed on cracked UCS sample to investigate the relationship between microstructure and long-term mechanical properties. Finally, possibility of using UCS and indirect tensile (IDT) strength to determine the shear strength parameters (c and φ) for CPB was assessed with proper validation based on both experimental test and numerical simulation. For all these studies

and investigations conducted in this research, various laboratory experiments, such as uniaxial compressive strength (UCS) test, indirect tensile (IDT) strength test, slump test, yield stress test, triaxial test and SEM analysis, with analytical correlation techniques and numerical simulation were employed.

Slag blended cement (60% Slag + 40% Portland cement) can be used as replacement of cement binder in preparation of CPB with less dosage to achieve similar strength and stiffness as like cement binder, even in short curing time. This significant reduction in Portland cement usage not only leads to the significant cost saving, but also may slightly contribute for a sustainable development. In addition, through the extensive laboratory experiments on rheological properties, it is found that the there is hardly any difference between the cement and slag blended cement binders on flow properties namely the yield stress and slump, while the binder dosage has an effect.

The smaller cylindrical slump device appears to have good potential for slurries like mine tailings or dredged mud that have high water content for slump test as there was strong correlation between the two different slump test devices used. Also, It is found that there is strong inter-relationship among solid content, slump, yield stress, and bulk density of CPB.

In addition, a simple and proper curing method for CPB samples for the laboratory tests was recommended. In addition, the mechanical properties of CPBs cured in this proposed method show less variability for UCS and Young's modulus with relatively small coefficient of variation of less than 10% and 25%, respectively and hence these small variabilities of mechanical properties demonstrates the consistency of sample casting, curing, and testing methods.

Furthermore, it is found that there is a positive relationship between microstructure and mechanical properties of CPB. Finally, the estimated shear strength parameters of CPB using the UCS and IDT strengths show good agreement with experimental and numerical

simulation. Throughout the thesis, sets of empirical models and correlations were proposed to predict the long term UCS, stiffness, yield stress, slump height, and cohesion.

In summary, the great potential of partial replacement of existing cement binder using slag blended cement in preparation of CPB is identified through various laboratory tests. In addition to the mechanical properties, the microstructure and flow properties of modified CPB were extensively investigated. This research will not only help to reduce the cement consumption in CPB production but also provides an alternative way of recycling industrial waste, such as slag and fly ash in vast volumes.

List of Publications

Journals

Sivakugan, N., Veenstra, R., and Niroshan, N. (2015). **"Underground Mine Backfilling in Australia Using Paste Fills and Hydraulic Fills."** *International Journal of Geosynthetics and Ground Engineering*, *Springer,* 1(2), 1-7. doi: 10.1007/s40891-015-0020-8

Niroshan, N., Sivakugan, N., and Veenstra, R. L. (2017). **"Laboratory Study on Strength Development in Cemented Paste Backfills."** *Journal of Materials in Civil Engineering, ASCE*, 29(7), 04017027. doi: 10.1061/(ASCE)MT.1943-5533.0001848

Niroshan, N., Yin, L., Sivakugan, N., and Veenstra, R. L. (2018). **"Relevance of SEM to Mechanical Properties of Cemented Paste Backfill."** *Geological and Geotechnical Engineering, Springer,* doi: 10.1007/s10706-018-0455-5

Niroshan, N., Sivakugan, N., and Veenstra, R. L. (2018). **"Flow characteristics of Cemented Paste Backfills."** *Geological and Geotechnical Engineering, Springer,* doi: 10.1007/s10706-018-0460-8

Niroshan, N., Sivakugan, N., and Veenstra, R. L. (2018). **"Effects of curing methods on UCS test specimens and variability of mechanical properties of cemented paste backfill."** *Journal of Materials in Civil Engineering, ASCE* (Under 2nd review)

Referred Conferences Proceedings

Niroshan, N., Sivakugan, N., and Lovisa, J. (2015). **"A Review on Use of Pozzolanic Materials and Geopolymers in Stabilizing Mine Tailings and Dredged Mud."** *Proc., Int. Conf. on Geotechnical Engineering, Sri Lankan Geotechnical Society (SLGS), Colombo, Sri Lanka* 375-378, https://www.issmge.org.

Niroshan, N., Sivakugan, N., and Veenstra, R. (2016). **"Effects of Different Binders on the Strength and Stiffness of Paste Fills."** *Proc., 4th GeoChina International Conference, Shandong, China*, 197-205, doi: 10.1061/9780784480083.025

Table of Contents

List of Figures

List of Tables

1 Introduction

1.1 Background

Mining is one of the major economic activities in many countries such as Australia, Brazil, Canada, Chile, China, India and South Africa, producing millions of tonnes of waste materials every year (Boger 1998). Due to the strict guidelines, these waste materials (extracted waste rock and processed tailings) need to be disposed in a responsible manner. Surface mining (Fig 1.1(a)) and underground mining (Fig 1.1(b)) are two different ways of mining to recover shallow and deep ore bodies, respectively. In underground mining, the ore is extracted through blasting and excavation. The excavated voids, which are commonly referred to as ‘‘stopes’’ are in the form of rectangular prisms, with plan dimensions of 20–50 m and heights of about 50–200 m. These stopes are backfilled, generally using waste materials in the form of cemented paste backfills (CPB), hydraulic fills and other types of backfills (e.g., cemented aggregate fill, cemented rock fill etc.). Tailings are generally used to make hydraulic fill and CPB, while waste rock is used for cemented rock fill.

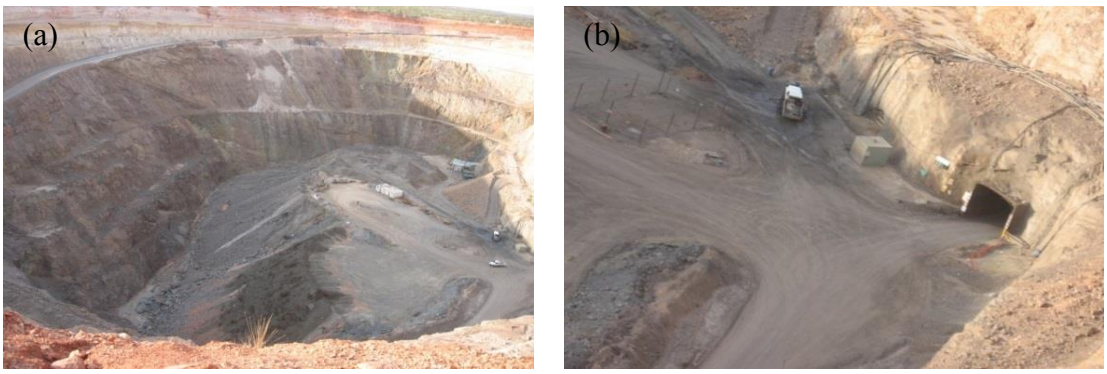

Fig. 1.1 (a) Open pit (surface) mine and **(b)** underground mine in Queensland, Australia

CPB is produced by mixing tailings, water, and a binder. When a stope is backfilled with CPB, a plug consisting of paste fill with high cement content is poured at the base of the

stope to a certain thickness before the rest of the stope is filled, often continuously, with paste of lower binder content. Using CPB to fill the underground voids is an effective way of disposing a large quantity of tailings (up to 60%), which have to be otherwise disposed at the ground level in a tailing storage facility (Brackebusch 1995). The CPB also provides regional ground support for mining operations and increases the ore recovery. The CPB is transferred to underground via pipes from the paste plant and is placed into the mine voids in the form of thickened slurry. The pulp density, binder content, and binder type determine the mechanical and rheological properties of CPB.

A small dosage of binder (typically 3% to 10% of the solids mass) is added to the paste fill to enhance strength (Belem and Benzaazoua 2008; Benzaazoua et al. 2002). As cement is currently used as a base material in the binder, the mining industry currently consumes millions of tonnes of cement per year to produce underground backfills. Due to high cement cost and environmental issues related to cement production, mines worldwide are considering using slag and fly ash to partially replace the Portland cement to form blended cement. Blended cements can consist of various proportions of Portland cement and the replacement materials such as slag or fly ash, depending on the strength and flowability requirements.

In underground mining, stope wall heights can be significant (more than 100m) and providing a stable wall is essential to undertake adjacent stoping in order to maximise ore recovery. There is no typical backfill type or mix design in backfill system as it is mine-specific. It is important, therefore, to ensure that thorough investigation is carried out to determine the most suitable backfilled type when designing a backfill system. The static stability requirements can be satisfied by designing the backfill masses with sufficient strength to ensure the vertical faces of the backfilled stopes remain stable throughout the mining of the adjacent stopes. Typically, excavation of adjacent (secondary) stope is commenced after 28 days curing period of primary stope when it would have attained most of its strength. If the paste backfill becomes unstable, the adjacent faces may collapse, causing high levels of dilution and, significant loss of mining economies.

Therefore, when using CPB, the key consideration is how quickly the backfill attains the necessary strength. Quicker development of strength and stiffness enable faster mining sequences but usually requires higher cement content which can have significant cost increases. Consequently, mining operations can be quicker due to the better support attained in the stope in a shorter time and reduced excess water problems in the stope due to CPB.

1.2 Problem Statement

Cemented Paste Backfill (CPB) is one of the many backfill materials used to fill the large underground mine voids that are created by the mining activities around the world. CPB is produced by mixing the mine tailings, binder, typically 2 to 10 wt.% (Benzaazoua et al. 2002) and required amount of water as per the consistency of CPB materials required for the flow through pipes. In terms of production benefits, the use of CPB, compared to the hydraulic fill, results in significant time saving in stope filling. Archibald et al. (1999) reported that the time requirement for filling a stope with satisfactory backfill strength is 45 days for CPB and 87.5 days for hydraulic fills. Therefore, the usage of CPB results in almost 50% reduction in mining cycle time, barricade preparation requirements, and capacity to fill stope voids with higher solid contents.

Cement is the common binder, which is currently being used in most of the mines in Australia. In an effort to control backfilling costs, investigations are being currently carried out for the use of some alternative binders for CPB. De Souza et al. (2003) reported that the cost of ordinary Portland cement in CPBs to be around 42% of the overall backfill cost. Due to the arising environmental sustainability concerns world-wide and increasing backfill cost, the possibilities of replacing the cement by alternate environmental friendly binders, i.e., large percentage of supplementary cementitious materials (SCMs) along with relatively small percentage of cement, in CPB have been already extensively assessed by the by researchers, both from industry and academia (Belem and Benzaazoua 2008; Belem et al. 2000; Ercikdi et al. 2009; Ercikdi et al. 2014;

Fall et al. 2007; Ouellet et al. 1998; Pirapakaran et al. 2007; Rankine and Sivakugan 2007; Sivakugan et al. 2006; Sivakugan et al. 2015; Thomas 1979; Yilmaz et al. 2010) all over the world. In Canada, it was noted that the principal alternatives were blended cement, which is a combination of OPC with either fly ash or slag from different industrial applications in different percentages as per a comprehensive review by Chew (2000).

However, the results of these investigations cannot be easily generalised, since the physio-chemical behaviour of a certain material is related to its origin (Manca et al. 1983). In addition, there is no typical backfill type or mix design for all applications as the backfill system is mine-specific. A thorough study to quantify the effects of additives, such as blast furnace slag and fly ash with ordinary Portland cement in certain percentages on CPB could save large sums of money for Australian mining companies, if the required cement percentage is reduced in binder for CPB. The majority of alternative binders are waste products from other industries. Therefore, the usage of this by products in underground mine offers environmental benefits while increasing revenues to the waste providers. In addition to the cost savings and technical benefits that can be realised by using alternative binders at appropriate dosage, there are environmental benefits. Especially, the environmental issues related to greenhouse emission and global warming due to the excessive cement production are reduced.

In addition, there is no standardised process for sampling, curing, and testing the paste backfill materials in laboratory. Their mechanical properties are governed by not only the characteristics of tailings, binders, and mixing water but also the chemical mineralogical properties of these materials. Even though the test results of in situ samples from the underground are often different from the laboratory experiment, standardised procedure, as for concrete or soil, for sampling, curing, and testing is necessary to minimise the error and variation between the lab and in situ samples.

In an attempt to dispose more tailings underground, the mines prefer increasing the solid content to the maximum possible limit, as dense CPB needs less binder to achieve a target strength. On the other hand, a high solids content slurry has both increased yield stress

and viscosity, which increase the likelihood of blocking the reticulation pipeline. As CPB is transported through a pipe system, the flow characteristics of the CPB are governed by its rheological parameters. Gravity based delivery methods are utilised for slurry based systems with the dense tailings slurry being delivered by pipeline to the disposal point in the stope. Flow characteristics play a key role as the CPB more commonly flows by gravity down a mine shaft to fill the void. Therefore, it is necessary to establish a balance to optimize the solid content and flow properties of CPB.

1.3 Objectives of the Research

The major focus of this thesis was to study the mechanical, flow, microstructure, and shear strength properties of CPB utilising tailing materials supplied by Glencore's George Fisher Mine (GFM), which is located North Queensland, Australia. The objectives of this thesis are:

- To suggest the best practice for sample preparation and curing in laboratory for the Uniaxial Compressive Strength (UCS) samples prepared using CPB;
- To assess the variability of mechanical properties of CPB and to validate the casting, curing and testing methods of CPB at laboratory;
- To investigate the effects of different binder materials and dosages on strength and Young's modulus development and flow characteristics of CPB;
- To find out the relevance of microstructure to long term (i.e., 112 days of curing period) mechanical properties of CPB;
- To determine the shear strength parameters, such as cohesion (c) and friction angle (φ), of CPB using laboratory results of UCS and indirect tensile (IDT) strength and compare these results with experimental results, such as triaxial tests and the numerical simulations using FLAC^{3D}; and

- To propose some simple correlations equations to estimate the strength, stiffness, slump, yield stress, cohesion, and friction angle of CPB in certain solid content.

1.4 Relevance of the Research

CPB is one of the popular and relatively new techniques, where the backfills are derived from mine tailings by adding small percentage of binders and water. The popularity is mainly due to its high strength achieved in a short time and its capability of standing alone without confinement, during the ore removal from adjacent secondary stope. The early strength gain enables the mining operations to be quicker. CPB is an engineered fill material, where the strength enhancement is achieved through the binder. By carrying out a proper mix design, through a series of trials, it is possible to achieve the optimum mix that will give the appropriate strength gain at certain time. The primary motivation for this research is to investigate the strength and stiffness development of cemented paste backfill after replacing the cement binder by other alternatives while carefully study the flow characteristics of modified CPBs.

Binders have a significant role in backfilling operations, especially in CPB. As binder is the major cost component in CPB, there have been several attempts by researchers worldwide to reduce the percentage of cement and explore the possibilities of offering other pozzolanic materials, such as flyash, slag and others as partial or sometimes total substitutes. From this research, it may lead to following positive aspects for the mining industry:

- Significant reduction in Portland cement usage in mine industry, which would lead to sustainable development as mining industries are consuming vast amount of cement binder in the form of CPB in Australia;
- Significant reduction in catastrophic failures and increase in productivity due to the better understanding on strength and stiffness development of CPB throughout curing period up to 112 days;

- Significant cost savings through altering current binder type and dosage, and proposing alternative ways to estimate the strength, stiffness, flow properties, and shear strength parameters using simple correlations;
- Increase safety in mine practices while increasing the productivity and without affecting ore recovery; and
- Reduce the maintenance cost as well as the interruption in operation due to blockages in pipelines through a better understanding on flow properties of CPB for certain range of solid content.

1.5 Organisation of Thesis

This chapter introduces the problem statement of the research, objectives and significance of the findings. The following Chapter 2 outlines brief insight in the mining and related sections while reviews the current binders and its effectiveness of producing CPB throughout the world. Most of the sections of this chapter were published as "Sivakugan, N., Veenstra, R., and **Niroshan, N**. **(2015)** "Underground Mine Backfilling in Australia Using Paste Fills and Hydraulic Fills." *Int. J. of Geosynth. and Ground Eng.*, 1(2), 1-7, doi: 10.1007/s40891-015-0020-8", and as "**Niroshan, N.**, Sivakugan, N., and Lovisa, J. **(2015)** "A Review on Use of Pozzolanic Materials and Geopolymers in Stabilizing Mine Tailings and Dredged Mud." *Proc., Int. Conf. on Geotechnical Engineering*, Sri Lankan Geotechnical Society (SLGS), Colombo, Sri Lanka 375-378.", which was a peer reviewed International conference article.

Chapter 3 describes the geotechnical characteristics of mine tailing used in this study, where the specific gravity, grain size distribution, Atterberg limits, grain shape and chemical characterisations were briefly assessed and discussed. This chapter was submitted as part of a journal article and published as **Niroshan, N.**, Sivakugan, N., and Veenstra, R. L. **(2018)** "Flow characteristics of Cemented Paste Backfills." *Geological and Geotechnical Engineering,* doi: 10.1007/s10706-018-0460-8.

UCS Specimen preparation including casting and curing samples is explained in Chapter 4. A proper curing method for UCS specimen is proposed by experimentally assessing the five different curing methods based on the attained mechanical properties in 28 days and 56 days. In addition, the variability of mechanical properties of CPB is statistically assessed by testing separate 25 identical samples from each mix. This chapter has been submitted as *journal article to Journal of Materials in Civil Engineering (ASCE)* for publication as **Niroshan, N.**, Sivakugan, N., and Veenstra, R. L. **(2018)** "Effects of curing methods on UCS test specimens and variability of mechanical properties of cemented paste backfill", which is under second review.

Chapter 5 elaborates the findings from an extensive laboratory test program carried out to understand the effects of binder dosage and solid content on the strength development over 56 days of curing. In addition, two simple strength models were developed to express UCS as a function of time and the 14 day UCS. Finally, the relative effect of increasing the solid content or binder dosage was studied in this chapter. This chapter was published as "**Niroshan, N.**, Sivakugan, N., and Veenstra, R. L. **(2017)**."Laboratory Study on Strength Development in Cemented Paste Backfills." *Journal of Materials in Civil Engineering*, 29(7), 04017027. doi: 10.1061/(ASCE)MT.1943-5533.0001848" Part of the results were published in an International conference as "**Niroshan, N.**, Sivakugan, N., and Veenstra, R. **(2016)** "Effects of Different Binders on the Strength and Stiffness of Paste Fills." *Proc., 4th GeoChina International Conference*, Shandong, China, 197-205, doi: 10.1061/9780784480083.025".

Comparison between micro structure and long-term mechanical properties of CPB is demonstrated in Chapter 6. The uniaxial compressive strength (UCS) tests were conducted on all samples after curing for 112 days to obtain their mechanical properties. scanning electron microscope (SEM) analysis was conducted on fractured samples to understand the failure mechanisms at the microstructural scale. This chapter was published as "**Niroshan, N**., Yin, L., Sivakugan, N., and Veenstra, R. L. **(2018)**

"Relevance of SEM to Long-Term Mechanical Properties of Cemented Paste Backfill." *Geotechnical and Geological Engineering*. doi: 10.1007/s10706-018-0455-5".

Chapter 7 deals with the flow characteristics (i.e., rheological properties) of CPB. In this chapter the slump measurements and yield stress of CPB are critically analysed and some useful correlations are proposed to predict the yield stress and slump in the mine site. This chapter has been submitted as main part of a journal article and published as **Niroshan, N.**, Sivakugan, N., and Veenstra, R. L. **(2018)** "Flow characteristics of Cemented Paste Backfills." *Geological and Geotechnical Engineering,* doi: 10.1007/s10706-018-0460-8.

Chapter 8 describes the determination of shear strength parameters, i.e., c and φ, of CPB for purpose if design and stability analysis. In this chapter, the shear strength parameters are determined in two different ways, such as experimental and analytical procedure. Unconsolidated Undrained (UU) Triaxial test was used to find the experimental values of c and φ, while UCS and IDT were performed to analytically find the values of c and φ of CPB using already developed analytical equations. These two outcomes from two different testings (analytical and experimental approaches) were compared and proposed a correlation to find one from other one. In addition, a numerical simulation using FLAC^{3D}, which is a finite different modelling (FDM) software, was carried out to compare the outcome with laboratory test. This chapter will be submitted as a research article to journal upon thesis submission. Finally, Chapter 9 gives the summary of the work done, discusses the main findings and provides recommendations for future research.

2 Literature Review

2.1 Mining

Mining is a multi-billion dollar industry in many countries around the world. Australia, Brazil, Canada, Chile, China, India, South Africa and United States are some of the countries that are at the forefront in the mining and exploration activities. Australia holds the world's largest known economic resources of bauxite, lead, zinc, silver, uranium, industrial diamonds and mineral sands. Most of the mines in Australia are located in the states of Queensland, Western Australia, New South Wales and Northern Territory. Mining industry is the largest generator of solid wastes in Australia (Boger 1998).

Open pit (Fig. 2.1(a)) and underground mining (Fig. 2.1(b)) are two different ways of mining to recover shallow and deep ore bodies, respectively. The study in this whole research is limited to backfilling underground mines, which are located from hundreds to thousands of metres below the ground level that are accessed through ramps, shafts and tunnels. Sometimes, when the near surface ore is recovered through open pit mining, the deep mineral resources can be accessed through underground mining process. For example, Osborne mine in Queensland started its operation as an open pit mine, and later developed as an underground mine.

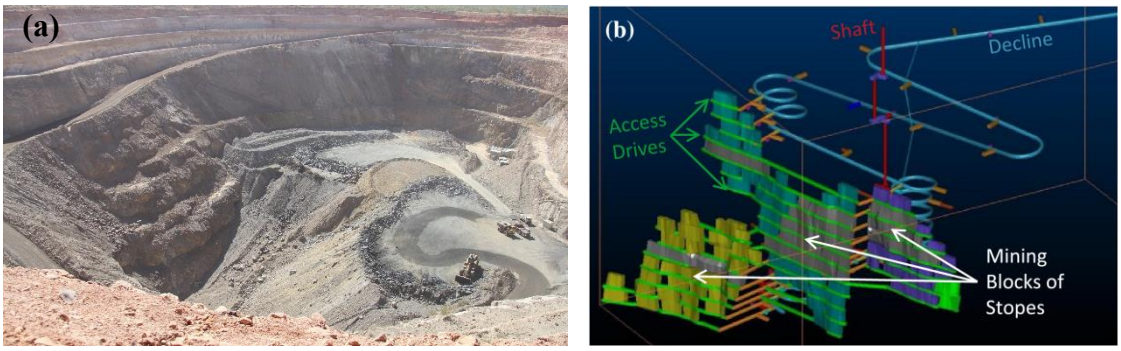

Fig. 2.1 (a) Open Pit mine, and **(b)** underground mine

Millions of tonnes of ore are removed from the ground, to extract a very small fraction of valuable minerals, leaving the bulk of the waste materials at the ground level for disposal. In addition, the ore removal leaves very large underground voids. These voids have to be backfilled before proceeding with excavation of nearby orebodies. Backfilling the voids ensures regional stability, minimises ore dilution, provides a working floor, controls subsidence and facilitates subsequent excavation and ore removal nearby. In addition, there are environmental regulations requiring that the mine site is left in good condition on the completion of mining operation, with all underground voids backfilled, all waste materials disposed in a responsible manner, and the flora and fauna in the region are protected. By sending the waste tailings to where they came from, the large underground voids are backfilled while the tailings are also disposed effectively in an environmentally friendly way. However, the success of a tailings backfill design and operation ultimately depends on the characteristics, strength and flowability properties of the tailings material, and physical conditions (i.e., shape and size) of the underground voids.

2.1.1 Underground Mining

When the parent rock of unit weight of 25–35 kN/m^3 and very low porosity is crushed and the small fraction of the valuable minerals are removed, there is a substantial quantity of crushed rock that has to be disposed. The crushed rock waste can be present in a range of grain sizes, and the smaller fractions are known as tailings. When the parent rock is crushed, the porosity increases from insignificant levels to 40–45% when it is placed underground in the form of tailings. With the dry unit weight of the waste tailings in the order of 15–20 kN/m^3 and porosity of 40–45%, only little more than 50% of the tailings can be disposed underground. The rest of the tailings have to be disposed through tailing dams on the surface.

The ore is extracted through blasting, and excavation in large blocks known as stopes. There are horizontal tunnels known as access drives at different levels for transporting

the ore (Fig. 2.2). The void left behind has to be backfilled before the nearby stopes can be excavated.

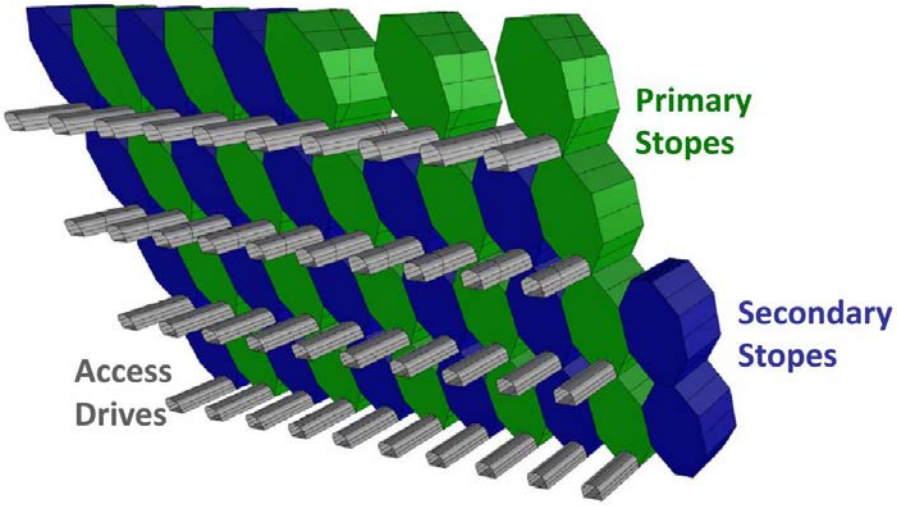

Fig. 2.2 Schematic diagram showing a primary-secondary stope extraction sequence with access drives in an underground mine (Sivakugan et al. 2015)

The tailings are transported through pipelines and boreholes over long distances. For ease of transport, they are generally pumped through pipes and boreholes in the form of slurry. In an attempt to dispose as much tailings as possible, the mines tend to increase the solid content to the maximum possible value, which is currently as high as 75–80 % in the case of paste fills, and slightly lower for hydraulic fills. Here, solid content is defined as the ratio of the mass of solids to the total mass, expressed in percentage. Increasing the solid content makes the flow through pipe difficult, leading to clogging. Therefore, it is necessary to arrive at the optimum solid content that will give satisfactory flow characteristics while maximising the tailing disposal. The flowability of the tailing slurry is generally quantified in terms of slump measured through a slump test or yield stress measured using a rheometer. With increasing solid content, slump decreases and yield stress increases. Fig. 2.3 shows the paste fill tailing slurry pumped through a pipe. Pipe diameters of 5–25 cm have been reported in the literature (De Souza et al. 2003).

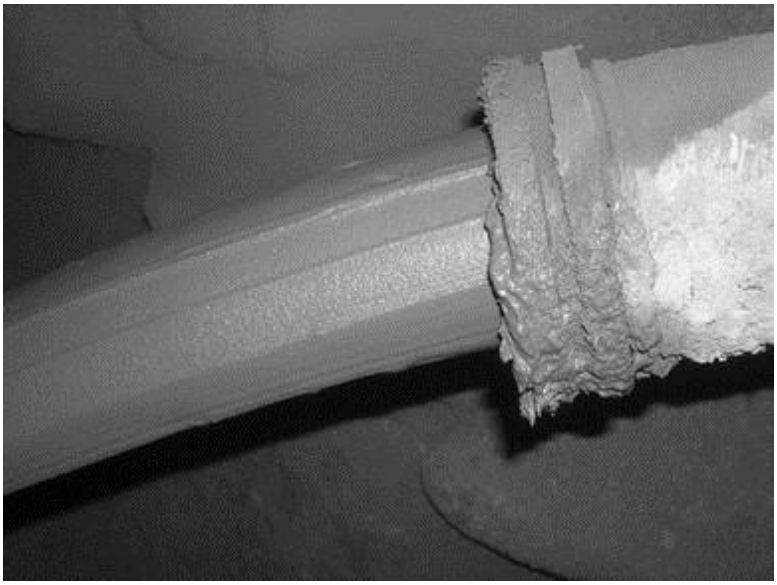

Fig. 2.3 Paste fill being discharged into a stop via pipeline

The empty stopes are filled by the tailing slurry over several days. In the case of hydraulic fills, depending on the rate of production of the tailing slurry at the plant, 12 h fill followed by 12 h pause or similar filling schedules have been reported in the literature, with pour rate of 1000–5000 tonnes of dry tailings per day. When paste fill is poured into the stope, a high-strength plug consisting of paste fill with high cement content is formed at the base before the rest of the stope is filled often continuously. When the wet slurry of tailings is placed within the empty stope, it is necessary to barricade the access drives to isolate the rest of the working environment in the mine. Failure of the barricades can lead to inrush of tailings into the other areas of the mine, causing economic damage and sometimes fatalities. Fig. 2.4 shows a barricade covering the drive of a paste fill stope, shotcreted prior to filling.

Fig. 2.4 Shotcreted barricades for a paste fill stope

2.2 Backfills

Backfills can be uncemented or cemented geomaterials such as tailings, sands or waste rocks. The uncemented backfills include hydraulic fills, sand fills, aggregate fills and rock fills. The majority of the uncemented backfills are rock fills and hydraulic fills. Fig.2.5 shows the rock fills used in backfilling an underground mine in Queensland, Australia. The yellow marker in the Fig. 2.5 is 350 mm in length. The rock fill consisted of gravel size to boulder size materials. The abundance of the rock fill material from the previous open pit operation dictated the selection of rock fills over any other type of fill. The most common cemented backfills are cemented paste backfill (CPB), cemented hydraulic fills and cemented rock fills.

Fig. 2.5 Rock fill used in an underground mine in Queensland, Australia

To expedite ore removal, the backfilled stopes may have one or more of the vertical walls exposed when the adjacent stopes or pillars are blasted and excavated. To ensure that the backfilled stopes remain stable during such exposures, a small dosage of binder is added to the tailings to enhance their strength. These cemented backfills include cemented paste backfill (CPB), cemented hydraulic fill (CHF), cemented aggregate fill (CAF) and cemented rock fill (CRF). De Souza et al. (2003) noted that a mining company could consume as much as 100,000 tonnes of cement per year. Therefore, there is good reason for any attempt to reduce the binder content even by 1 percent.

In addition to the large carbon footprint associated with the cement production, due to the high transport cost to the mine site, cement adds significant cost to the backfills, even in such small dosages in the order of 3–6 wt.%. The mines have been trying to replace cement with blended cements, which consist of cement mixed with fly ash and/or slag, with considerable success.

Fig. 2.6 shows scanning electron micrographs (SEM) of mine tailings that are present in CPBs and hydraulic fills. It can be seen that the hydraulic fill grains are very sharp and angular. This is not the case with the soil grains encountered in nature, which have undergone thousands of years weathering and tend to become more rounded, sub-rounded or sub-angular. The angularity is not obvious in the case of paste fills, which contain significant clay fraction.

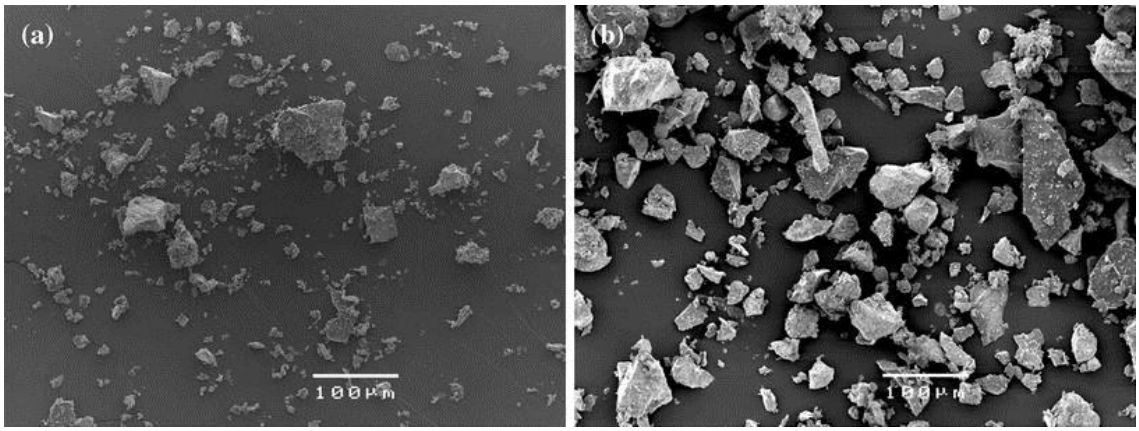

Fig. 2.6 Scanning electron micrograph of mine tailings. **(a)** Paste fills **(b)** hydraulic fills

Fig. 2.7 shows the grain size distributions of paste fills, hydraulic fills, ordinary Portland cement (OPC), and dune sand. The three different zones of fine, medium, and coarse-grained tailings are clearly indicated along with their suitability in paste fills and hydraulic fills.

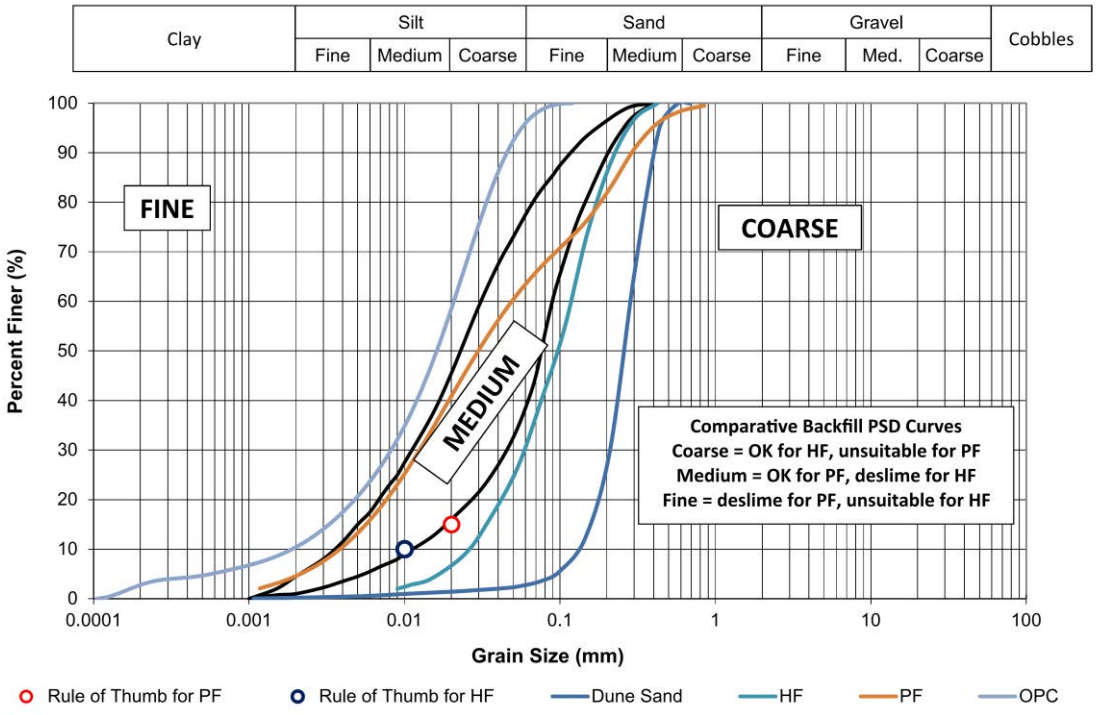

Fig. 2.7 Grain size distributions of Paste fills and Hydraulic fills (Sivakugan et al. 2015)

2.2.1 Paste Backfills

The use of paste as an underground backfill started in 1979 when it was used at Preussag's Bad Grund Mine in Germany. However, paste fill (PF) did not gain much widespread use until the mid-1990s when several plants were built in Canada and Australia. It is estimated that over 150 paste plants have now been built (some are not currently operating) with the industry having added approximately 5 paste plants a year since 2000 (Stone 2014).

Paste is a high density slurry thickened until it is non-settling, which usually occurs at solid contents ranging from 70–80 % ($Mass_{solids}/Mass_{total}$) depending on the constituent materials. Fig 2.8 shows the typical component of CPB. Paste also generally uses the entire tailings stream (fine-grained soils with fine sand). Fig. 2.7 can be referred for comparison of the particle size distributions.

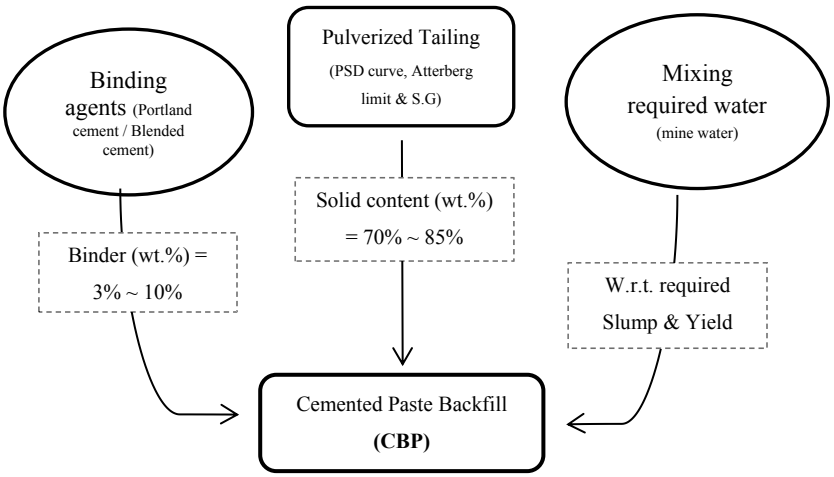

Fig. 2.8 Components of CPB (modified from Belem and Benzaazoua (2008))

It is common practice to make CPB by adding a small dosage of binder, in the range of 2–10 % binder ($Mass_{cement}/Mass_{solids}$), to enhance the CPB's strength. This strength is dependent on the CPB's application (type of exposure, size of exposure, etc.). Note that uncemented paste fill is not used in an underground mining operation due to liquefaction concerns. Historically most CPB was made with a binder containing 100 % OPC. However there is a recent trend to use blended cements for manufacturing CPB in mining operations. These blended cements contain other cementitious materials, such fly ash and/or slag, mixed with OPC in various proportions.

CPB is usually delivered to the underground void via a reticulation pipeline driven by either a pure or pump-assisted gravity system. However, given the thickened nature of the paste slurry it is critical to understand how the flow properties of paste slurry impact the design and successful operation of the reticulation system.

The flow of CPB closely conforms to the Bingham plastic flow model, which is strongly non-Newtonian in its behaviour. Fig. 2.9 shows Newtonian and non-Newtonian fluid models and plots the change in shear stress as a function of the shear rate. Water is the

best example of a Newtonian fluid, exhibiting no shear strength at a shear rate of zero and linear increases in shear stress with increases in shear rate.

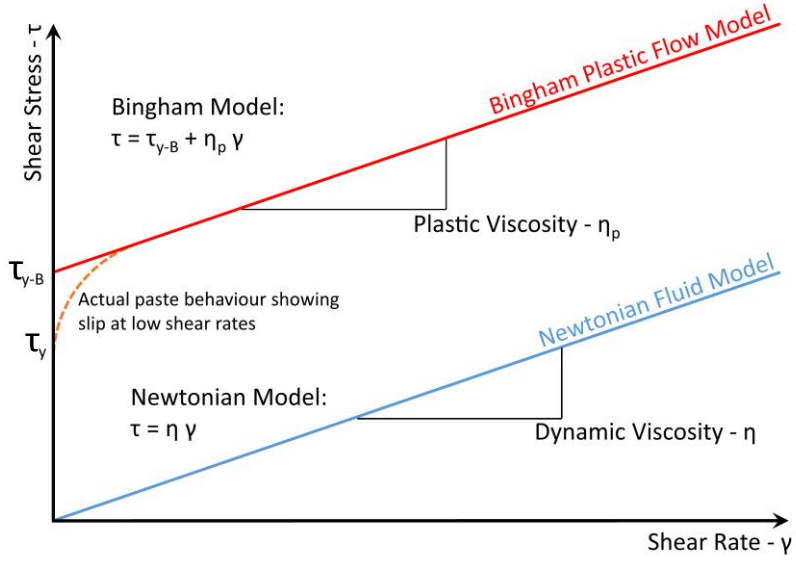

Fig. 2.9 Comparison of Bingham plastic and Newtonian flow models

Bingham plastics in general, and pastes in particular, exhibit a significant shear stress which must be overcome before movement (shearing) commences. This value of shear stress is commonly referred to as yield stress (τ_y). Once shearing has commenced, the rate of rise of shear stress with shear rate is closely linear. The gradient of this line is the viscosity of the paste. Note that the linear Bingham model predicts a yield stress ($\tau_{y\text{-}B}$) that is higher than the actual yield stress (τ_y) of the material. This means that actual paste generally exhibits a non-linear behaviour at low shear rates.

The flow characteristics (τ_y and η_p) of the paste can be determined through the use of a shear-vane rheometer (laboratory-scale) or a pipe loop (field-scale) testing. Pipe loop testing generally gives better results but requires specialized equipment to complete. Mines typically operate at a yield stress around 250 Pa, although operating yield stresses can range from 50 to 500 Pa depending on a particular mine's CPB and reticulation system. For ease of use, paste plant operators typically use either a conical or cylindrical

slump test to provide an indication of their CPB's ability to flow (similar to the cement and concrete industries). The amount of slump varies for each mine site but is generally between 235 to 275 mm for most of the mine in North Queensland, Australia.

Increasing the density of a paste also increases its yield stress (and a decrease in its slump). In general, the cement content required to achieve a specific strength is reduced as the density increases. Therefore, the primary economic goal of a paste plant operator will always be to decrease the amount of cement added by maximising the CPB density. This is typically done by minimising the addition of water. However, this means that the reticulation system will be operated in a narrow band of densities. Flow will only occur when the driving head exceeds the total pipeline wall shear stress. If the density of the CPB is too high, flow will not occur and the CPB will set in the borehole, which leads to pipeline blockages. Conversely, if the density is too low the CPB will be of lower strength, it may experience sediment settlement in low velocity areas, and it may cause excessive pipeline wear at high velocity areas. Nowadays, there are several chemical additives available commercially that can increase the slump, reduce the yield stress and enhance the flow without reducing the strength of the paste fill when it cures.

Once the CPB is deposited in the stope, the binder starts to hydrate and gain strength with cement curing age. The typical industry measure of backfill strength is the UCS tests. This testing is typically carried out on samples prepared in the laboratory or at the paste plant for quality control purposes. Mix design testing is conducted to determine the strength of a CPB mix proportion at different curing ages and appropriate mix proportions are selected based on the strength required (again, exposure type, exposure size etc.).

Fig. 2.10 shows a strength gain curve for an Australian mine's CPB recipe using 4 % OPC at approximately 76 % solids. Three sets of results are plotted. The first two are the mix design and the paste plant QC samples. The third set of data is the horizontal dashed line showing the average strength of four-month old in situ samples. The results show that the paste plant and in situ samples are higher than the mix design and that these results are more similar to each other than to the mix design. This trend has been observed

at mining operations (though the reverse is also observed) but the amount of in situ samples obtained by mining operations is limited, making such comparisons difficult.

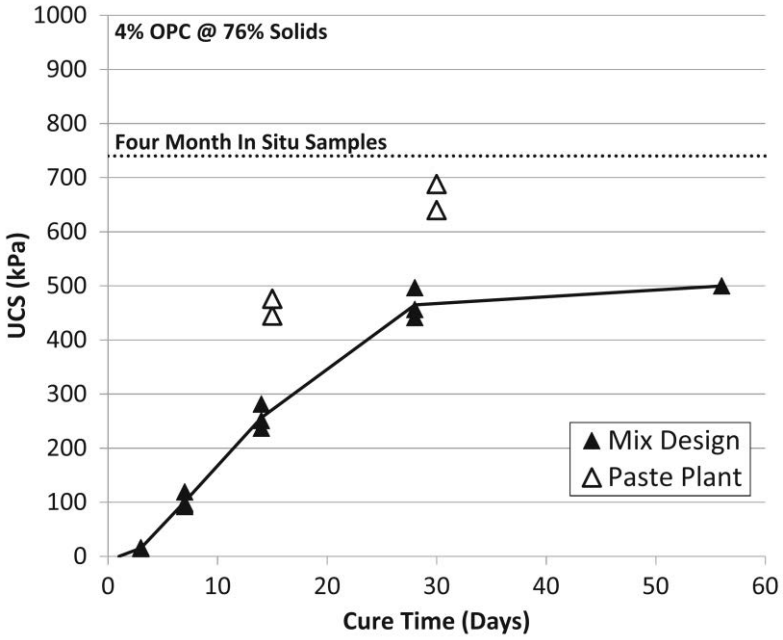

Fig. 2.10 Strength gain curves for 4% OPC CPB at 76% solids (Sivakugan et al. 2015)

If one assumes that the required backfill strength is 400 kPa, this chart indicates that a curing age over approximately 25 days would give the required strength whereas a required strength of 300 kPa would be achieved just before a 20 day cure.

Unlike hydraulic fills, excess water is not a problem in paste fills. The water in the slurry is partly used in the hydration and the rest stays within the clay matrix, without any excess water obvious to the naked eye. The main advantages of the paste fills are that the mining operations can be quicker due to the better support achieved in the stope in a shorter time, reduced excess water problems, and more tailings being disposed underground, leaving less for the surface tailing disposal facilities.

2.3 Binders

In most cases, a CPB must have enough strength to support its own weight following exposure. The strength is gained from binders that become a key ingredient of a CPB mix. The most common binders are cement or natural pozzolans, which control the time-dependent fill strength development. Strength gain will continue as long as un-hydrated cement and water is present. However, to expedite the mining operations, the mines want to reduce the time for curing, i.e., quicker strength achievement is expected. In order to achieve the required strength within a stope extraction period, the correct water to cement ratio must be known and adhered to as closely as possible.

In general, the choice of binder depends on the strength and durability requirements of a particular CPB operation. Therefore, a cost-effective mix design with optimum strength can be achieved by selecting the right binder for given tailings and mixing water. Cement cost often constitutes a large proportion of the total CPB production cost. Mine operators use combinations of other materials that have cementitious properties to reduce the amount of cement needed (Grice 1989). Alternate binders include fly ash, granulated iron blast-furnace slag, and silica fume, which can be used to replace partially or fully the cement binder in CPB. Generally, fly ash and slag are used in various percentages as a constituent of blended cement or in combination with normal Portland cement. In either case, the normal proportion of fly ash is 20-40%, while slag is 30-80% of total cement.

2.3.1 Pozzolanic Binders

Pozzolans are siliceous or aluminosiliceous materials that are generally added to enhance properties of soil and concrete. Waste glass, lime, fly ash, granulated blast furnace slag and silica fume are the examples of pozzolanic material. Among these, fly ash and granulated blast furnace slag are the waste and by-products of coal power plants and metal furnaces, respectively. These two pozzolanic materials containing a certain percentage of cement are also used to produce building materials as well as to stabilize soil in a cost effective manner. Cement is used to improve the properties of backfilling

material. Cement can be partially replaced with pozzolanic mineral admixtures in CPB. Furthermore, the utilization of pozzolanic admixtures can reduce binder costs substantially (which may constitute 40–70% of the operating costs in a CPB plant) since many industrial wastes with pozzolanic characteristics are available in large quantities and at low cost.

The use of the pozzolanic additives can affect the stress–strain behaviour of CPBs due to their filler and pozzolanic effect (Mehta 1989). The more slag in the binder, the greater its hydraulic reactivity in the presence of alkaline activators (Detwiler et al. 1996). Although behaviour of different CPB with different types of binders have already been investigated experimentally and numerically (Chindaprasirt and Rukzon 2009; Doven and Pekrioglu 2005; Fall et al. 2007; Helinski et al. 2011; Rankine and Sivakugan 2007), the research reported in this dissertation focuses mainly on slag blended cement consisting 60% slag and 40% GPC.

2.3.2 Fly Ash

Fly ash (FA) is one of the by-products of coal-burning thermal power plants, which produce around 40% of global electricity nowadays (Heidrich et al. 2013). From a typical 1,000 MW thermal power plant, approximately 650,000 t of FA and bottom ash are obtained, annually (Tokyay 2016). Generally, most fly ash consists of silica (SiO_2), alumina (Al_2O_3), iron oxide (Fe_2O_3), lime (CaO) and magnesium oxide (MgO).

Fly ash is the finely divided residue resulting from the combustion of ground or powdered coal, which is transported from the firebox through the boiler by flue gases (ACI Committee 116 1988). Fly ash is usually finer than the normal Portland cement, has very rounded shape and lower specific gravity (generally 1.9 – 2.4) than cement. ASTM C618 standard (ASTM 2015) classifies fly ash based on the source of mineral coal. It defines two classes of fly ash suitable for use in concrete - Class F and Class C. While the two classes have identical physical characteristics, they are distinguished by their chemical compositions. The Class F fly ash, which normally results from the burning of anthracite

or bituminous coal, is the more readily available of the two. It also has low (typically less than 10%) calcium oxide (CaO) content. Whereas, the Class C fly ash has a high CaO content (between 10% and 30%). In this research, the class F fly ash is used.

The chemical and mineralogical compositions as well as the physical properties of fly ashes vary depending on the source of the coal used in the thermal power plant, method of burning, combustion equipment, and collection methods, etc. Therefore, one can expect relatively large variations between fly ashes obtained from different thermal power plants and even within the same power plant at different times.

2.3.3 Granulated Blast Furnace Slag

Granulated blast furnace slag (GBFS) is the by-product of iron manufacturing and is produced by direct water cooling of molten blast furnace slag. The activity of GBFS is determined by the quantities and the properties of amorphous glass, the chemical compositions, as well as the fineness (Öner et al. 2003). For its use in blended cements, GBFS is generally ground to improve its reactivity during cement hydration. Fine grinding leads to formulation of a larger surface area, which significantly improves the mechanical activation of the components in blended cement (Boldyrev et al. 1996; Kumar et al. 2004; Sajedi and Razak 2011). It is also claimed that slag gives higher strength development compared to clinker for the same incremental increase in fineness (Patzelt 1993). The main constituents of GBFS include CaO, SiO_2, and Al_2O_3. In addition, it generally contains small amounts of MgO, FeO, SO_3, and sulphide as CaS, MnS, and FeS.

Though the replacement of cement clinker by GBFS usually results in lower early strength, the early strength gain phenomenon (1-7 days) purely depends on the grade of the slag used in accordance with ASTM C989 (ASTM 2014) and ACI 233R-03 report (ACI Committee 233 2003). In accordance with ASTM C989 (ASTM 2014), slag is classified into three performance grades: Grade 120, 100 and 80, which are determined by their respective mortar UCS when they are mixed with equal mass of Portland cement.

The three grades are classified according to their slag activity index (i.e., relative strength), which is average UCS of the slag-reference cement cubes (SP), divided by the average UCS of the reference cement cubes (P), multiplied by 100.

$$\text{Activity Index (i.e., Relative Strength), \%} = \frac{SP}{P} \times 100$$

When compared to GPC, grade 120 slag typically results in reduced strength in the early ages (1 to 3 days) and increased strengths in the latter ages (7 days and beyond). Grade 100 slag results in lower strengths in the early ages (1 to 21 days), but equal or greater strength in the latter ages. Grade 80 generally shows lower strength at all ages (ACI Committee 233 2003). The slag blended cement used in this research can be categorised as grade 100 or 120 as per their activity index.

2.3.4 Geopolymer

The term ‘‘geopolymers’’ was introduced by Davidovits in the mid-1970s. Geopolymer binder is used to produce building materials in a cost effective manner. Geopolymerization could convert a wide range of waste alumina silicate materials into building materials with excellent physical, chemical and mechanical properties as well as long-term durability (Davidovits 1991; Davidovits et al. 1994).

The geopolymer can be synthesized from pozzolanic material under activation using alkaline solution. The ratio between alkaline activator and fly ash is found to have a great influence on the UCS of the geopolymer. Al Bakri et al. (2012) concluded that the alkaline activator/fly ash ratio of 0.4 has the optimum amount of alkaline liquid, which could activate the fly ash in highest rate of geopolymerization. NaOH 10M and slurry of $NaAlO_2$ in NaOH 10M solution are generally used as alkaline solutions. The specimens were cured at 25° C and 100% RH for different ageing times. The weight ratio NaOH 10M and $NaAlO_2$ solid was equal to 3.5. Verdolotti et al. (2008) found that pozzolanic

material treated with 10M NaOH and $NaAlO_2$ slurry was more effective than material treated with 10M NaOH alone.

UCS of geopolymeric specimens prepared with certain percentages of class C fly ash (containing more than 20% lime), granulated blast furnace slag (GBFS), sodium silicate (water glass) solution and sodium hydroxide (NaOH), were tested by (Bagheri and Nazari 2014). In these tests, a specimen with 30 wt.% GBFS and NaOH concentration of 12M after being cured at 90°C for 16h showed the highest UCS, which is over about 65MPa.

2.4 Rheology of CPB

CPB is delivered from the paste plant to the stope via its reticulation pipeline. The transport of this material depends on the CPB's rheological characteristics, such as the CPB's yield stress and viscosity, and these can be quantified in the laboratory by using a rheometer. Rheology (i.e., flow characteristics) is the study of flow and deformation of materials under applied forces. To accurately define the rheology of paste fill, the yield stress (τ_y) and dynamic viscosity (μ) must be measured (Belem and Benzaazoua 2008). As CPB rheology closely fits the Bingham plastic flow model of a non-Newtonian fluid, there is a resistance known as the yield stress that is required to start the flow. A perfect Newtonian fluid has no yield stress (e.g., water). The viscosity of a fluid is defined as the increase rate of shear stress over the increase in shear rate (1/sec). Fig. 2.11 shows the general rheology of Newtonian and non-Newtonian fluids. Rankine et al. (2007) state that the key parameter in CPB rheology is the yield stress, with it exponential to the solid density of the mix before the hardening effect of cement.

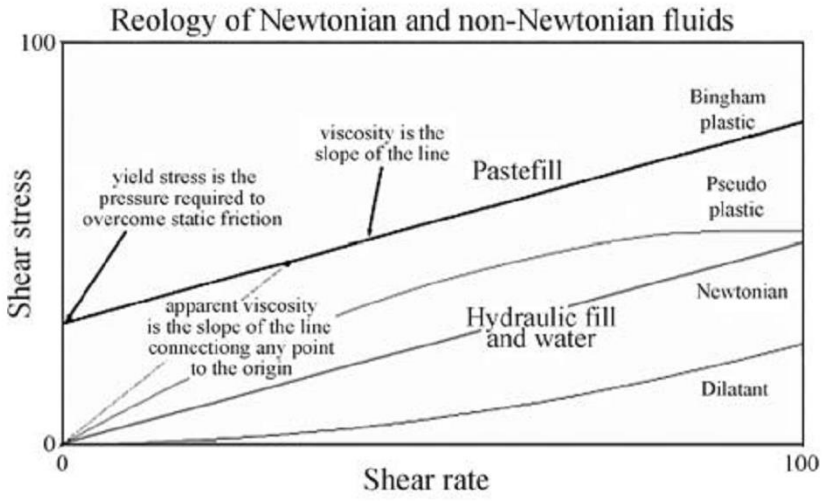

Fig. 2.11 Rheological curves for particulate fluids (Rankine et al. 2007)

The direct measurement of rheological properties in pastes can be very difficult due to the complexity of experimental devices (e.g. rheometer) used in the testing. Due to the simplicity of the standard slump test (Fig. 2.12), it is a popular method of determining paste backfill flowability. A slump test (similar to those carried out on concrete) is an indirect method for determining yield stress at the paste plant using established correlation between slump and yield stress for a particular tailing. Yield stress and slump are closely related, where higher solid content gives higher yield stress and a reduced slump. Both are used as a measure of how easy the slurry can flow through the pipes (Belem and Benzaazoua 2004; Belem and Benzaazoua 2008). CPB's with higher solid content generally have higher strengths than CPB's with lower solid content. However, increasing a CPB's solid content increases its yield stress. If the solid content is increased too much then the CPB will not move through the reticulation pipeline. Hence, there is always a trade-off between the CPB's solid content and yield stress when determining the CPB's optimum design.

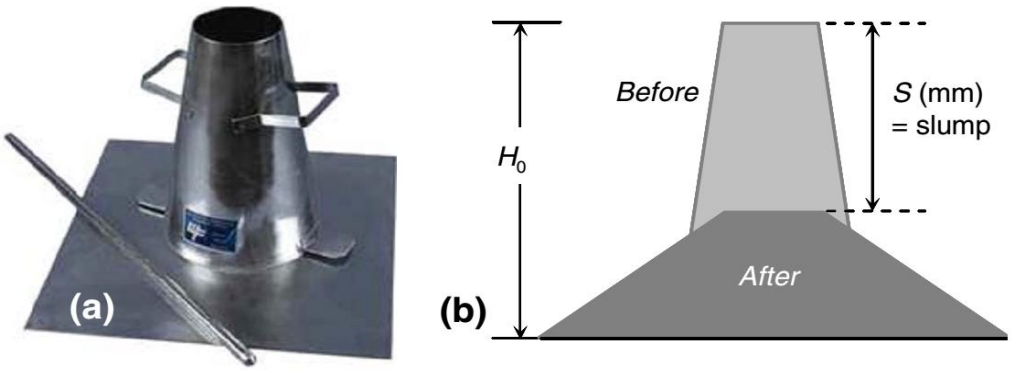

Fig. 2.12 (a) Slump cone mould **(b)** Schematic view of slump ((Belem and Benzaazoua 2008)

Similarly, increasing the binder dosage will increase the strength, but at a cost. The optimum dosage with regards to cost depends on the solid content and the strength gain required. For a certain solid content, the optimum binder type and dosage are generally determined through a well-planned mix design testing program.

The optimum slump of paste fill for pumping is suggested as 150 mm to 250 mm (Belem and Benzaazoua 2008; Li 2013) but this is dependent on the transport method adopted. Many properties can affect the slump behaviour of CPBs, such as yield stress and density, which are further dependant on the composition, particle specific gravity and particle size.

A strong interest in yield stress of fluids in the last two decades has led to developments of a variety of experimental methods and techniques for measuring the yield stress (Nguyen and Boger 1983). While each method has its own advantages and limitations, and although some techniques may be more popular than the others, no single method has been universally accepted as the standard for measuring the yield stress. Since yield stress measurements are extremely difficult to interpret, it is not unusual to find variations in the results obtained from different methods with the same material, prepared and tested in the same laboratory (Nguyen et al. 2006).

Rheology is one of the important performance properties highlighted in this review, with the other being UCS. The UCS is heavily affected by the tailing component characteristics of binder, and therefore an understanding into binders is necessary to reflect on UCS findings.

2.5 Uniaxial Compressive Strength of CPB

In literature, it is recommended that the uniaxial (i.e., unconfined) compressive strength (UCS) of CPB at 28 days reaches 0.7 – 2.0 MPa for most applications (Ercikdi et al. 2009; Fall et al. 2008). Strengths of 1 MPa are expected to maintain stability of the stope in the long term (Cihangir et al. 2012). As the required strength is based on the intended functions, strength of 5 MPa may be required to provide adequate ground support, while free-standing applications may require lower than 1 MPa (Belem and Benzaazoua 2008).

The strength of CPB varies significantly across backfill operations and is affected by the fineness of particles (Fall et al. 2005; Kesimal et al. 2003), high-sulphide content (Benzaazoua et al. 2004; Cihangir et al. 2012), sample curing (Benzaazoua et al. 2004; Fahey et al. 2011) and binder type and dosage (Cihangir et al. 2012; Ercikdi et al. 2009). Therefore, it is necessary to rely on the experimental results in each specific case to get an understanding of how the strength can vary across CPB mix designs. Binder type and dosage are the most important area of research as the binder content is estimated to be a major cost in backfill operations (Benzaazoua et al. 2004; Li 2013). Importance has been placed on analysing the strength development over time as sulphate attack has been observed to decrease the long term strength of CPBs, more specifically relating to calcium rich binders such as GP Portland cement (Ercikdi et al. 2009). It can be hard to find an exact analytical CPB design solution as most mine tailings have varying properties. A review of current literature can give an indication to the performance of different binders and dosages.

In a study of the effect of binder on high-sulphide CPB, a general idea can be reached into strength properties achieved from the use of GP Portland Cement (i.e., GPC).

The results show the strength of a CPB with approximately 77% solid content and a slump of 190 mm (Cihangir et al. 2012). Although the CPB suffers a loss of strength due to sulphate attack, the peak UCS gives an indication of the strength achievable in the CPB (Fig. 2.13).

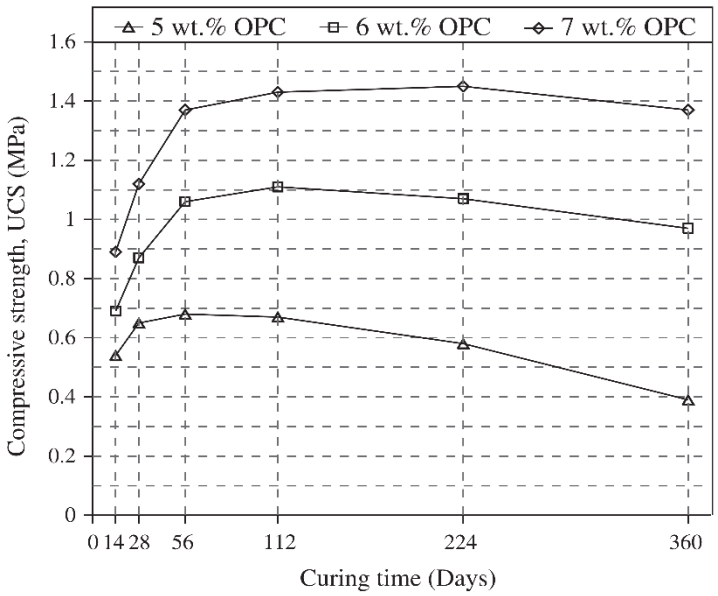

Fig. 2.13 Effect of GP cement dosage on strength of CPB (Cihangir et al. 2012)

Benzaazoua et al. (2004) had performed research into the effect of different binders in sulphide-rich tailings. At 28 day testing, GP Portland cement with slag (20/80%) achieved 1.05 MPa, Type GP and V Portland cement as well as high silica fume cement achieved 0.7-0.8 MPa, while the worst performing Portland cement and fly ash mixes (50/50%) achieving 0.4 MPa. Reviewing the effect of binder dosage, all mixes significantly increased strength with an increase in binder dosage from 3% to 6% weight of tailings.

Research into the strength associated with different binders in sulphide rich CPB used GP Portland cement, Portland composite cement and sulphide resistant cement (Ercikdi et al. 2009). The binder content was kept at constant 5% with GP cement having the earliest strength development. Over time, the GP cement samples strength decreased and

the sulphide resistant cement blends achieved approximately 40% more strength at 360 days. When the Portland composite cement dosage was increased to 6% and 7% it showed higher strength development as expected.

Cihangir et al. (2012) were one of the first to use alkali-activated slag as a binder in CPB. Two types of slags were activated with sodium silicates and NaOH, separately. Slag samples activated by NaOH showed higher 28-day strengths than sodium silicates. Overall, the study revealed the long-term superiority of alkali activated slag binders suitable for use sulphide-rich tailing CPB, with UCS of up to 4.75 MPa.

Ahmari and Zhang (2013) studied the feasibility of enhancing the physical and mechanical properties and the durability of geopolymer bricks made of copper mine tailings (CMT) and cement kiln dust (CKD). The effects of CKD content (0–10%), NaOH concentration (10M and 15M) and initial water content (12–20%) on unconfined compressive strength (UCS), water absorption, and weight and strength losses after immersion in water were studied. Addition of CKD results in significant improvement in the physical and mechanical properties and the durability of CMT-based geopolymer bricks. Furthermore, addition of CKD decreases the loss of weight and UCS of samples after submerging in water, while increases water absorption slightly.

Binding agents comprising 100% PC, 75% PC with 25% fly ash and 30% PC with 70% slag were used for the optimization exercise carried out by Pirapakaran et al. (2007). In this study, by adding 3%, 3.5% and 4% of binding agents by total dry mass of Cannington paste fill tailings having solids contents of 79%, 80% and 81%, specimens were prepared and tested for UCS after curing periods of 7, 14, 28 and 56 days. The 3.5% binding agent (25% fly ash blended with 75% PC) mixture with 80% tailings solids content was identified as the optimal alternative mix, considering strength, rheology and binder cost. Solid content chosen in this study appears to be high and it may not be satisfy flow characteristics in certain mine unless the high power is preferred for pumping the CPB from batching plant to underground stope.

Use of pozzolanic additives, such as waste glass (WG), fly ash (FA), granulated blast furnace slag (GBFS) and silica fume (SF), for the partial replacement of ordinary Portland cement (OPC) in CPB of Sulphide-rich mill tailings was investigated by Ercikdi et al. (2009). The pozzolanic wastes in the binder phase decreased the rate of strength development in the CPB samples.

The strength of CPB samples produced from exclusively OPC dropped after an initial curing period of 56 days as shown in Fig. 2.14. The addition of WG (10–30 wt.%), as a partial replacement of OPC, further reduced the strength of the CPB samples. Although GBFS, FA and SF appear to improve the long-term performance of CPB samples, only up to 20 wt.% GBFS (shown in Fig. 2.14) and 15 wt.% SF should be allowed into the CBP sample to maintain consistently higher strength.

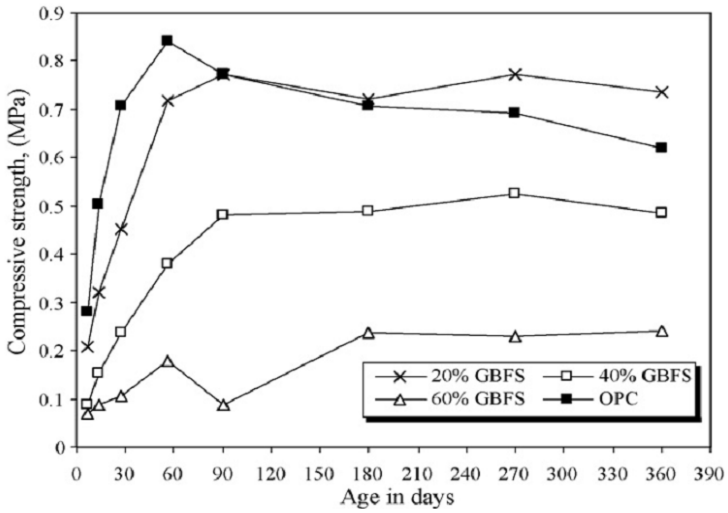

Fig. 2.14 Effect of GBFS addition on the strength of CBP samples (Ercikdi et al. 2009)

Waste rock dumps offer high strength, high permeability and low compressibility characteristics while tailing deposits typically have low permeability, slow time rate consolidation properties and long-term stability concerns associated with shear strength. Wickland and Wilson (2005) found that mixtures with approximately 5:1 waste rock to

tailings by dry mass were found to have a hydraulic conductivity similar to tailings alone and total settlements similar to waste rock alone.

2.6 Shear strength of CPB

Cohesion (c) and friction angle (φ) are the shear strength properties of any geomaterials including CPB, which are important values in assessing their stability and load resisting capabilities. For CPB, they are essential to carry out detailed numerical models in order to analyse the stability of both individual backfilled stopes and the entire mining sequence. These properties can be experimentally derived from the most direct methods in laboratory. To determine the shear strength properties for one specific mix, at least three triaxial tests at three different confining pressures must be performed. Then, by allowing the Mohr-Coulomb failure envelope, c and φ, can be determined. However, these experiments are very time consuming and expensive, in addition to requiring expensive and high-quality test equipment. Reducing the cost and effort is possible by using simpler testing methods to determine the c and φ. The analytical correlation method was initially proposed by Christensen Jr and Bonaquist (2002) for use on asphalt concrete base material to estimate the shear strength parameters by performing UCS and Indirect tensile (IDT) tests in laboratory. Compressive strength (UCS or σ_c) and tensile strength (IDT or σ_t) of CPB can be derived through the UCS and IDT strength test in laboratory, respectively. Further research by Piratheepan et al. (2012) and Sivakugan et al. (2014) utilised the correlation for lightly stabilised granular material, and rocks respectively. The theoretical framework of this alternate method for determining c and φ is strongly relating to the Mohr-Coulomb failure criterion the derivation is described in detail by Piratheepan et al. (2012). The equations presented in the paper by Piratheepan et al. (2012) were simplified by Sivakugan et al. (2014) and can be seen in Equations 2.1 & 2.2.

$$c = \frac{0.5\sigma_c\sigma_t}{\sqrt{\sigma_t(\sigma_c - 3\sigma_t)}} \quad \textbf{(2.1)}$$

$$\varphi = sin^{-1}\left(\frac{\sigma_c - 4\sigma_t}{\sigma_c - 2\sigma_t}\right) \quad \textbf{(2.2)}$$

The length to diameter ratio used for both rocks and stabilised granular material is 1:2 (Piratheepan et al. 2012; Sivakugan et al. 2014). Previous studies found that the UCS of CPB can be in excess of 4 MPa, as rock can be classified as a geological material with a UCS greater than 1 MPa. It can be assumed that CPB should follow similar criterion (Bieniawski 1989; Yumlu 2010). This thesis aimed to test the applicability of the correlative equations as a means to calculate the c and φ easier and quicker than conventional triaxial tests or direct shear for CPB. Typical shear strength parameters, such as cohesion and friction angle of CPB derived based on unconsolidated undrained triaxial test at 28 days curing were 208 kPa and 39˚, respectively as per studies by Saw and Villaescusa (2013). However, the solid content and the binder type and dosage used to prepare this particular CPB were unclear.

2.7 Numerical Simulation

Numerical simulations by means of the finite element method (FEM) of finite different method (FDM) have become a valuable tool in geotechnical and mining engineering to predict and to understand the behaviour of complex geomaterials and underground structures. The application of suitable nonlinear material models allows the prediction of damage and then failure mode of geomaterials and underground structures in different specific loading scenarios.

Fast Lagrangian Analysis of Continua (FLAC) in 2D version 7.0 and 3D version 6.0 from ITASCA (2017), both geotechnical and mining computer modelling programs, are used for explicit continuum modelling of non-linear materials behaviour. In past, FLAC software used in many ways for different problems associated with underground mining by many researchers Coulthard (1999) carried out numerica1l modelling using FLAC^{3D} for the analysis of underground mining problems, including the study of stresses generated when an open stope is filled with cemented rockfill. Pierce (2001) developed and utilized FLAC^{3D} numerical models for the stability analysis of paste backfill exposures at the Brunswick mine, Canada. Li et al. (2003) studied arching in a narrow

backfilled stope using FLAC software. Rankine (2004) investigated the arching mechanism in paste fill during a complete mining sequence using FLAC^{3D}. Pirapakaran (2008) developed FLAC^{3D} models on arching for the square and rectangular backfilled vertical stopes and also developed approximate axisymmetric solutions using FLAC to 3-Dimensional models.

2.8 Summary

After conducting a literature review, there was evidence to suggest that CPB performance is affected by the physical, mineralogical and chemical properties as well as type and dosage of binder. In particular, strength and rheology are two important performance properties highlighted while binder type and dosage had the largest effect on UCS. The slump test is a primary method in determining an empirical rheological factor but further investigation is required into the use of a rheometer/viscometer in CPB to take advantage of a more accurate method of quantifying slurry consistency. There are opportunities to significantly reduce the cost in production of CPB by suggesting a more economical binder type as it contributes to typically 8% - 15% of total mining operating costs (Li 2013). It is proposed more investigation into types of binder and dosage be performed in this thesis. In particular, there is very limited literature on the use of alkali-activated pozzolan in CPB. The opportunity to further study the performance of GP cement compared to cement composites (cement and Pozzolans) will also be undertaken. The strength development will be analysed over a longer period to ensure there is no significant loss in strength over time while understanding the flow behaviour of CPB.

3 Geotechnical Characterisation of the Mine Tailings

3.1 Introduction

The mine tailings for this research project were provided by Glencore from their George Fisher Mine (GFM) operations, which is a hard rock underground mine. It is located 20 km north of Mt Isa in North Queensland, Australia. The tailings provided were in a relatively dry state and sealed in 20 L containers. Grains size lager than 4.75mm in around 5% were present within the tailings and it was recommended the tailings be sieved to a maximum particle size of 4.75 mm to achieve a more homogeneous material. This chapter highlights geotechnical properties including chemical characterisation and, grain shapes of the mine tailings. Some of these are important in the analysis and test methodology and others are merely to gain an understanding of mine tailings characteristics.

This chapter was submitted as minor portion of a journal article and published as Niroshan, N., Sivakugan, N., and Veenstra, R. L. (2018)."Flow characteristics of Cemented Paste Backfills." *Geological and Geotechnical Engineering,* doi: 10.1007/s10706-018-0460-8.

3.2 Moisture Content

The existing (i.e., initial) moisture content of the tailings material was required for both strength and rheology methodologies so that the exact amount of water to be added can be determined. Moisture content (w), which is a mass ratio and used to quantity the amount of water present in a soil, is defined as in Equation 3.1,

$$w = \frac{M_w}{M_s} \times 100\% \qquad \textbf{(3.1)}$$

where, M_w is mass of the water and M_s is mass of the dry soil grains.

A sample was placed in an oven at 105°C for 24 hours as per ASTM D2216 (ASTM 2010) to measure the dry mass. Throughout this thesis, the initial moisture content of each 20 L bucket was determined by averaging two samples. The average moisture content was in the range of 8% –13%.

3.3 Grain Size Distribution

The relative proportions of the different grain sizes in mine tailings are quantified in the form of grain size distribution. Grain size distribution is performed through sieve analysis according to ASTM D6913 (ASTM 2009) and laser analysis. Laser analysis in fine-grained tailings is conducted using Malvern Mastersizer 3000 laser particle size analyser.

Figure 3.1 shows the grain size distribution of mine GFM tailings used in this experimental study. It shows that the tailings are fine-grained soil as the fine fraction is above 50%. Moreover, it shows that the percentage passing 20 μm is 28%, which is above than the percentage required for the paste fill preparation.

The median particle size (D_{50}) of the tailings is 49.5 μm. Based on the grain sizes mine tailings, approximately 28% are clays, 26% are silts, and 46% are coarse grained tailings.

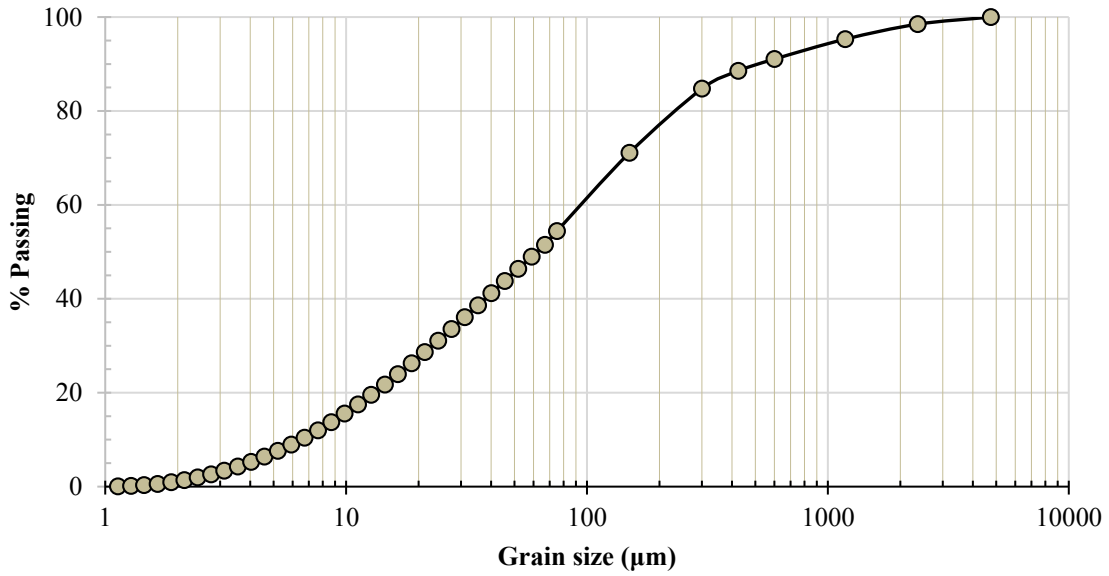

Fig. 3.1 Grain size distribution of George Fisher Mine Tailings

3.4 Specific Gravity

The specific gravity of a soil grain (G_s) is the ratio of density of the soil grain to the density of water. The specific gravity (G_s) of particles was determined in accordance with

ASTM D854 (ASTM 2014). The G_s of the tailings material is an important parameter required in the paste fill analysis and evaluation of sample curing methods. Due to the presence of heavy metals in mine tailings, the specific gravity can be in the range of 2.70 – 4.50, which is significantly higher than inorganic soils including sands, silts and clays (Sivakugan 2008). The specific gravity of GFM tailings was determined as 2.90.

3.5 Atterberg Limits and Linear Shrinkage

Atterberg limits are the borderline water contents to separate different consistencies in fine grain soils. The limits are liquid limit (LL), plastic limit (PL) and shrinkage limit (SL) (Sivakugan and Das 2010). Liquid limit, plastic limit and plasticity index are determined in accordance with ASTM D4318 (ASTM 2010). Though different methods are available to determine the liquid limit, the fall cone method is used herein to evaluate the liquid limit of the GFM tailings.

The liquid and plastic limit of the tailings were determined as 22% and 15%, respectively. While there are substantial fines present within the tailings, the tailings in this testing program show very little or no plasticity. Based on the Atterberg limit test in addition to the grain size distribution the mine tailings used can be classified as low plastic sandy silty clay (CL-ML) according the unified soil classification system ASTM D2487 (ASTM 2011).

The basic geotechnical properties of the GFM tailings are summarised in Table 3.2. Specific gravity of GFM tailings is 2.90, which is slightly higher than the natural soils (normally 2.65) due the presence of heavy metals in mine tailings. Average in-situ moisture content and the bulk density of the tailings used are 9% and 1950 kg/m^3, respectively.

Table 3.1 Physical properties of George Fisher Mine (GFM) tailings

Physical Properties	Values
Initial water content (%)	8.0 - 13.0
Bulk density, ρ_b (kg/m^3)	1,950
Specific gravity	2.90
D_{10} (μm)	6.5
D_{50} (μm)	49.5
Coefficient of uniformity, C_u	7.62
Coefficient of curvature, C_c	1.57
Liquid limit, LL (%)	22.0
Plastic limit, PL (%)	15.0
Plastic index, PI (%)	7.0
Linear shrinkage (%)	2.5

3.6 Consolidation and Permeability

Consolidation is the process in which water is squeezed out from the fine-grained soil. The reduction of water within the fine-grained soil leads to a reduction in the void ratio, thus leading to settlement on the soil. Whereas, the permeability (i.e. hydraulic conductivity) is the measure of how easily water is able to pass through a soil sample. Permeability has an important influence on both the consolidation behaviour of the tailings, as it controls the water flow characteristics. The purpose of the consolidation and permeability tests was to determine the consolidation and permeability behaviour of tailings over the effective stress range of 6–800 kPa. The saturated permeability at the end of each applied stress increment was also determined through direct measurement by applying a falling head difference across the sample to measure the upward flow through the sample.

In this study, GFM tailings were used to prepare uncemented backfill contains 100% tailings (i.e., no binder) with approximately 75% solid content for the consolidation and permeability testing. The consolidation test was carried out in accordance with ASTM D2435 (ASTM 2011). 75 mm diameter with 20 mm height sample was prepared in this study. The consolidation parameters, i.e., the coefficient of consolidation, coefficient of volume compressibility, and permeability, were then calculated from the test results from each load increment.

Automatic Computerised Oedometer (ACE) apparatus was used in this study to measure the consolidation parameters and permeability and test setup for consolidation with permeability measurement is shown in Figure 3.2.

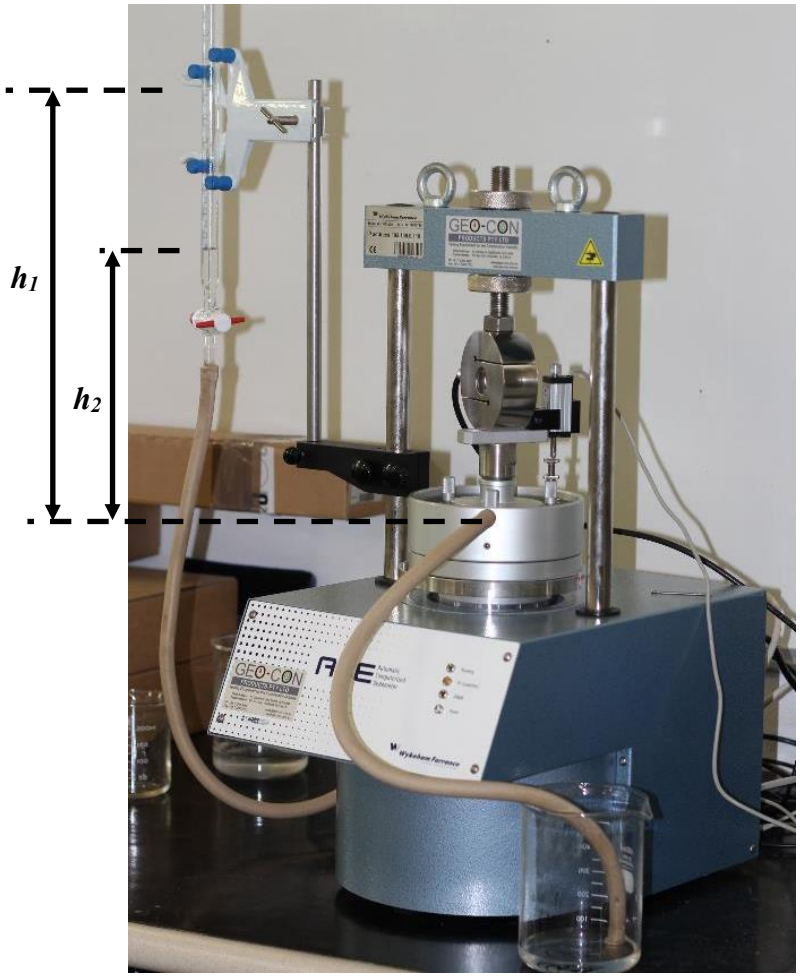

Fig. 3.2 Test setup for the consolidation and permeability measurements

In the laboratory, permeability can be determined used either constant head or falling head methods. However, the permeability (k) of the uncemented backfill were determined through a falling head method in this study in accordance with ASTM D5084 (ASTM 2003). Figure 3.3 shows the inlet and outlet positions for permeability measurement in the ACE consolidation apparatus.

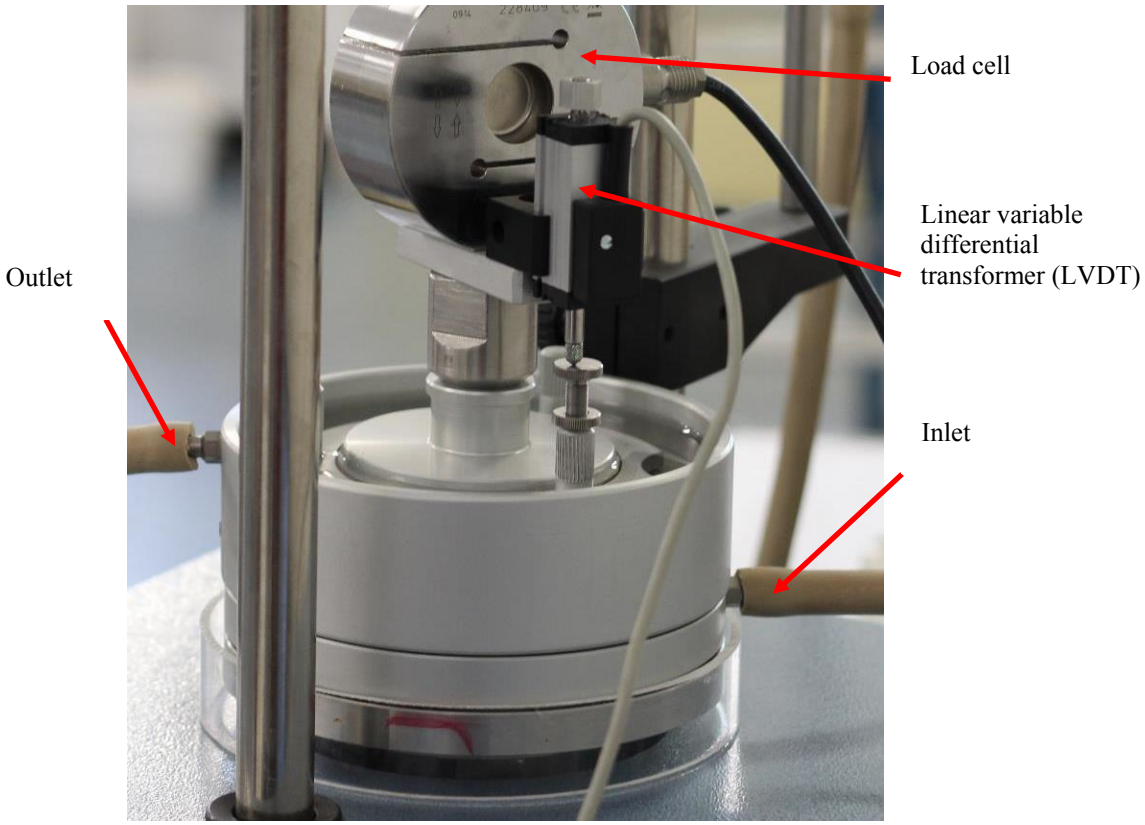

Fig. 3.3 Positions of inlet and outlet valves during permeability measurements in ACE consolidation apparatus

In a falling head permeability test, water passes through a soil sample with a known height (L) and surface area of soil specimen (A). During the permeability test, initial head (h_1) and the final head (h_2) of the water in the standpipe are measured over a specific time (t). These measurements are taken between stress increments in a consolidation test, while there is no excess pore pressure within the specimen. In addition, the cross section area

(a) of water standpipe is measured. Using these data, the permeability (k) of the paste backfill is calculated using the Equation 3.2 (Sivakugan and Das 2010)

$$k = \frac{aL}{At} ln \frac{h_1}{h_2} \quad \textbf{(3.2)}$$

The setup used in this study to measure the permeability of paste backfill facilitates the investigation on permeability changes with vertical effective stress increment.

Generally, the coefficient of consolidation (c_v) is determined using both Casagrande's and Taylor's methods, which heavily rely upon the shape of the settlement curve. However, testing has shown (Figure 3.4) that the settlement curves produced by the paste fill is not comparable to the graphs for both Casagrande's and Taylor's methods. Because the methods rely on the shape of the graph and the graph produced by paste backfill is different these methods cannot be used to produce and accurate value for the coefficient of consolidation.

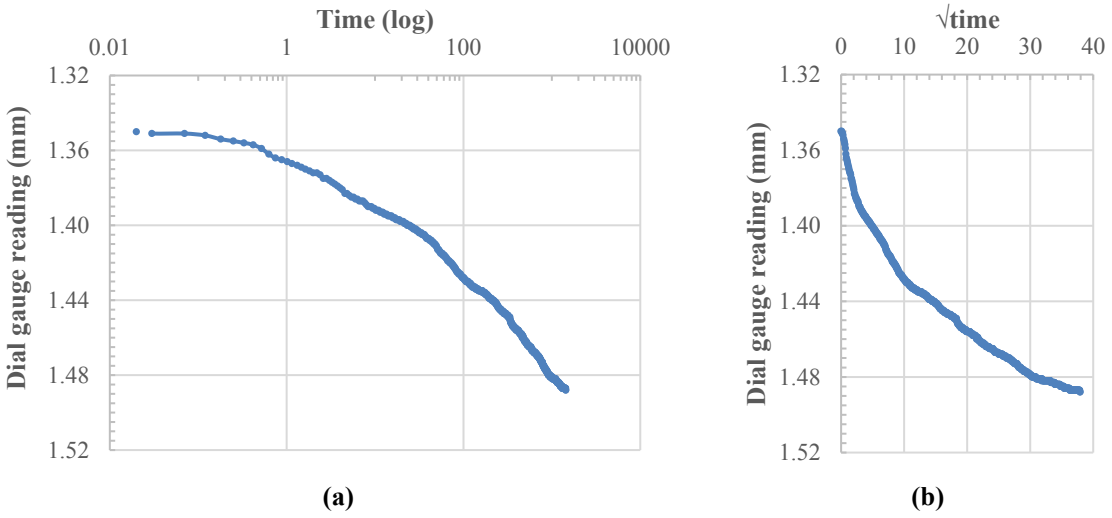

Fig. 3.4 Settlement curve of paste fill for determination of c_v **(a)** Casagrande's log time method **(b)** Taylor's square root of time method

Therefore, an alternate method is used to calculate the coefficient of consolidation using results obtained during the one dimensional consolidation test. In conventional consolidation theory the coefficient of consolidation can also be calculated using the Equation 3.3

$$c_v = \frac{k}{m_v \times \gamma_w} \quad \textbf{(3.3)}$$

where, the c_v is coefficient of consolidation, k is the permeability of Paste fill, m_v is the coefficient of volume compressibility and γ_w is the unit weight of the water.

Figure 3.4a shows the changes of void ratio with effective stress of paste fill (no binder). The compression index (C_c) and re-compression index (C_r) of paste fill are 0.087 and 0.011, respectively. It is noted that the re-compression index is about 8 times lesser than the compression index for paste fill with no binder. The value of the C_c for the GFM tailings were within the range obtained by Qiu and Sego (2001).

Figures 3.5(b) and 3.5(c) show the coefficient of volume compressibility (m_v) and coefficient of consolidation (c_v) changes with vertical effective stress (σ_v'). In general, the c_v increases with increasing σ_v', whereas the m_v reduces with increasing σ_v'. The m_v of the paste fill reduces from around 2.20 MPa^{-1} to 0.04 MPa^{-1} when the stress increases from 10 kPa to 800 kPa. However, the c_v of the paste fill increases from 2.4×10^{-6} m^2/s to 4.1×10^{-5} m^2/s over the vertical stress change from 6 kPa to 800 kPa. The values of the coefficient of consolidation (c_v) for the GFM tailings at 100 kPa stress form this study was much higher than this presented by Qiu and Sego (2001) (3.31×10^{-6} m^2/s for Gold tailings and 2.54×10^{-6} m^2/s for Copper tailings). However, the c_v value at 100 kPa of GFM tailings was similar to the values obtained by Volpe (1979) (1.50×10^{-5} m^2/s for the copper tailings at pond area)

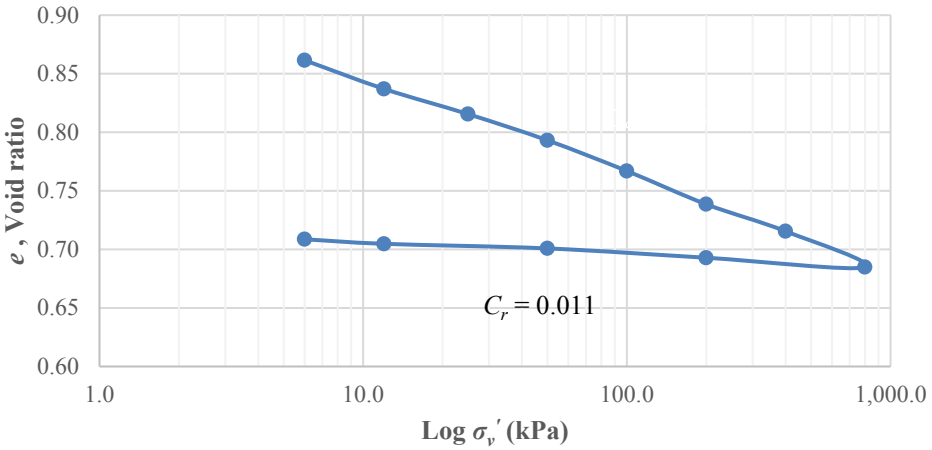

(a)

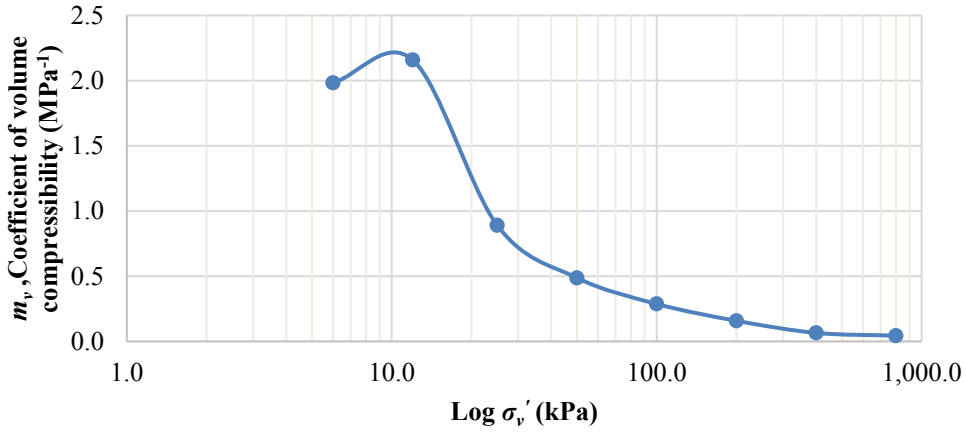

(b)

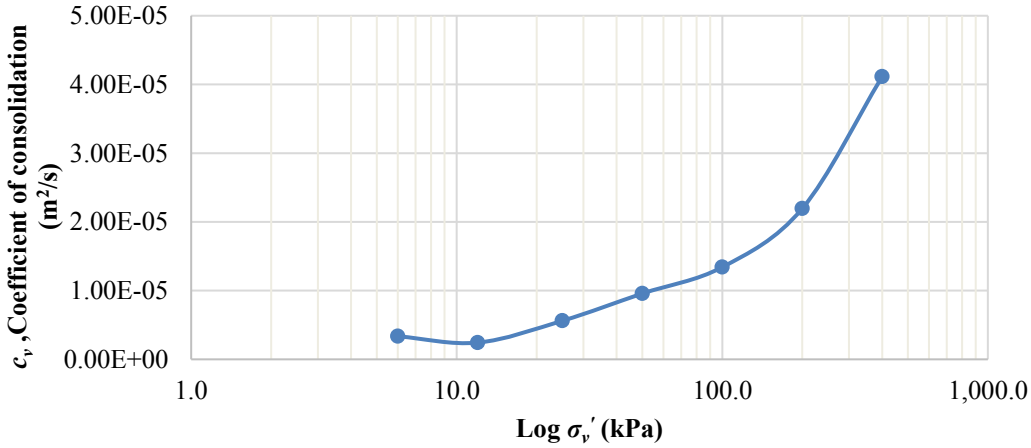

(c)

Fig. 3.5 (a) Void ratio (e), **(b)** Coefficient of volume compressibility (m_v) and **(c)** Coefficient of consolidation (c_v) changes with log $\sigma_{v'}$ for paste backfill (no binder)

Figure 3.6 shows the permeability changes with vertical effective stress for uncemented backfill. It is worth noting that the permeability (k) almost linearly reduces with increasing vertical effective stress (σ_v'). The k values of GFM tailings are between 6.52×10^{-6} and 2.65×10^{-6} cm/s.

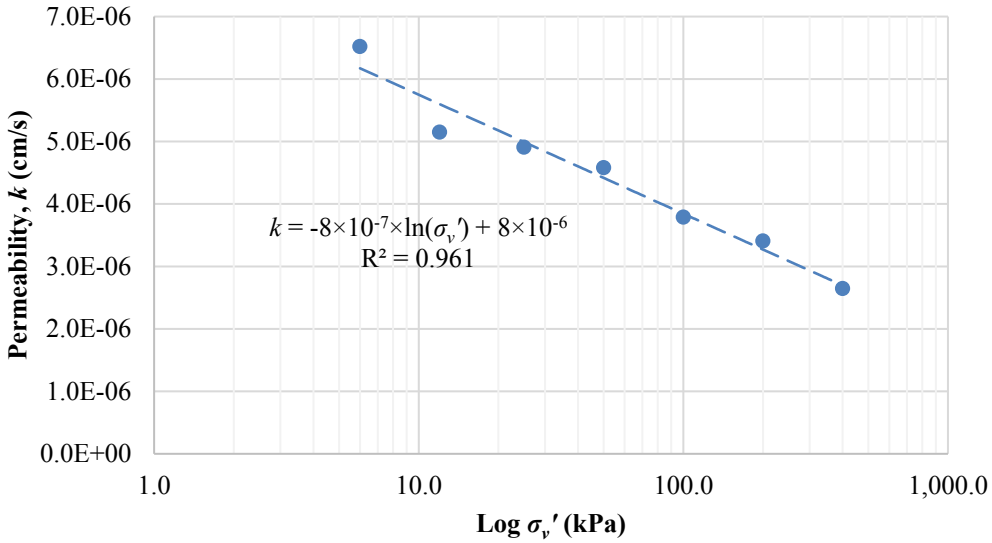

Fig. 3.6 The permeability of GFM tailings changes with vertical effective stress

3.7 Grain Shape and Chemical Composition

The grain shape, mineralogical and chemical properties play an important role in the performance of paste backfill. Although it was not a major focus of this thesis, these shapes and chemical composition give a better understanding of the mine tailings material from GFM used in the paste backfill. The facilities at the Advanced Analytical Centre at James Cook University were utilised to perform the scanning electron microscope (SEM) analysis and X-ray Fluorescence (XRF) analysis.

3.7.1 Scanning Electron Microscope (SEM) Analysis

SEM analysis was performed to identify the shape of individual tailings particles. For this analysis, tailings sample was dried, powdered and gold-coated to view using the SEM facility. Scanning electron micrographs of the dry GFM tailings is shown in Figure 3.7. Based on this SEM image, shapes of most grains are angular while some are sub-rounded. Due to the presence of more angular shaped grains in the tailings, the tailings would show greater strength and stiffness due to the interlocking ability between them. In addition, further SEM analyses of tailings and CPBs are given in detail in the Chapter 6.

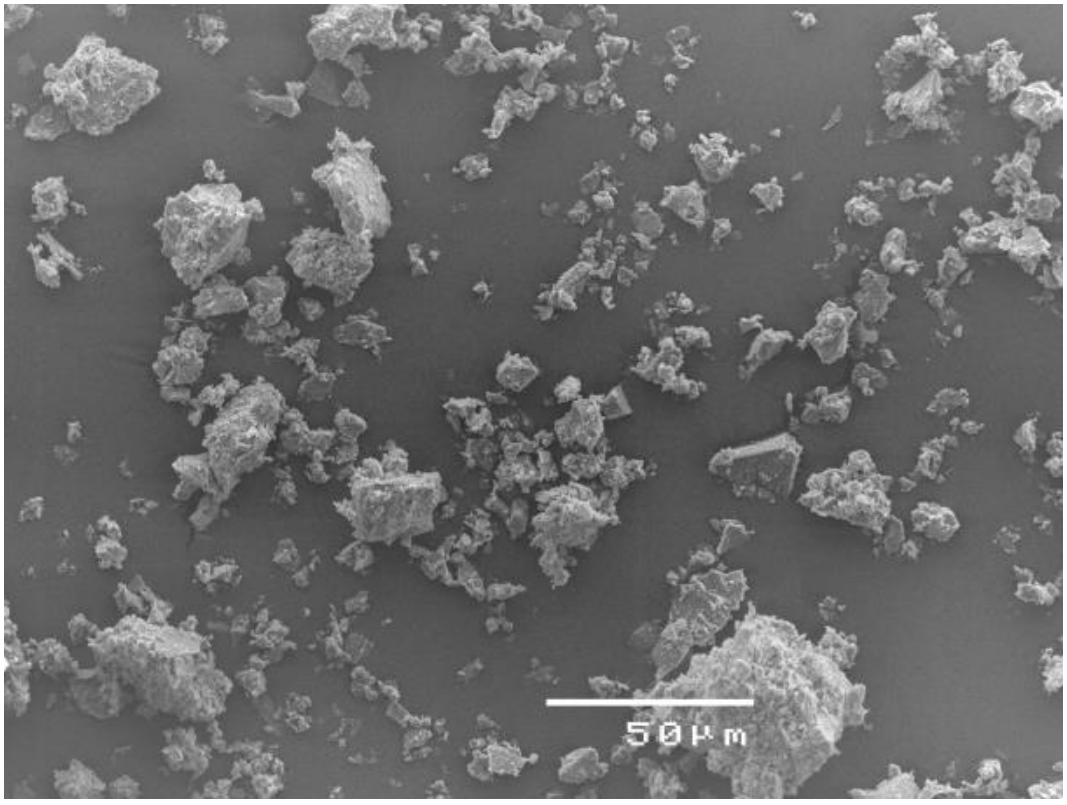

Fig. 3.7 Scanning electron micrograph (SEM) of the GFM tailings

3.7.2 Chemical Characterisation

A semi-quantitative X-ray fluorescence (XRF) analysis was carried out to identify the chemical concentration of different compounds in the mine tailings. Table 3.1 shows the

chemical content of the GFM tailings. In GFM tailing the sulfide content, possibly coming from pyrite in the tailings, was relatively low.

Table 3.2 Chemical analysis of the GFM tailings, (wt. %)

Compound	Al	Ca	Cu	Fe	Mg	O	S	Si	Zn	K	Na
Concentration	2.3	10.0	0.1	7.27	4.14	54.3	3.29	15.9	0.36	1.37	0.18

3.8 Summary

The basic geotechnical properties of the George Fisher Mine tailings were determined, as per the relevant ASTM standards, inclusive of; moisture content, specific gravity, grain size distribution, Atterberg limits, grain shapes and chemical composition. The mine tailings used for this experiment is categorised as low plasticity Sandy Silty Clay (ML-CL). Grain shapes of GFM tailings particles are mostly angular with 28% finer than 20 μm. The specific gravity was found to be 2.90 while the existing moisture content in sample containers ranged from 8-13%. The most common chemical elements were oxygen (54.3), Silicon (15.9), Calcium (10.0) and Iron (7.27).

4 Specimen Preparation – Casting and Curing

4.1 Introduction

There is no standardized process for sampling, and curing of paste backfill materials for testing in laboratory. Their mechanical properties are determined by not only the characteristics of tailings, binders and mixing water but also the chemical and mineralogical properties of these materials. Even though the test results of in situ samples from the underground are often different from the laboratory experiment, standardised procedure, as in the case of concrete or soil, for sampling, curing and testing, is quite essential to minimise the error and variation between the lab and in situ samples.

During the mix design, where the optimum mix proportions are identified through trials, several cemented paste fill specimens of different proportions are cast, cured and tested for the mechanical properties such as uniaxial compressive strength (UCS) and Young's modulus. Curing process, which ensures a humid environment, plays a vital role in the strength development within the CPB. Several different methods of curing are tried in this laboratory test program to assess the differences in the strength development. The findings are discussed in this chapter.

The cement content in concrete is in the order of 16% and is much higher than that in the CPB mixes where the cement content is about 2-6%. Further, the concrete specimens reach strengths in the order of 30-40 MPa in 28 days, whereas CPB reaches 500 – 2000 kPa of strength over the same period. The concrete specimens are cured by submerging them in water baths for 28 days, which is not possible for the CPB specimens due to their lower strength at early ages. In addition, since the CPB specimens require significantly less water for the hydration process with the smaller cement content, it is not necessary to fully submerge them for curing. A simple method, that mimics the curing at the site conditions, is proposed for the curing process. The effects are discussed and the alternate curing methods are compared.

The nature of the geomaterials such as soils or rocks is such, there can be significant variabilities associated with the parameters determined in the laboratories. Part of the variability is due to the inherent nature of the materials and the rest come from the test procedures. The UCS sample preparation, curing and test procedure suggested in this chapter are assessed through 25 replicate samples and a thorough statistical analysis. The results are discussed in this chapter.

There is always uncertainty associated with the design parameters of materials determined from laboratory tests. These can be quantified through typical values for the coefficient of variation (COV). The values of COV can be used in defining the plausible lower and upper bounds, for a specific risk level. While the structural strength or Young's modulus of materials such as concrete or steel have lower variability with COV less than 10%, there is substantial variability associated with the properties of geomaterials, including paste backfills. Typical values of COV for the different soil parameters are summarized by Das and Sivakugan (2017). Phoon and Kulhawy (1999); Phoon and Kulhawy (2008) noted that good quality lab test results can have COV as high as 30% and that the geotechnical correlations can lead to COV up to 50%. In addition, an attempt is made in this chapter to define the statistical distributions for the UCS and Young's modulus, the two major parameters derived from the UCS test.

A preliminary description of the variability of a design parameter can be obtained from the descriptive statistical analysis. A complete description can be obtained by plotting the information graphically in the form of a histogram. Geotechnical engineers often work with the data that can be thought of as a random samples from some population. In many such cases, it is important to determine a probability distribution that approximately describes the population of the random variable. The measured mechanical properties (e.g., UCS and Young's modulus) of CPBs are the two random variables in this study. It is shown that both parameters can be considered as normal variates.

Probability plot provides sample distribution in a good way to check whether the random samples are normally distributed. It is also more reliable than the histogram for small to

moderate size samples. Probability plotting typically uses special axes that have been scaled for the hypothesized distribution. We generally focus primarily on normal probability plots because many statistical techniques are appropriate only when the population is (at least approximately) normal. It is also good to elaborate the experimental data in probability density function (PDF). Then one can easily understand from the PDF plots how the experimental results are scattered. This scatter will give strong evidence on quality of lab experiments and methods of sample casting, curing and testing.

Therefore, the objective of this chapter are:

- To propose the best method for curing UCS specimens by studying five different methods; and
- To assess the variability of UCS and Young's modulus through a statistical analysis of values derived through the laboratory test of 25 identical samples from each CPB mixes tested on 28 and 56 days.

UCS test is used to estimate the mechanical properties of each single CPB specimen. Finally, different techniques, such as histogram, probability plot and probability density functions, were used to understand the scattering pattern of mechanical properties obtained from the 25 identical samples from each mixes, which provides insights into the quality of laboratory test.

This chapter was submitted as journal article for publication in *Journal of Materials in Civil Engineering (ASCE)* co-authored by Niroshan, N., Sivakugan, N., and Veenstra, R. L. (2018) "Effects of curing methods on UCS test specimens and variability of mechanical properties of cemented paste backfill", which is under second review.

4.2 Materials

Mine tailings from George Fisher Mine (GFM), which is a hard rock underground mine located in north Queensland, Australia, were used to prepare CPB for this laboratory testing program.

General Purpose (GP) cement, which is a normal Portland cement or type I Portland cement according to ASTM C150 standard (ASTM 2007), was used as a binder in preparation of the CPB specimens. The GP cement binder was received from Cement Australia. Water obtained from three sources in the mine were used to prepare CPB samples for the laboratory testing. The water analysis results of the three types of water is summarised in Table 4.1. Mine water 1 shows slightly higher pH values, and significantly lower total dissolved solids (TDS), chloride and sulphate when compare to other two mixing water types. Mine water 1 was from spring water source whereas, the Mine water 3 was pure bore water and Mine water 2 was mixed water from both sources.

Table 4.1 Water analysis of three different mine waters

Water Types	pH	Total Dissolved Solids (mg/l)	Chloride (mg/l)	Sulphate (mg/l)
Mine Water 1	7.80	170	36	29
Mine Water 2	7.65	2385	252	1115
Mine Water 3	7.51	4600	467	2200

4.3 Sample Preparation for UCS Test

UCS specimens were produced using cylindrical plastic mould, which are split longitudinally to facilitate specimen removal. Slightly longer (about 120 mm) cylindrical plastic moulds with bottom cap were used to cast the UCS specimens of 50 mm diameter and 100 mm height. The specimens in the mould were placed on the vibrating table for 2 minutes to eliminate air pockets within the specimens. Just before the UCS test, the cured specimens were extruded from the split mould, and the ends were trimmed off with a

steel straight edge to ensure the surfaces were flat and parallel. The binder content, solid content and water content are defined as follows.

$$\text{Binder content (\%)} = \frac{\text{Mass of binder}}{\text{Mass of (dry tailings+binder)}} \times 100 \quad \textbf{(4.1)}$$

$$\text{Solid content (\%)} = \frac{\text{Mass of (dry tailing+binder)}}{\text{Mass of (dry tailings+binder+water)}} \times 100 \quad \textbf{(4.2)}$$

$$\text{Water content (\%)} = \frac{\text{Mass of water}}{\text{Mass of (dry tailings+binder)}} \times 100 \quad \textbf{(4.3)}$$

Trimmed UCS specimen was tested according to ASTM C39 (ASTM 2005). In this test, the compressive load was applied axially to the cylindrical sample at strain rate of 0.8 mm/min to axial strain of 4-8%, which was well past the peak load (i.e., UCS). For all mix designs, duplicate specimens were tested for compressive strength at each curing period. Since the UCS tests are undrained tests, the cross sectional areas increase during the loading period. The new cross sectional area, A at axial strain of ε is computed as per Equation 4.4

$$A = A_0 \times \frac{1}{(1-\varepsilon)} \quad \textbf{(4.4)}$$

where, the A_0 is the initial cross section area of UCS specimen. The Young's modulus of each UCS specimen was calculated as the slope of the linear segment (initial tangent method) of corresponding stress-strain plots. Niroshan et al. (2017) have described how the Young's modulus can be estimated from the stress-strain plots.

4.4 Effect of Curing Method

GFM tailings with 2% GP cement was used to prepare CPB specimens for curing method evaluation based on mechanical properties. In this experimental study, the solid content of CPB was 75%, approximately. In all five curing methods studied herein, prepared samples were cured in buckets with about 2 cm of water at the bottom, and fully covered by a lid to maintain constant humidity for initial 7 days. Since the cemented paste with high slump (approximately 260 mm slump) was used to cast cylinder samples, the

extrusion from their respective mould was not possible before 7 days with no damage or disturbance to the sample. Duplicate specimens per mix were tested in all five methods. Beyond the first 7 days, the specimens were cured by five different methods for the rest of their curing time, as shown in Figure 4.1. This exercise is solely to assess the different curing methods. Each method is described below briefly.

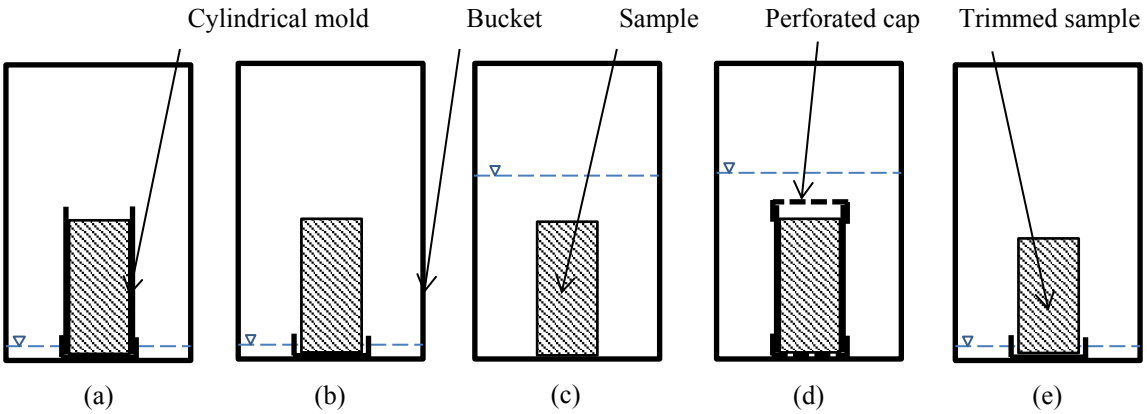

Fig. 4.1 CPB samples curing methods: **(a)** Method-1, **(b)** Method-2, **(c)** Method-3, **(d)** Method-4, **(e)** Method-5

Method- 1: Curing is continued as for the first seven days, as shown in Figure 4.1(a). i.e., the UCS specimen with the plastic mould and the bottom cap is placed at the bottom of a bucket with 2 cm water and the lid was covered to ensure humid environment. On the day of testing, samples were removed from the bucket and the ends trimmed prior to UCS testing.

Method- 2: After 7 days of curing, the sample was taken out from the plastic mould and placed with the bottom cap in a bucket with 2 cm water at the bottom and the top covered by a lid to maintain humidity, as shown in Figure 4.1(b). On the day of testing, samples were removed from the bucket and the ends trimmed prior to UCS testing.

Method- 3: After 7 days of curing, the sample was taken out from the plastic mould and then fully submerged into water, without the bottom cap, for curing as shown

in Figure 4.1(c). On the day of testing, samples were taken out from the water and trimmed prior to UCS testing.

Method- 4: After 7 days of curing, the sample was taken out of the bucket and perforated caps were placed both ends of plastic mould and then fully submerged into water for curing for the rest of the time as shown in Figure 4.1(d). On the day of testing, samples were removed from the bucket, extruded from the plastic mould and trimmed prior to UCS testing.

Method- 5: After 7 days of curing, the sample was taken out of the bucket and removed from the plastic mould and the ends trimmed. The trimmed sample was placed in a bucket with a bottom cap to prevent direct contact with water. The bucket was filled with about 2 cm of water in the bottom, and fully covered by a lid to maintain constant humidity as show in Figure 4.1(e). On the day of testing, samples were removed from the bucket for UCS testing.

In each method, duplicate samples with 50 mm in diameter and 100 mm long per mix were used for UCS testing at 28 days and 56 days of curing time as per ASTM standard.

Though, five different curing methods were implemented in order to propose a proper curing method for UCS specimens, only the cured samples in first four methods were tested after 28 days. Then, two most effective curing methods among the first four methods were chosen and continued with curing in the same condition, in addition to the fifth method, and cured samples were tested after 56 days of curing. Figure 4.2 shows the stress-strain plots of some samples in 28 days curing by the first four methods.

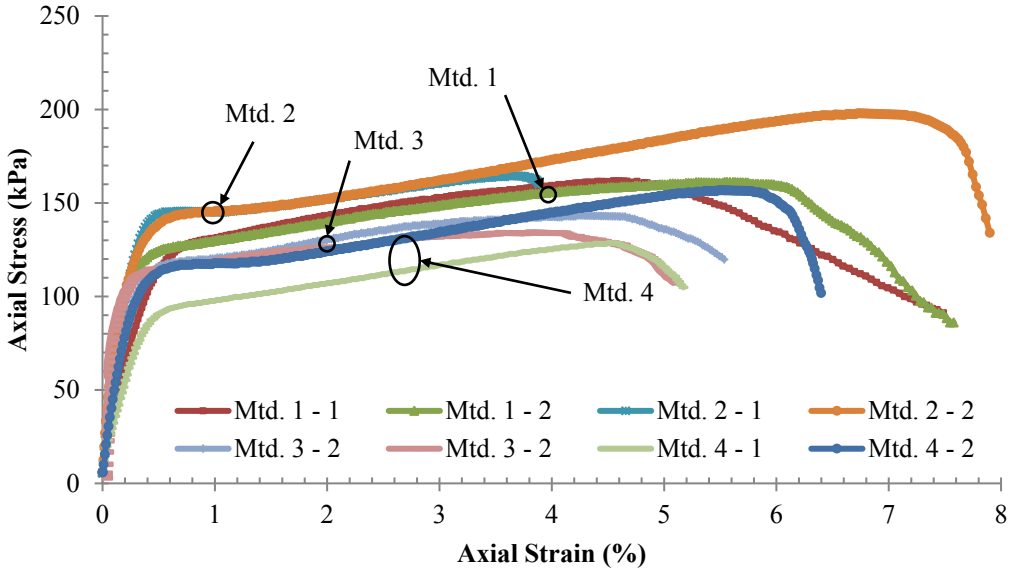

Fig. 4.2 Stress-strain plots of CPB samples in 28 days of curing

All the mixes show similar trend in the stress-strain plot generated during uniaxial compressive strength test. All the samples, irrespective of the curing methods, yield at approximately 0.5% axial strain during the testing. However, the maximum stress (i.e., UCS) of each sample is considerably different not only between different curing methods but also within the same curing method. However, it is noted that the samples cured in method-2 show slightly higher strength and Young's modulus than method-1 in 28 days testing, even though it was hard to see any significant difference in the trend. As mentioned previously, curing methods 1 and 2 were chosen, in addition to the method-5 for 56 days testing. It appears that submerging the specimens (methods 3 and 4) is of very little or no value; the 2 cm water at the bottom of the bucket (methods 1, 2, and 5) is adequate for maintaining the humidity and for curing.

Figure 4.3 illustrates the variation of stress with strain for the CPB samples cured for 56 days by the three different curing methods 1, 2, and 5. As noted in the trend of stress-stain curves for 28 days curing (Figure 4.2), 56 days cured samples also yield at approximately 0.5% strain and reached the maximum shear stress at 6 to 8% strain. As can be seen, the trend of the stress-strain plot of 56 days cured samples in the curing

method-1 is significantly different from the other methods. The UCS is significantly higher in this case. The Young's modulus values determined from the initial linear segments are not very different for the three methods of curing

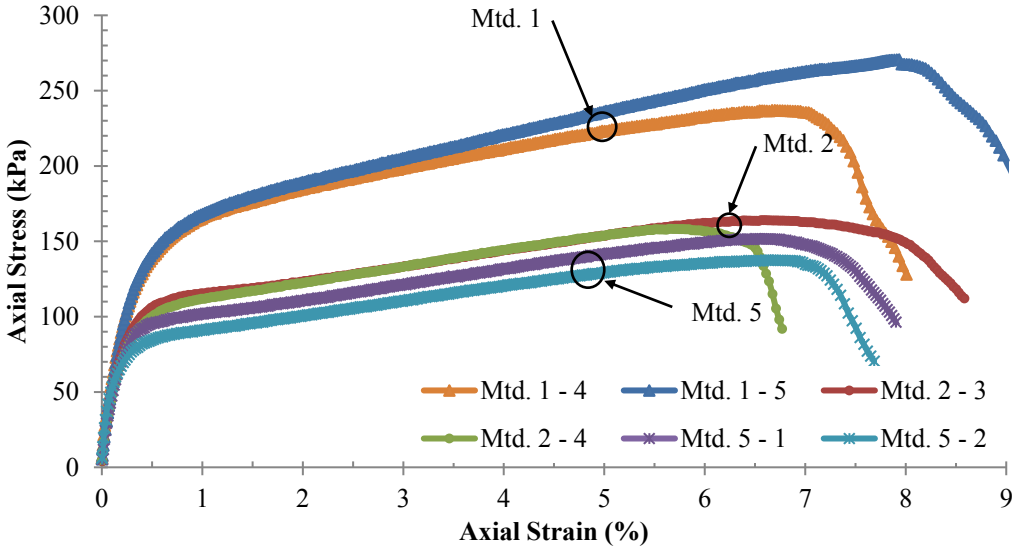

Fig. 4.3 Stress-strain plots of CPB samples in 56 days of curing

Figure 4.4 summarises the average UCS and Young's modulus of the CPB samples cured in different methods. Both UCS and Young's modulus in 7 days curing period are equal for all methods as the condition of curing was the same for the first 7 days and changed only after 7 days of curing. Method- 1 gives the highest UCS and Young's modulus after 56 days. Here, both UCS and Young's modulus increase over the 56 days period. Further, this method is the simplest of all five for curing the UCS specimens in any laboratory. In addition, the CPB samples in methods 3 and 4, where samples were fully and partially submerged in the water, respectively, show lower strength than methods 1 and 2 and hence excluded in the 56 days testing.

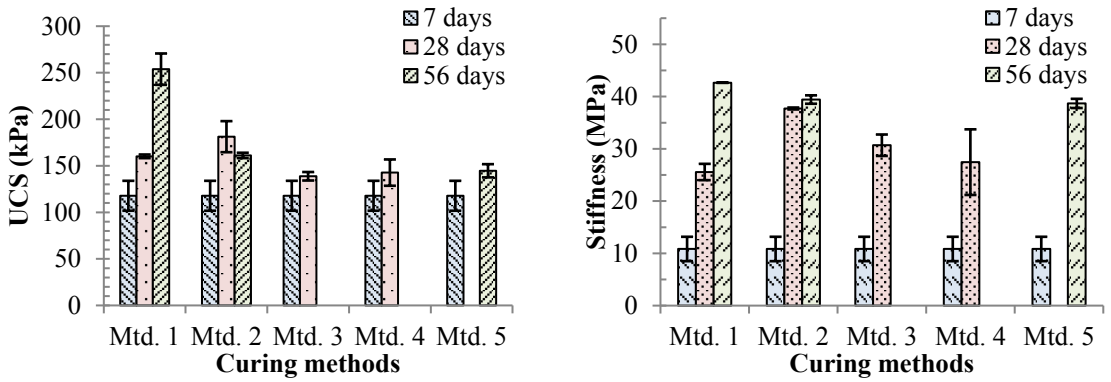

(a) (b)

Fig. 4.4 Mechanical properties of CPB samples cured by different methods for 7, 28 and 56 days: **(a)** Strength, **(b)** Young's modulus

Furthermore, method-5 was included in 56 days testing to evaluate the trimming effect of sample on mechanical properties. The difference between both methods (methods 2 and 5) is the trimming, which was carried out after (in method-2) or before (in method-5) curing the CPB samples. Both methods show similar trend in the stress-stain plots and approximately equal values for UCS and Young's modulus. Therefore, it can be concluded that the trimming has no effect on their mechanical properties and the trimming can be performed either before or after the curing process. With lower but adequate strength after 7 days, it is easier to trim the specimen after 7 days and hence method-5 is preferred over method-2.

The variation of moisture content and saturation with curing time for the five different methods are shown in Figures 4.5(a), 4.5(b), respectively. The moisture contents were determined at 0, 28 and/or 56 days only. All samples were at initial moisture content of 32.7%, which reduced slightly with the curing time. Nevertheless, al all stages of curing, the moisture content remained above 28%.

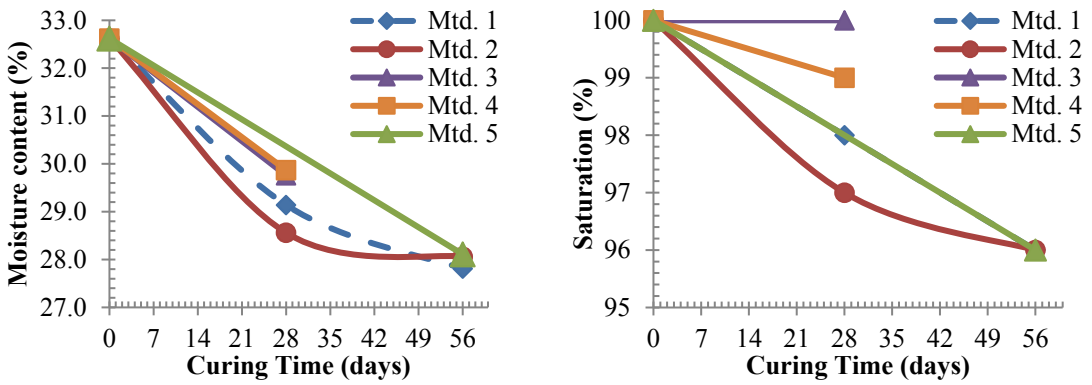

Fig. 4.5 (a) Moisture content **(b)** Degree of saturation of CPB samples changes with curing days in different curing methods

From the Figure 4.5(b) it is clear that at all stages during the curing process, and for all five methods, the degree of saturation remained above 96%. This exercise clearly shows that there is adequate moisture present for the hydration purposes in all five methods of curing and that it is not necessary to submerge the samples in water (methods 3 and 4) as in the case of concrete specimens. Method-1 appears to be the simplest of all five methods, with the highest UCS and Young's modulus values, with steady gains during the 56 days. The method-1 was adopted for the curing process of the rest of the samples discussed in the statistical analysis.

4.5 Variabilities in Mechanical Properties – A Statistical Approach

Table 4.2 shows the testing program for the analysis of variability of mechanical properties of the CPB specimens. Three different CPB mixes, each mix containing 25 samples, were cast and tested as per ASTM standard to find the UCS and Young's modulus of each sample. The three sample sets consisting 25 samples per mix can be considered representative random samples from each CPB mix. For this statistical study, all CPB samples were cured as per method-1 as shown in Figure 4.1 (a). UCS tests were conducted on samples cured for 28 and 56 days. Solid content of CPB sample slightly varies between the mixes in the range between 73.5 and 75. 5%. These were the solid

contents required for 260 mm slump height, derived through the standard slump test as per ASTM standard C143 (ASTM 2015).

Table 4.2 Mix design for statistical analysis

Mix Ref.	Binder	Solid content (%) required for 260 mm Slump	Water	Curing days	Number of Samples per mix
Mix 1	4% GP Cement	75.0	Mine Water 1	28	25
Mix 2		73.5	Mine Water 2	28	25
Mix 3		75.5	Mine Water 3	56	25

In descriptive statistical analysis carried out herein, mean, standard deviation, skewness and coefficient of variation (COV) are mainly calculated for the two variables UCS and Young's modulus of each CPB mix. The COV is a normalized measure of the amount of dispersion around the mean, and is calculated using Equation 4.5

$$COV = (\sigma/\overline{x}) \times 100\ \% \quad \textbf{(4.5)}$$

where, σ is the standard deviation and $\overline{x}$ is mean. In the sample, which is normally distributed, the probability that the true population mean lies within a certain distance of the sample mean can be readily calculated. For sample populations, the estimated standard error ($SE(\overline{x})$), of the sample mean is calculated using Equation 4.6

$$SE(\bar{x}) = \sigma/\sqrt{n} \quad \textbf{(4.6)}$$

where, σ is the standard deviation and n is number of sample. Again, to avoid dimensional problems, a non-dimensional measure of skewness known as the skewness coefficient can be found using Excel function SKWE (data range). However, the coefficient of skewness can also be calculated using Equation 4.7 (Harr 1977), and the result is the same as from the Excel function.

$$Skewness\ coefficient = \frac{\frac{1}{N}\sum_{i=1}^{N}(x_i-\mu)^3}{\sigma^3} \quad \textbf{(4.7)}$$

Values for Kurtosis can be calculated based on Excel in-built function called "KURT (data range)". The kurtosis calculated based on KURT excel function is sample excess

kurtosis. Therefore, actual coefficient of kurtosis (CK) can be calculated by adding three with excess kurtosis.

In addition, histogram, cumulative occurrence plot, probability density function (PDF) plots, and probability plot are employed to analyse the variability in the mechanical properties of the CPB samples.

Table 4.3 elaborates the average experimental results and some analysis to shed some light on the variability in the UCS and Young's modulus, which reflect the quality of the sample preparation and test procedure. Existing moisture content of CPB sample, measured just prior to the UCS testing, has shown a positive linear relationship with corresponding dry density, and mechanical properties (i.e., UCS and Young's modulus). Though Mix 1 and 3 have initial solid content approximately equal during the casting, the UCS of Mix 1 at 28 days is higher than the UCS of Mix 3 at 56 days due to the different water used in the mix (see Table 4.2). However, CPBs gain strength throughout the curing period till 56 days (Niroshan et al. 2017). As mentioned early, water used to prepare Mix 3 (i.e., mixing water 3) has significantly higher TDS, chloride and sulphate compared to mixing water 1. Thus, as expected, mixing water also plays a vital role in strength development of CPB mixes.

Table 4.3 UCS test results and analysis

Mix Ref.	Mean					Standard Deviation			Coefficient of Variation (%)	
	Dry density (g/cm^3)	**Moisture content (%)**	**UCS (kPa)**	**Failure strain, ε_f (%)**	**Young's modulus, E (MPa)**	**UCS (kPa)**	**Failure strain, ε_f (%)**	**Young's modulus, E (MPa)**	**UCS**	**Young's modulus, E**
Mix 1	1.985	30.6	439.46	3.61	107.75	28.65	1.80	19.52	6.52	18.11
Mix 2	1.931	34.0	321.59	0.77	101.73	19.63	0.15	13.24	6.10	13.02
Mix 3	1.969	32.1	375.11	2.33	112.85	39.16	1.59	27.78	10.44	24.61

The COV of UCS and Young's modulus of CPB were in the range of 6.10-10.44% and 13.02-24.61%, respectively. However, these COVs are well below the levels suggested by past researchers for soils (Baecher and Christian 2005; Fredlund and Dahlman 1972; Harr 1977; Matsuo and Kuroda 1974; Morse 1971). As per Phoon and Kulhawy (2008), in geotechnical engineering, the COV of less than 30% for strength properties of geomaterials can be considered as low property variability and typically these can be expected in good quality laboratory or field testing. The COV values observed suggest that the test procedures including curing by method-1 are adequate for general UCS testing. From the overall analysis, we can conclude that the sample casting, current practice of curing methods and testing in the laboratory are very consistent and reliable to get meaningful results for the mechanical properties of CPB samples over certain curing period.

Figure 4.6 shows the moisture content changes with curing time for the three different CPB mixes. These moisture contents are averaged over the 25. All three mixes were cured by method-1. Mixes 1 and 2, tested after 28 days, show only 2-3% reduction in the moisture content during the entire curing period. In the case of mix 3, tested after 56 days, the drop in the moisture content is insignificant. Niroshan et al. (2016) reported that moisture contents of the UCS samples prepared using CPB slightly vary (~ 3-5%) during the first 28 days of curing period. As can be seen, the moisture content of sample during testing was above 30% in all mixes, which is adequate for the hydration process of CPB sample during the curing period. Therefore, the moisture content measurements of CPB samples suggest that the current curing method (method-1) adopted in this study is adequate. Noting that the specimens are nearly saturated, with very little room for absorbing any more water, there is little value in submerging them in water.

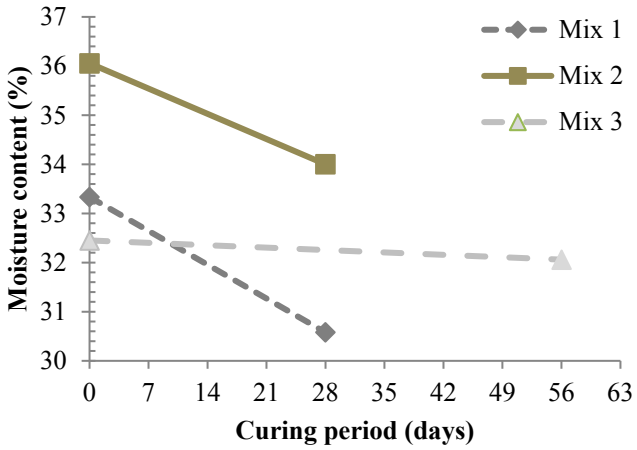

Fig. 4.6 Moisture content changes with curing time of CPB mix

Table 4.4 shows the parameters from a descriptive statistical analysis of the two mechanical properties of CPB mixes, UCS and Young's modulus. The maximum value for UCS and Young's modulus can be found from the Table 4.3 for corresponding CPB mixes. The coefficient of skewness (CS) measures the degree of asymmetry of observations around the mean. The closer the CS is to zero, the lesser the degree of skewness. Positive values suggest right-skewed distributions and vice versa. On the other hand, coefficient of kurtosis (CK) measures the degree of kurtosis (i.e., the peakedness or flatness) of population. The skewness and kurtosis values of three different mixes tested indicate that the distributions of mechanical properties (i.e., UCS and young's modulus) are near normal (near-zero skewness and kurtosis). As CS values of UCS are between 0.5 and 1.0 for Mix 1 and 2, the degree of skewness is moderate, whereas the CS of UCS for Mix 3 and Young's modulus of all mixes are between -0.5 and 0.5, which indicate relatively symmetrical distributions. Thus, the variability in the mechanical properties, (i.e., UCS and Young's modulus) of CPB is relatively small.

Table 4.4 Descriptive analysis of mechanical properties of CPB samples

	UCS			Young's modulus		
	Mix 1	**Mix 2**	**Mix 3**	**Mix 1**	**Mix 2**	**Mix 3**
Mean	439.46	321.59	375.11	107.75	101.73	112.85
Standard Error	5.73	3.93	7.83	3.90	2.65	5.56
Median	434.33	318.88	376.91	102.87	103.23	110.84
Standard Deviation	28.65	19.63	39.16	19.52	13.24	27.78
Sample Variance	820.93	385.21	1533.39	380.84	175.36	771.57
COV	**6.52**	**6.10**	**10.44**	**18.11**	**13.02**	**24.61**
Kurtosis	1.14	0.15	0.18	-0.49	-0.85	-0.66
Skewness	0.90	0.55	-0.24	0.39	0.00	0.02
Range	125.53	81.37	162.83	74.71	47.65	104.45
Minimum	393.30	284.78	285.52	75.29	78.14	60.50
Maximum	518.83	366.16	448.35	150.00	125.79	164.95
Count (sample tested)	25	25	25	25	25	25
Confidence Level (95.0%)	11.83	8.10	16.16	8.06	5.47	11.47

In this study, 25 identical samples per mix are considered, and hence the degree of freedom is 24. As the samples are normally distributed, the true mean of UCS and Young's modulus will be within ± 2.064 standard errors of the sample mean 95 times out of 100 (i.e., where the probability, $P = 0.05$) and these limits are the 95% confidence limits. A confidence interval always specifies a confidence level, which is a measure of the reliability of the procedure. By reliability, it is understood that if this testing was repeated over and over again, 95% of all samples results would be within the confidence interval that contains the true mean mechanical properties. The 95% level of confidence value of mean mechanical properties for CPB mixes can be calculated using from Table 4.4 and Equation 4.8. It may be possible to accurately predict the actual behaviour of CPB by using these predicted mean values in the any designs stage.

$$95\%\ confident\ level = mean \pm 2.064 \times standard\ error \quad \textbf{(4.8)}$$

A preliminary description of the randomness in a variable can be obtained from the numerical values of the parameters derived from a descriptive analysis as discussed above. However, a more complete description can be obtained by plotting the information graphically in the form of a histogram.

Histograms and cumulative distributions of mechanical properties of CPB samples are shown in Figure 4.7. From this figure, the symmetric bell-shaped distribution of the mechanical properties measurements can be noticed. This display often gives insight about possible choices of probability distributions to use as a model for the population.

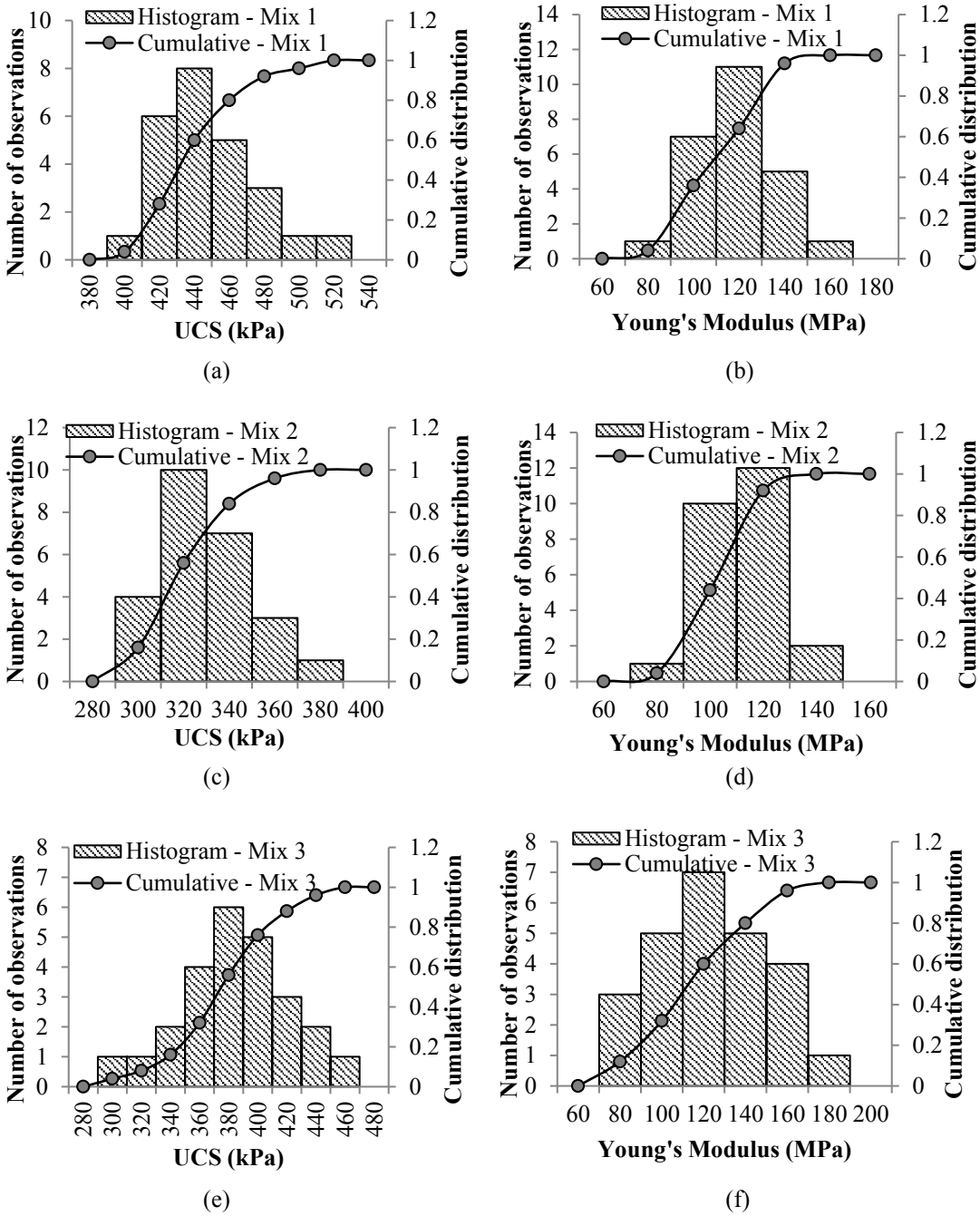

Fig. 4.7 Histogram and cumulative distribution of mechanical properties of CPBs: (a) UCS – Mix 1, (b) Young's modulus – Mix 1, (c) UCS – Mix 2, (d) Young's modulus – Mix 2, (e) UCS – Mix 3, (f) Young's modulus – Mix 3

Figure 4.8 shows the normal probability plots obtained from standardized normal UCS and Young's modulus of CPBs. In Figure 4.8, the z-values indicate the standardized values of corresponding mechanical properties and it can be obtained using Equation 4.9. These points in the probability plots lie on a straight line with strong coefficient of correlation (R^2) and hence can be concluded that the random variables UCS and Young's modulus of the different mixes are normally distributed.

$$z = \frac{X - \mu}{\sigma} \qquad \textbf{(4.9)}$$

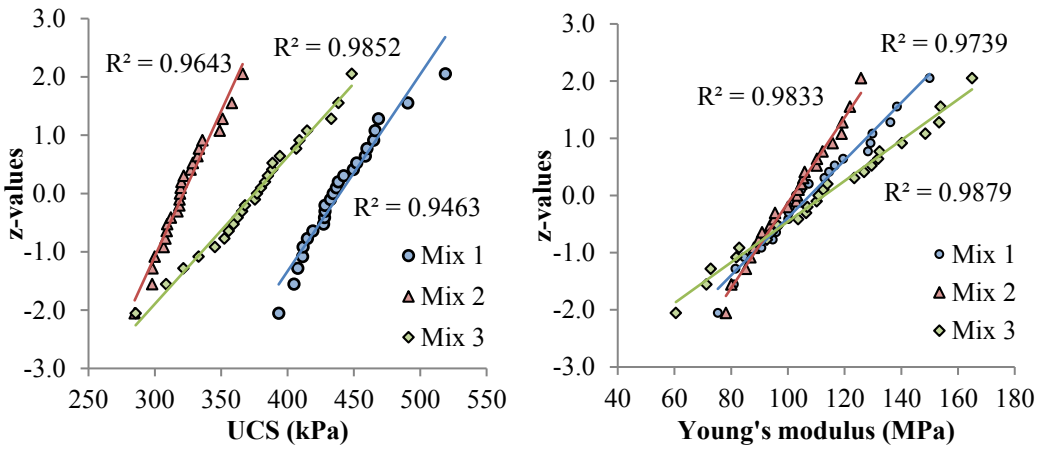

Fig. 4.8 Normal probability plots for **(a)** UCS **(b)** Young's modulus of CPB samples

Sample populations for soil properties in geotechnical engineering commonly show a long tail of values to the right of the distribution (i.e., they are right-skewed) (Wang et al. 2015). However, the mechanical properties (i.e., UCS and Young's modulus) of CPB are almost normally distributed as per the standard probability plots (Figure 4.7).

The sample data will not plot exactly on a straight line, even though the underlying population is exactly normal (Montgomery and Runger 2010). Some judgment and experience are required to evaluate the plot. Generally, if the sample size is $n < 30$, there can be significant deviation from linearity in normal plots. Therefore, in these cases only a very severe departure from linearity should be interpreted as a strong indication of non-

normality. As *n* increases, the linear pattern will tend to become stronger, and the normal probability plot will be easier to interpret and more reliable as an indicator of the form of the distribution.

Figure 4.9 shows the PDF of mechanical properties for different CPB mix samples. CPB Mix 2 shows the least spread of UCS and young's modulus, whereas Mix 3 shows the highest spread of mechanical properties. As the area under the PDF plot is unity, mix showing high spread of mechanical properties exhibits low peak and vice versa. In addition, the mean and standard deviation of mechanical properties for each mix were highly varied mainly because of the solid content changes in corresponding mix.

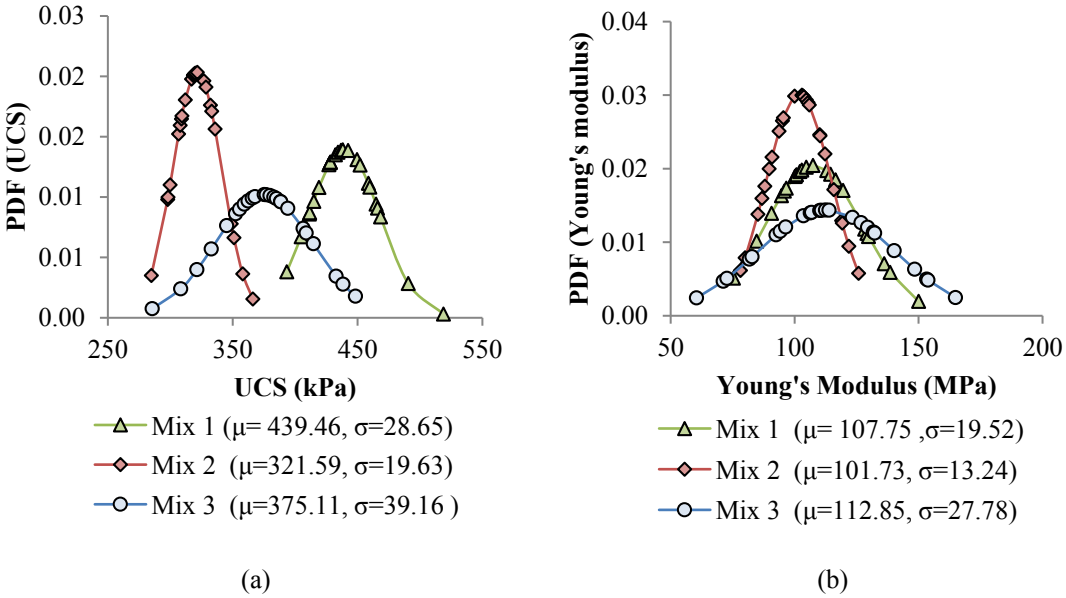

Fig. 4.9 Probability density function (PDF) of mechanical properties of CPBs **(a)** UCS **(b)** Young's modulus

4.6 Summary

George Fisher Mine tailings and General Purpose Cement with water from three different sources in the mine were used to cast the cemented paste backfill (CPB) specimens for UCS experiments in this study. In an attempt to suggest an effective curing method, five different methods were studied. In all of them, samples were cast, cured in different ways and the mechanical properties, the moisture content and degree of saturation were

computed at 7, 28 and 56 days. It was suggested that the method-1 is the simplest of all five methods, which also gave steady gain in UCS and Young's modulus, while the saturation remaining close to 100% with only a slight drop in the moisture content during the curing period. In this method, the UCS specimen with the plastic mould and the bottom cap is placed at the bottom of a bucket with 2 cm water and the lid was covered to ensure humid environment. It is suggested that this method be practiced for curing UCS specimens.

Separately, 25 identical samples were cast and tested to study the variabilities of mechanical properties generally derived from the laboratory tests. In this study, the variability of mechanical properties of CPBs and the consistency of sample casting, curing, and testing methods were validated with relatively small coefficient of variation for UCS and Young's modulus of less than 10% and 25%, respectively. In addition, the calculated dry densities and mechanical properties of CPB mixes show a negative linear relationship (i.e., when one increases the other decreases) with the measured existing (i.e., final) moisture contents of correspondent CPB mixes. The normal probability plots shows that the measured mechanical properties of CPB samples are normally distributed. Finally, the variability of mechanical properties can be used in numerical modelling to optimize design values of CPBs for the mining industry.

5 Effect of Different Types of Binders on Strength and Stiffness

5.1 Introduction

In cemented paste backfill, increasing the binder dosage will increase the strength, but at a cost. The optimum dosage with regards to cost depends on the solid content and the strength gain required. For a certain solid content, the optimum binder type and dosage are generally determined through a well-planned mix design testing program, as recommended by Niroshan et al. (2015), where a series of CPB mixes are prepared and the samples are tested for strength after 7, 14, 28, and 56 days of curing.

This chapter discusses the laboratory tests carried out to understand how the strength and stiffness of CPB develop over time. This was accomplished by conducting uniaxial compressive strength (UCS) testing on CPB samples cured to different times. In addition, this chapter then suggests typical values for the E/UCS ratios of CPB, which have not been reported in the literature. E/UCS is a useful parameter that is used in soils and rocks (Sivakugan et al. 2013). Knowing E/UCS will enable realistic estimates of Young's modulus based on the UCS. Furthermore, two simple analytical models are proposed to estimate the UCS at any time, based on the UCS at 14 days (UCS_{14}). Finally, the inter-relationship among solid content, binder content and UCS is critically assessed. The relative contributions to the UCS from solid content increase and the binder content increase are quantified.

This chapter is published as Niroshan, N., Sivakugan, N., and Veenstra, R. L. (2017). "Laboratory Study on Strength Development in Cemented Paste Backfills." *Journal of Materials in Civil Engineering*, *ASCE*, 29 (7), 04017027, doi: 10.1061/(ASCE)MT.1943-5533.0001848.

5.2 Laboratory Experimental Program

The tailings used in this study were received from George Fisher Mine (GFM) located in North Queensland, Australia. CPB typically contains at least 15% of grains finer than 20 μm to sustain water in the soil matrix (Sivakugan et al. 2006; Sivakugan et al. 2015). The particle size distribution of the tested tailing was determined using sieve analysis in accordance with ASTM C6913 (ASTM 2009) and laser analysis (Malvern Mastersizer 3000 Hydro EV). Figure 5.1a shows the grain size distribution of the mine tailings, where approximately 28% (by mass) of particles were less than 20 μm in size. A scanning electron micrograph (SEM) of the dry tailings is shown in Figure 5.1b. Based on this SEM image, shapes of most grains are angular and sub-angular while some are sub-rounded.

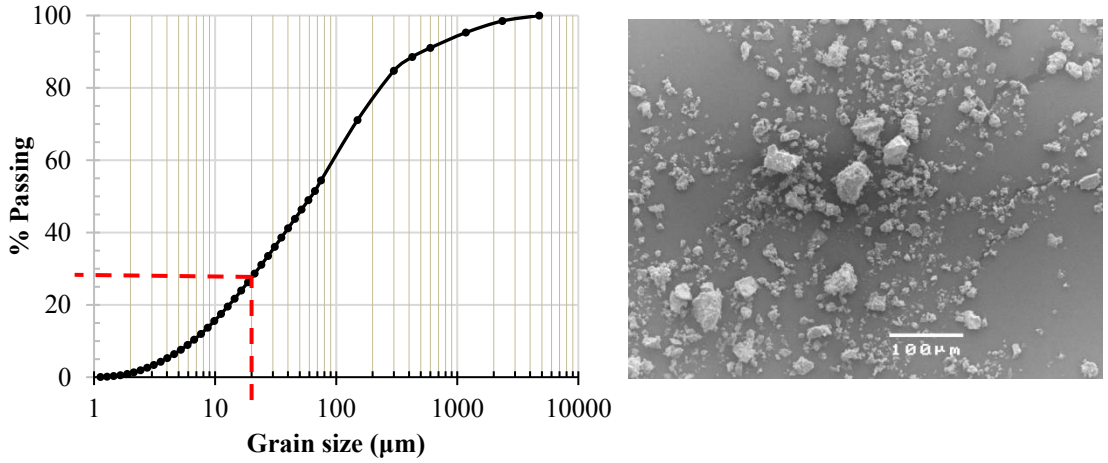

Fig. 5.1 Test results of the tailings: **(a)** Grain size distribution; **(b)** Scanning electron micrograph

Physical properties of tailings are shown in Table 5.1. The in situ water content of tailings varies between 8% and 13% and the specific gravity is between 2.87 and 2.91. In the Unified Soil Classification System, the CPB studied herein will be classified as clayey silt or silty clay, containing 54% fines smaller than 75 μm and 46% sand.

Table 5.1 Physical properties of the CPB mine tailings

Physical Properties	Ranges
In-situ water content (%)	8.0 - 13.0
Bulk density (kg/m^3)	1,900 - 2,100
Specific gravity	2.87 - 2.91

The grain shape, mineralogical and chemical properties play an important role in the performance of paste backfill. A semi-quantitative XRF analysis was performed to provide an indication of the chemical concentration of different elements in the mine tailing. Major element concentrations based on weight percentage are shown in Table 5.2.

Table 5.2 Chemical concentration of different compound in the tested tailings

Elements	Concentration (%)
Oxygen	54.30
Silicon	15.90
Calcium	10.00
Iron	7.27
Magnesium	4.14
Sulphur	3.29
Aluminium	2.30
Potassium	1.37

In the experimental program, two different binders were used: (a) 100% General Purpose Cement (GPC), which correspond to type I in ASTM C150 (ASTM 2007) and (b) blended cement (BC), consisting of 60% Granulated Blast Furnace Slag (GBFS) and 40% GPC. The chemical composition (in wt.%) and physical properties of the GPC, BC and GBFS are shown in Table 5.3, which satisfied the limitation specified in ASTM C989 (ASTM 2014) and ACI 233R-03 report (ACI Committee 233 2003). Moreover, the slag used in this study could be classified as grade 120 as the 28 days' activity index of slag was 110. The activity index (i.e., relative strength) is the average compressive strength of the slag-

reference cement cubes, divided by the average compressive strength of the reference cement cubes, multiplied by 100. On the other hand, the fineness or specific surface area of slag is slightly better than GPC cement (Table 5.3), which would lead to increase the rate of reaction in the early ages of BC mixes.

Table 5.3 Chemical composition and properties of the binders

Constituents / Property	**GPC**	**BC (60% Slag + 40% GPC)**	**Slag**
CaO (%)	63.9	49.6	41.3
SiO_2 (%)	19.2	29.0	35.2
Al_2O_3 (%)	5.0	10.4	14.5
Fe_2O_3 (%)	3.2	1.4	0.3
SO_3 (%)	2.4	2.3	1.09
MgO (%)	1.1	4.2	5.0
Na_2O (%)	0.4	0.4	0.21
Total Chloride (%)	0.019	<0.01	0.001
Fineness Index (m^2/kg)	375	415	430
Residue @ 45μm sieve (%)	5.2		2.0
Specific gravity	3.16	3.04	2.88
Relative strength - 28 days (%)	-	-	110

Ten different mixes were prepared, four using GPC and six using the BC. Eight specimens, 50 mm in diameter and 100 mm in length, were cast from each mix, to carry out uniaxial compression tests in duplicate samples for testing after 7, 14, 28 and 56 days of curing. The details of the ten mixes, including the binder type and percentages are summarised in Table 5.4.

Table 5.4 Mix design used for the lab experiments

Mix Reference	Binder	Binder content	Curing Time	Tests per mix	No. of Samples
Mix - 1	100% GPC	2.00%	7,14,28, 56 days	2	8
Mix - 2	100% GPC	3.00%	7,14,28, 56 days	2	8
Mix - 3	100% GPC	4.00%	7,14,28, 56 days	2	8
Mix - 4	100% GPC	6.00%	7,14,28, 56 days	2	8
Mix - 5	60% Slag, 40% GPC	2.00%	7,14,28, 56 days	2	8
Mix - 6	60% Slag, 40% GPC	3.00%	7,14,28, 56 days	2	8
Mix - 7	60% Slag, 40% GPC	3.50%	7,14,28, 56 days	2	8
Mix - 8	60% Slag, 40% GPC	4.00%	7,14,28, 56 days	2	8
Mix - 9	60% Slag, 40% GPC	4.50%	7,14,28, 56 days	2	8
Mix - 10	60% Slag, 40% GPC	6.00%	7,14,28, 56 days	2	8

The binder content, solid content and water content are defined as follows:

$$\text{Binder content (\%)} = \frac{\text{Mass of binder}}{\text{Mass of (dry tailings + binder)}} \times 100 \quad \textbf{(5.1)}$$

$$\text{Solid content (\%)} = \frac{\text{Mass of (dry tailings + binder)}}{\text{Mass of (dry tailings + binder + water)}} \times 100 \quad \textbf{(5.2)}$$

$$\text{Water content (\%)} = \frac{\text{Mass of water}}{\text{Mass of (dry tailings + binder)}} \times 100 \quad \textbf{(5.3)}$$

5.3 Slump Tests

The mine's typical solid content gives a slump of approximately 260 mm, corresponding to yield stress of 150-200 Pa. This correlation between yield stress and slump is based on the authors' own data for the same mine tailings. In order to determine which solid content generated a 260 mm slump, slump tests were carried out for 3-5 different solid

contents. Each slump test (Figures 5.2a & 5.2b) was carried out according to the ASTM C 143 standard (ASTM 2010). When these results were plotted, the solid content that gave 260 mm slump was determined. An example of this slump analysis is shown in Figure 5.2c, where, for Mix – 4, it was determined that 74% solid content gave a 260 mm slump.

(a) (b)

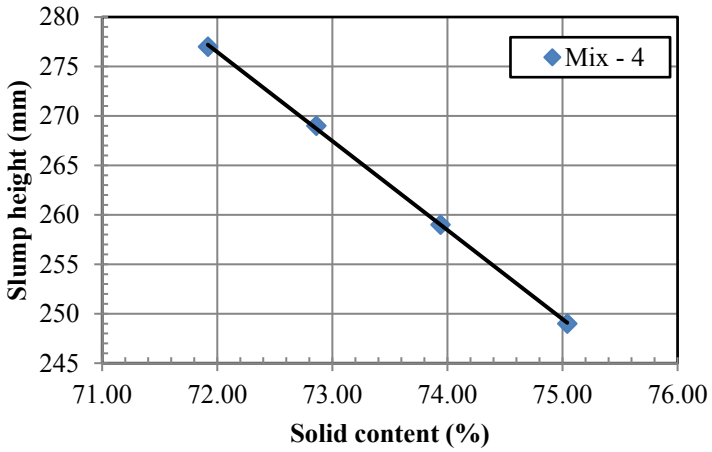

(c)

Fig. 5.2 Slump test of Paste fill: **(a)** Before; **(b)** After and; **(c)** Variation of slump height with solid content for Mix – 4

This exercise was repeated for all 10 mixes. The results are summarised in Table 5.5, where the solid content required for 260 mm slump lies in the range of 73-76%, irrespective of the binder type and dosage. It is an important observation that the slump or yield stress of the slurry depended on the binder dosage and the solid content.

However, it is important to note that the values could significantly vary depending on the mineralogical characteristics of specific mine tailings and binders. In addition, the water content and the water to binder ratio (W/B) are shown for each mix in Table 5.5.

Table 5.5 Solid content corresponding to 260 mm slump

Mix Reference	Binder type	Binder content (%)	Solid content (%)	Water content (%)	W/B
Mix - 1	100% GPC	2.0	75.0	33.3	16.7
Mix - 2	100% GPC	3.0	73.0	37.0	12.3
Mix - 3	100% GPC	4.0	74.0	35.1	8.8
Mix - 4	100% GPC	6.0	74.0	35.1	5.9
Mix - 5	60% Slag, 40% GPC	2.0	76.0	31.6	15.8
Mix - 6	60% Slag, 40% GPC	3.0	75.0	33.3	11.1
Mix - 7	60% Slag, 40% GPC	3.5	74.0	35.1	10.0
Mix - 8	60% Slag, 40% GPC	4.0	74.5	34.2	8.6
Mix - 9	60% Slag, 40% GPC	4.5	75.5	32.5	7.2
Mix - 10	60% Slag, 40% GPC	6.0	74.5	34.2	5.7

5.4 Uniaxial Compressive Strength (UCS) Tests

The specimens were prepared within plastic tubes, with nominal dimensions of 50 mm internal diameter and 120 mm length, split longitudinally to facilitate specimen removal. The CPB mix was cast within the tubes using the vibrating table to remove air pockets within the specimens. Prepared samples were cured in buckets with about 2 cm of water at the bottom, and fully covered by a lid to maintain constant humidity. On the day of testing, samples were removed from the bucket and trimmed to prepare UCS samples 50 mm diameter and 100 mm long. Figure 5.3 shows the specimens in the plastic tube where they were cast, and the ones before and after trimming.

(a) (b) (c)

Fig. 5.3 Sample preparation for UCS test: **(a)** Samples within the mould; **(b)** Before trimming; **(c)** After trimming

UCS tests on the CPB samples were performed over a curing period up to 56 days according to ASTM D7012 (ASTM 2014). Since the uniaxial compressive strength tests are undrained tests, the cross sectional areas increase during loading. The new cross sectional area (A) at axial strain of ε is computed as

$$A = A_0 \times \frac{1}{1-\varepsilon} \tag{5.4}$$

where, A_0 is the initial cross sectional area of the specimen computed from the specimen diameter, assuming circular cross section, and ε is the axial strain. Equation 5.4, which assumes no volume changes in the specimen, was used to compute the axial normal stress during testing. Figure 5.4 shows the experimental setup and sample stress - strain plot of the UCS test of a CPB sample in the laboratory.

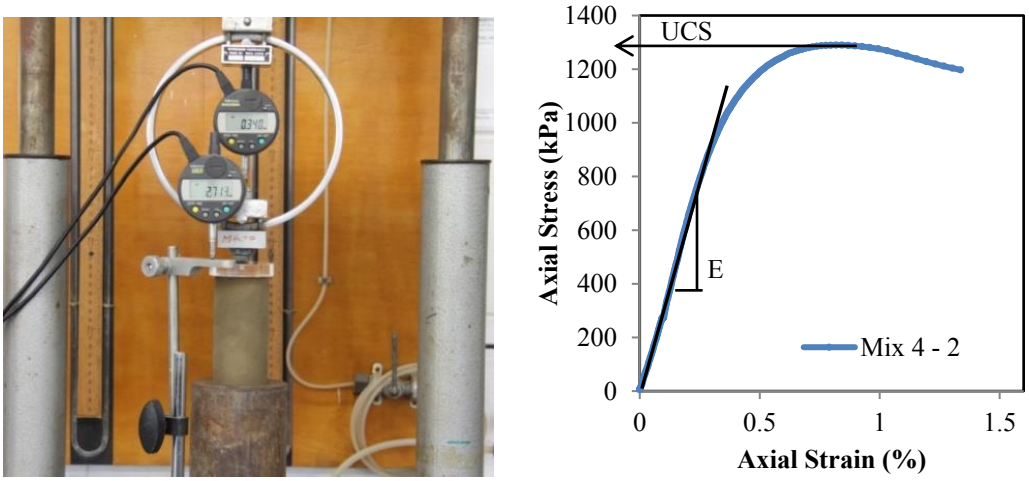

(a) (b)

Fig. 5.4 UCS Test: **(a)** Experimental setup; **(b)** Stress – Strain plot of a sample from Mix 4 (6% GPC) in 56 days curing

The UCS values after 7, 14, 28 and 56 days for the four GPC mixes and the six BC mixes are summarised in Figure 5a. For each of the 10 mixes, the strength increased with time as expected, with maximum values reached at 56 days. It is clear that the strength gains in the GPC mixes (1-4) are of the same order between successive durations. On the other hand, the BC mixes (5-10) showed steep increases in strength during the early days of curing, achieving more than 60% of the 56-day strength in 7 days, with little gain after 14 or 28 days. In addition, it can be seen that for the same dosage, BC mixes showed higher strength than the GPC mixes.

The Mix 1 (2% GPC) and Mix 5 (2% BC) samples had peak strengths of approximately 220 kPa and 35 kPa, respectively. In addition, Mix 5 (2% BC) samples showed little or no strength gain even after 56 days. These samples simply collapsed when removed from the plastic mould in the early curing period. Therefore, such small dosages (less than 3%) work better for GPC binders than BC binders. This is probably due to the low GPC presence (e.g., only 0.8% GPC in 2% dosage) within the blended cement mix.

Samples in Mix 2 (3% GPC) gained strength of about 75 kPa in the first 7 days and showed relatively steady strength increase, reaching 280 kPa after 56 days of curing time. However, samples in Mix 6 (3% BC) gained strength of about 320 kPa after 7 days, which is greater than the 56 days strength achieved by 3% dosage of GPC binder, and showed smaller increments over the subsequent curing periods reaching the maximum strength of about 485 kPa after 56 days. Due to the presence of grade 120 slag (finer than GPC) in BC, the extent of reactions would be higher in BC than GPC, especially in early ages (1-7 days). The samples in Mix 7 (3.5% BC) gained strength 400 kPa in 7 days curing time and reached 550 kPa after 56 days of curing. Although BC binder showed higher strength in 7 days than GPC binder, GPC binder mixes showed steady strength increment throughout the curing period than BC binder mixes.

Samples in Mix 3 (4% GPC) exhibited strengths of 255 kPa, 355 kPa, 485 kPa and 575 kPa in 7, 14, 28 and 56 days of curing, respectively, whereas samples in Mix 8 (4% BC) showed strengths of 690 kPa and 920 kPa in 7 days and 56 days of curing, respectively. Meanwhile, samples in Mix 9 (4.5% BC) showed strengths of 830 kPa after 7 days' cure and 1160 kPa after 56 days. Similarly, samples in Mix 4 (6% GPC) increased in strength from 630 kPa after 7 days to 1350 kPa after 56 days. However, Mix 10 (6% BC) samples showed strengths of 1180 kPa and 1690kPa after 14 and 56 days, respectively.

A comparison of the strength gain between Mix 4 (6% GPC) and Mix 8 (4% BC) showed that the BC mix had higher initial strengths (after 7 and 14 days) but lower strengths at the later curing periods. This illustrates a lower amount of BC binder could be used to achieve higher initial strengths but may not be an appropriate choice if higher strengths are required at later curing ages.

The UCS and the Young's modulus were calculated for all the samples as the maximum axial stress and the slope of the linear segment (initial tangent method) of the stress-strain plot (as shown in figure 5.4b) with the values summarised in Figure 5.5b.

(a)

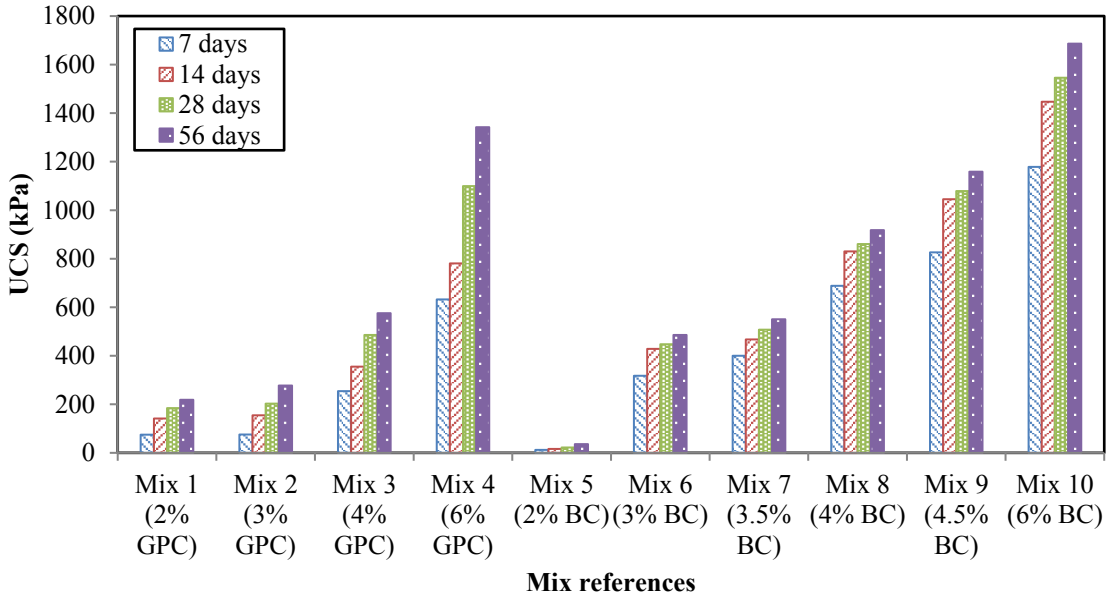

(b)

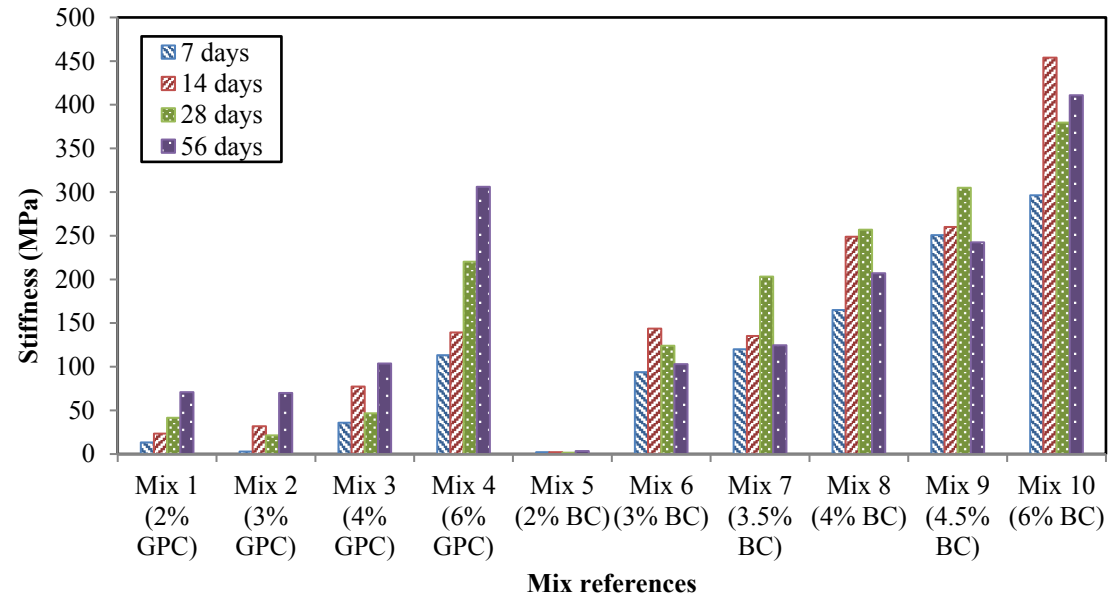

Fig. 5.5 UCS test results of the 10 mixes at 7, 14, 28 and 56 days: **(a)** UCS; **(b)** Young's modulus

All of the Mix 5 (2% BC) samples exhibited very low stiffness when compared to the Mix 1 (2% GPC) samples, which had values up to 70 MPa at 56 days. All GPC binder mixes showed a general stiffness increase with curing time, with all mixes reaching their maximum stiffness after 56 days. However, the stiffness of the BC binder mixes showed

an initial stiffness increase (over 14 to 28 days) and then stiffness reduction with increased curing age. It is seen that the stiffness of the Mix 6 (3% BC) samples were much higher than the Mix 3 (4% GPC) samples most of the time. Moreover, Mix 8 (4% BC) samples had higher stiffness until 28 days than Mix 4 (6% GPC) samples. Mix 5 (2% BC) samples gained little or no stiffness over the entire curing period. Overall, BC binder mixes showed relatively higher young's modulus than GPC binder mixes.

In conclusion, as expected, CPB increases in strength with an increase in the cement content as well as curing time. An additional phenomenon, which was quite interesting finding, is the development of significant early strength (1-7 days) of BC binder mixes. The fineness, chemical properties, and especially the grade 120 slag contained in BC mixes, enhance early strength dramatically, more so than GPC mixes. Furthermore, a 4.5% BC binder can replace a 6% GPC binder without affecting the strength and stiffness. In addition, a 6% BC binder could replace a 6% GPC binder in order to achieve 1.85 time higher short term strength and 1.25 time higher long term strength.

5.5 Further Interpretation of Laboratory Test Data

The UCS values normalised to their respective 28 days and 56 days UCS with curing time up to 28 and 56 days, respectively are shown in Figure 5.6. These results clearly show that the BC mixes have much higher early strength gain than the GPC mixes, which exhibit a much more gradual strength gain. A comparison of 14 days strength shows that the GPC and BC mixes gained about 60% and 87% of their 56 days strengths respectively.

a)

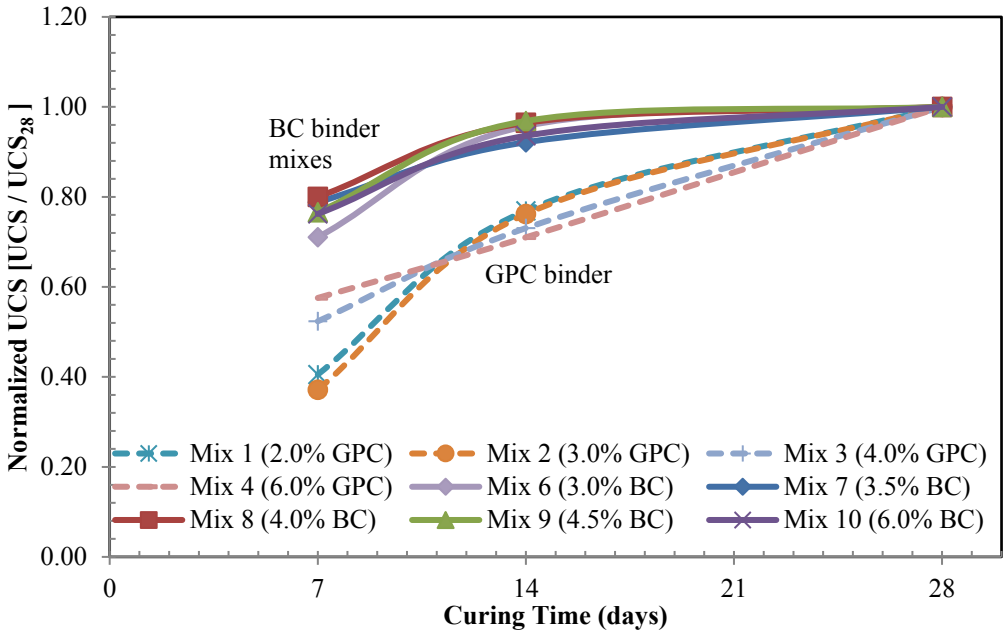

b)

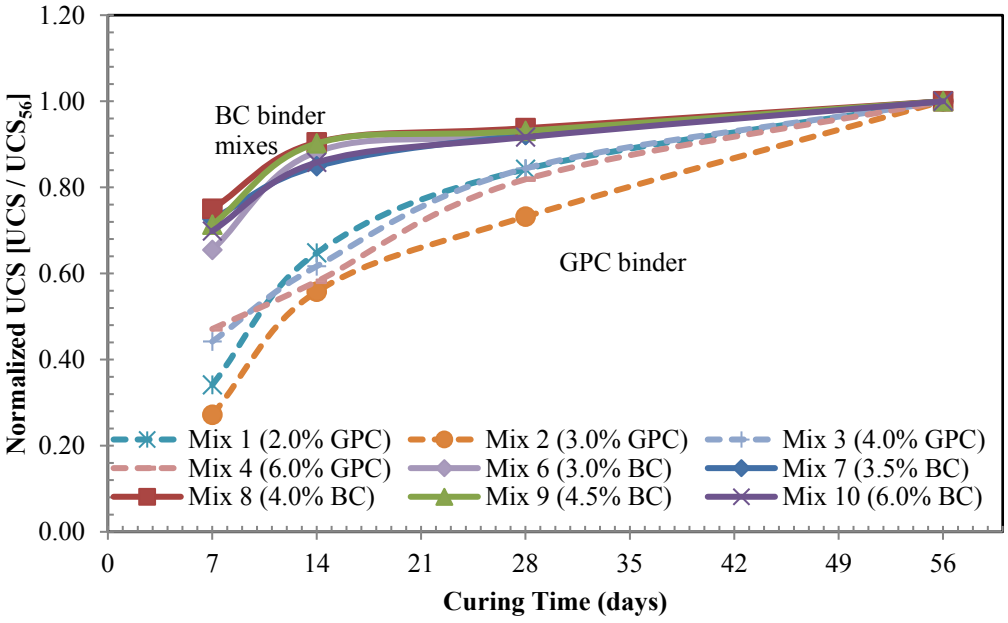

Fig. 5.6 Normalized UCS versus curing time: **(a)** 28 days; **(b)** 56 days

The ratio of E to UCS (E/UCS) is a unique material property for most civil engineering materials including steel, concrete, soils, and rocks (Table 5.6). These ratios can be used

as the basis for estimating a material's Young's modulus when the UCS of the material is known.

Table 5.6 E/UCS values of some civil engineering materials

Material	E / UCS	Reference
Soft clay	20 - 120	Lambe and Whitman (1969)
Firm to stiff clay	40 - 150	
Very stiff / hard clay	13 - 35	
Rock	300 - 500	Waltham (2009)
Steel	400 - 600	Hibbeler (2016) and Beer et al. (2012)
Wood	300 - 500	
Concrete	750 - 1000	
Cemented paste backfill (CPB)	***150 - 350***	**Niroshan et al. 2017**

Figure 5.7 shows E versus UCS variation for the 10 mixes, considering all curing times (i.e., 80 points in total). As can be seen, the ratio lies in the range of 150-350, with an average value of 250. The BC binder mixes appeared to give a slightly higher ratio than the GPC binder mixes.

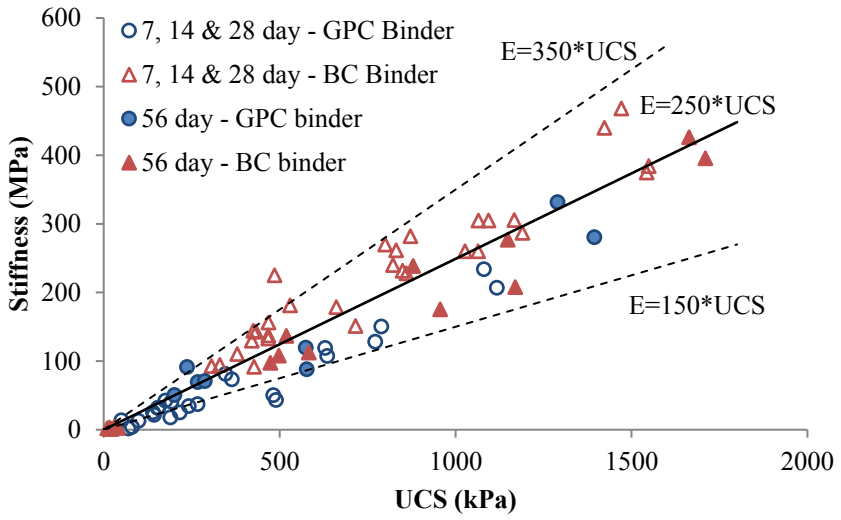

Fig. 5.7 E/UCS of CPB

5.6 Developing a UCS Model for Cemented Paste Backfill

Figure 5.8 shows the variation of UCS for all 10 mixes over 56 days. It is clear the strength continued to increase up to 56 days, with UCS reaching an asymptotic value in the long term. This section aims to propose a UCS strength model, using its corresponding 14 days' strength, to estimate the UCS values throughout the curing time.

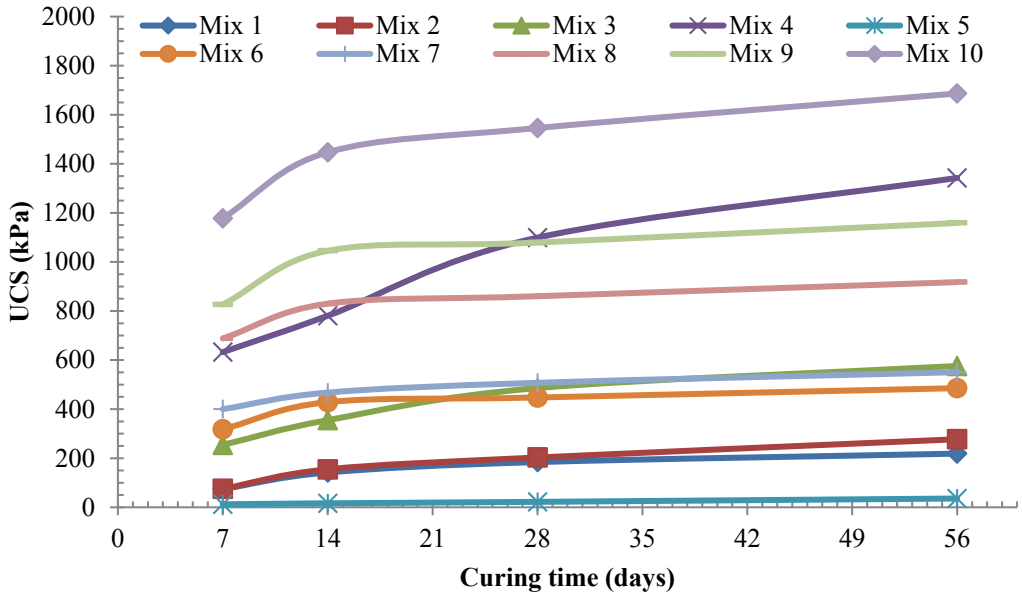

Fig. 5.8 UCS changes with curing time of paste fill mixes

It is proposed that a strength prediction model for CPB can be based on a similar equations used by the ACI committee (ACI Committee 209 1971) for predicting strength increase in concrete. This was done by tweaking Equations 5.5 and 5.6 to fit the data provided by determining appropriate values for the constants *a*, b, c and d.

$$UCS_t = \frac{t}{a + b.t} \tag{5.5}$$

$$UCS_t = c \times \left(1 - e^{-d.t}\right) \tag{5.6}$$

where,

- UCS_t is UCS gain in t days of curing,

- 't' is the curing time in days, and
- *a*, *b*, *c* and *d* are coefficients.

Here, the *a* and *d* coefficients are related to the rate of increase in UCS and the *b* and *c* coefficients are related to the asymptotic value of the UCS. The long-term or asymptotic UCS value is given by

$$UCS_{\infty} = \frac{1}{b} = c \approx UCS_{56}$$

The test results for the 10 mixes showed that after 14 days of curing, the UCS was about 56% and 83% of the UCS_{56}, for GPC and BC mixes, respectively. Therefore, for GPC mixes,

$$UCS_{\infty} = \frac{1}{b} = c \approx UCS_{56} \approx 1.8UCS_{14} \quad \textbf{(5.7)}$$

and for BC mixes,

$$UCS_{\infty} = \frac{1}{b} = c \approx UCS_{56} \approx 1.2UCS_{14} \quad \textbf{(5.8)}$$

Therefore, the coefficients *b* and *c* can be determined from UCS_{14}.

The *a* and *d* coefficients were determined through a curve-fitting exercise. For each of the nine data sets, Equations 5.5 and 5.6 were fit separately using Excel's nonlinear regression function. This was done using the *b* and *c* constants, determined from Equations 5.7 and 5.8. These values were plotted against corresponding UCS_{14} in order to find a relationship for coefficients *a* and *d* in terms of UCS_{14}, as shown in Figure 5.9 for the GPC and BC binders.

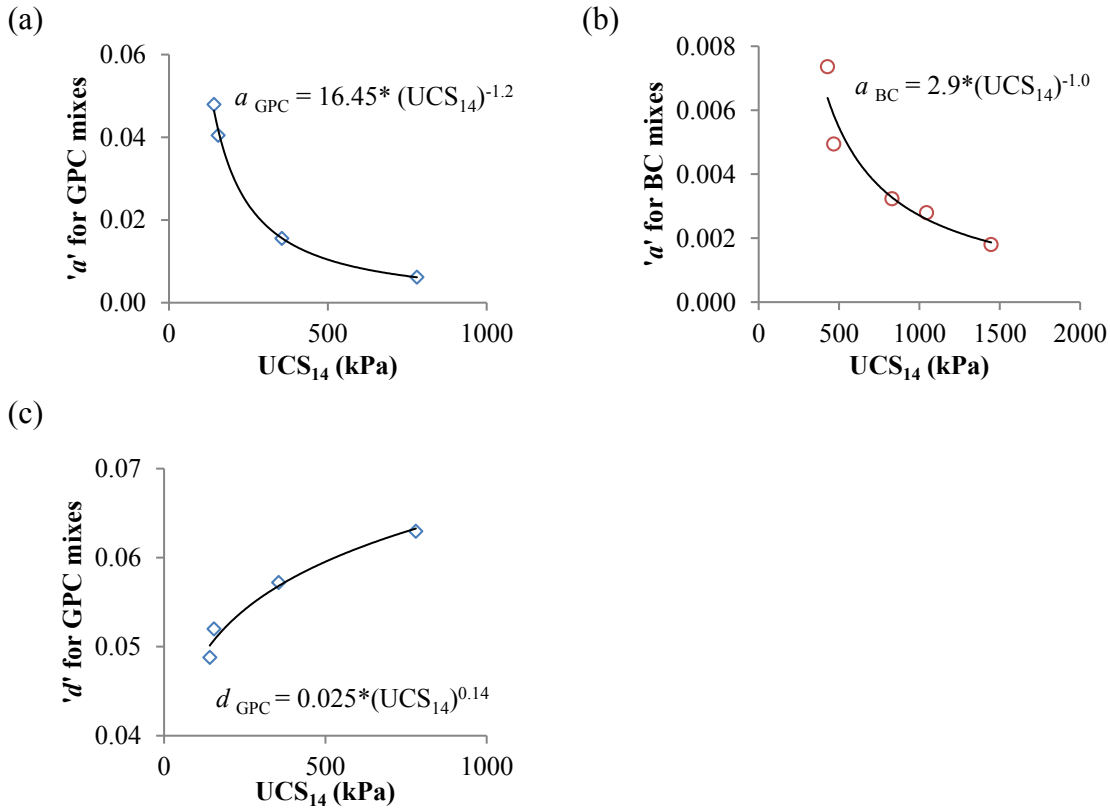

Fig. 5.9 Determination of coefficients: **(a)** *a* for the four GPC binder mixes, **(b)** *a* for the five BC binder mixes, **(c)** *d* for the four GPC binder mixes

For the BC mixes, *d* was approximately a constant, equal to 0.14.

The coefficients *a*, *b*, *c* and *d* for the GPC and BC mixes, in terms of UCS_{14}, are summarised in Table 5.7.

Table 5.7 Summary of coefficients for UCS model

Coefficient	GPC Binder	BC Binder
a	16.45 x $UCS_{14}^{-1.2}$	2.9 x $UCS_{14}^{-1.0}$
b	1 / (1.8 x UCS_{14})	1 / (1.2 x UCS_{14})
c	1.8 x UCS_{14}	1.2 x UCS_{14}
d	0.025 x $UCS_{14}^{0.14}$	0.14

5.6.1 UCS Strength Model Validation

Using the coefficients summarised in Table 7, the UCS values determined from Eqs. 5.5 and 5.6 were plotted with curing time for GPC and BC mixes in Figures 5.10a and 5.10b, respectively. The measured 7, 14, 28 and 56 days' UCS values were also plotted.

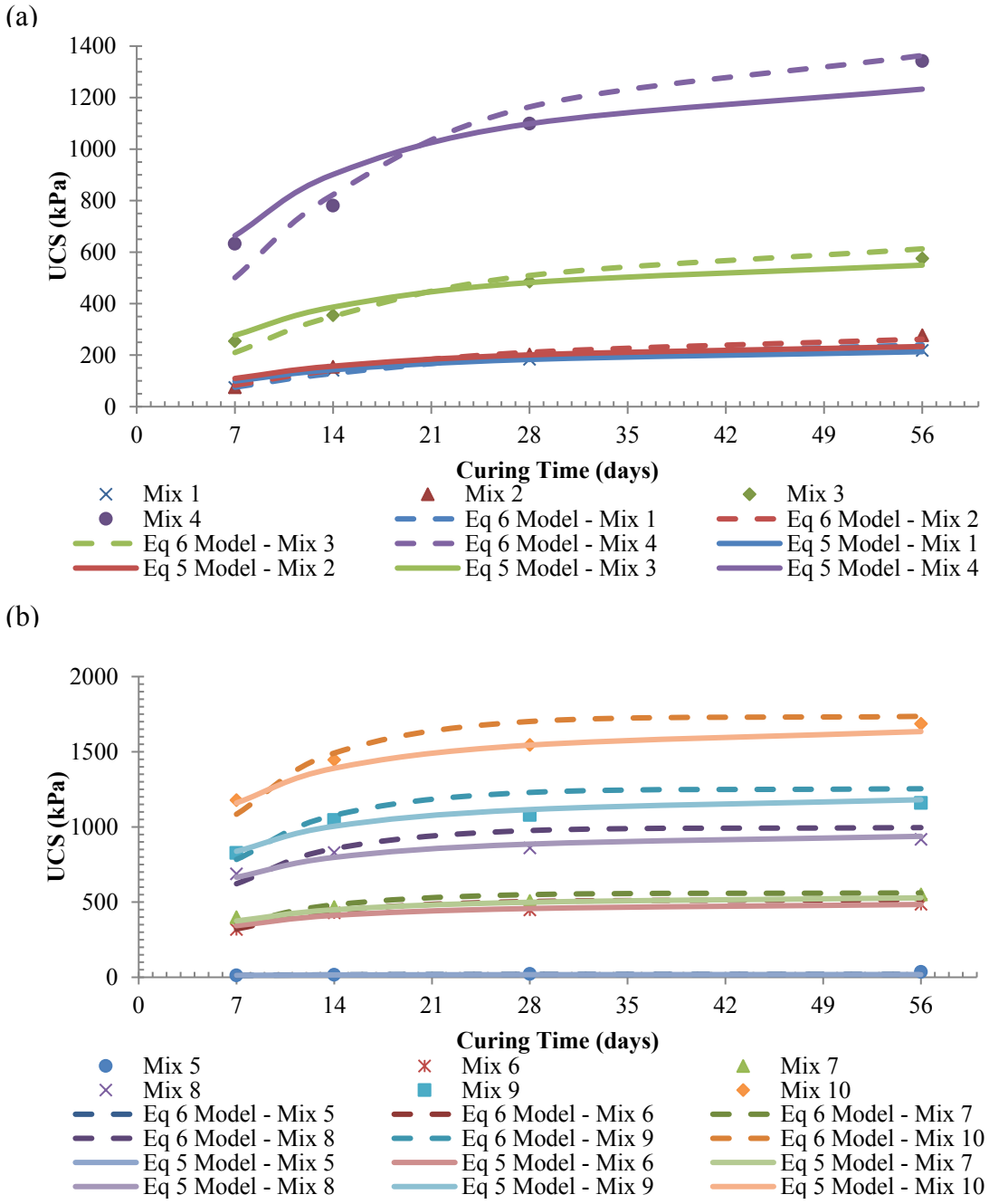

Fig. 5.10 Estimated UCS using each strength model varies over curing period for: **(a)** GPC binder mixes; **(b)** BC binder mixes

The calculated values of the coefficient of determination (R^2) based on Equation 5.9 are summarised in Table 5.8.

Table 5.8 Coefficient of determination values

Mix	Dosage and Binder	R^2	
		Eq. 5.5	**Eq. 5.6**
Mix 1	2.0% GPC	0.9212	***0.9585***
Mix 2	3.0% GPC	0.7374	***0.9720***
Mix 3	4.0% GPC	0.9501	***0.9602***
Mix 4	6.0% GPC	0.8697	***0.9477***
Mix 6	3.0% BC	***0.9174***	0.8620
Mix 7	3.5% BC	***0.9060***	0.8602
Mix 8	4.0% BC	***0.9421***	0.7937
Mix 9	4.5% BC	***0.9494***	0.8169
Mix 10	6.0% BC	***0.9555***	0.8801

$$R^2 = 1 - \frac{SS_{res}}{SS_{tot}} \quad \textbf{(5.9)}$$

where,

- SS_{res} = The sum of squares of residuals
- SS_{tot} = The total sum of squares

The UCS values estimated using Equations 5.5 and 5.6 for both GPC and BC mixes of the 9 mixes for 7, 14, 28, and 56 days were plotted against the measured values in Figures 5.11a and 5.11b, respectively. Also shown in these figures are the 10% deviation lines. It is evident that the two proposed equations could be used to predict the UCS at any time, with an error less than 10% for most of the mixes.

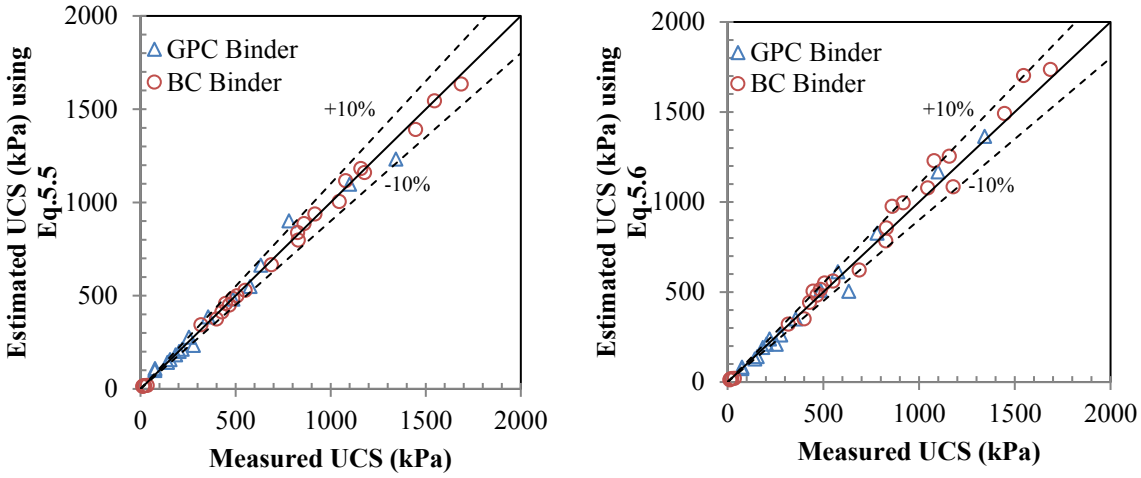

(a) (b)

Fig. 5.11 Measured UCS verses estimated UCS using model: **(a)** Eq. 5.5; **(b)** Eq. 5.6

These two strength models (Equations 5.5 and 5.6) are proposed to estimate the UCS values throughout curing time using its corresponding 14 days strength. While both equations fit the data reasonably well, the following conclusions can be made using table 5.8, Figure 5.11:

- For the GPC mixes, Equation 5.6 gives a slightly better fit, and
- For the BC mix, Equation 5.5 gives a slightly better fit.

5.7 Effects of solid content and binder dosage in UCS strength gain in CPB

In a typical CPB operation the solid content is usually kept constant and binder content is varied in order to reach the design long term strength. However, as mentioned previously, increasing the solid content can increase the strength of the mix, provided that the operation's reticulation system can handle the increased solid content.

This section presents the results of a laboratory program designed to determine the strength increase of CPB with increased solids content or binder content, and highlight the effectiveness of increasing the solid content or binder content of a specific mix. Since

BC binder is becoming increasingly popular in mining operations, this experimental program is limited to BC binder only.

Twenty different mixes, representing solid content in the range of 73-77% and binder content of 3.0-4.5%, were prepared, and UCS samples were cast in duplicate for determination of 28-day UCS (UCS_{28}) and 56-day UCS (UCS_{56}). Table 5.9 summarises the mix details and the UCS values. The UCS varied linearly with the solid content for all four binder contents. The equations of the lines of best fit were used as the basis for computing Δ_{UCS}, which is the increase in UCS for 1% increase of solid content or binder content, discussed herein.

Table 5.9 28 and 56 days UCS data for the BC binder samples

Sample No	Binder content (%) and Type	Solid content (%)	UCS_{28} (kPa)	UCS_{56} (kPa)
6-A	3.0 BC	76.14	801.46	735.70
6-B		75.04	697.91	708.70
6-C		74.80	703.56	668.61
6-D		74.40	674.00	627.69
6-E		73.78	651.12	611.73
7-A	3.5 BC	75.40	911.91	979.95
7-B		74.54	909.57	862.12
7-C		74.26	845.17	821.62
7-D		73.72	835.05	793.39
7-E		73.29	747.34	785.41
8-A	4.0 BC	76.58	1242.51	1462.32
8-B		75.70	1129.68	1326.08
8-C		75.20	1079.73	1264.65
8-D		74.58	1023.28	1184.31
8-E		73.94	924.09	1085.51
9-A	4.5 BC	76.05	1529.80	1850.79
9-B		75.47	1409.19	1672.70
9-C		75.24	1359.68	1598.56
9-D		75.07	1328.22	1542.10
9-E		74.20	1156.30	1394.81

Variations of UCS_{28} and UCS_{56} with % solids are shown in Figure 5.12.

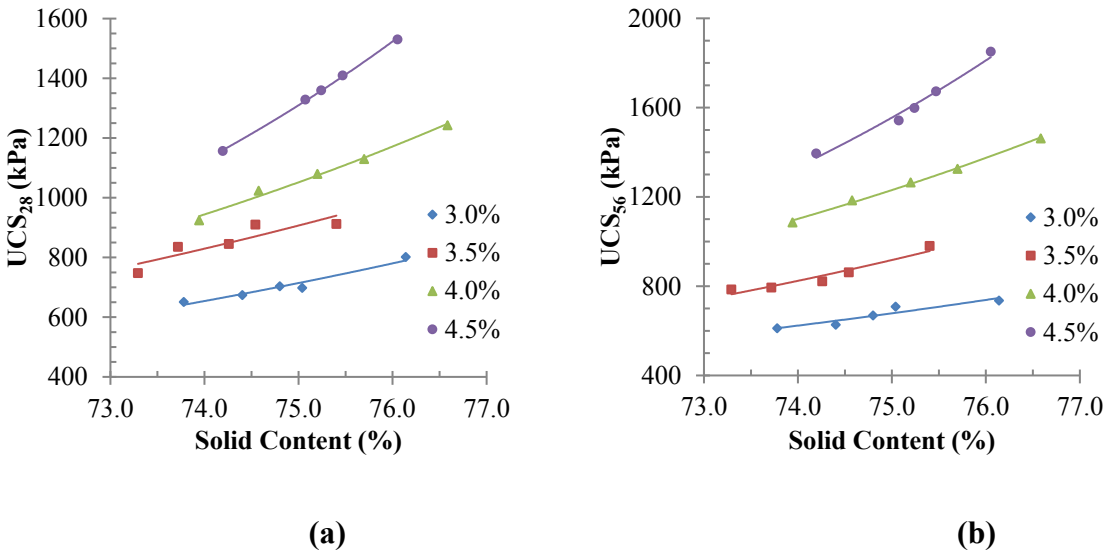

Fig. 5.12 UCS changes with solid content: **(a)** 28 days; **(b)** 56 days

Figure 5.13a shows the change in UCS change per 1% increase in solids content plotted against BC binder content. These results were calculated based on the experimental results shown in Table 5.9. It can be seen that Δ_{UCS} increases rapidly with the binder content, showing significantly higher values for Δ_{UCS} at higher binder content. In other words, increasing the solid content can increase the strength significantly when the binder content is high. The relationship between Δ_{UCS} and the binder content (%BC) is given by:

$$\Delta_{UCS,28} = 3.4\exp(0.9\times\%BC) \quad \textbf{(5.10a)}$$

$$\Delta_{UCS,56} = 2.7\exp(\%BC) \quad \textbf{(5.10b)}$$

Similarly, Δ_{UCS} per 1% increase in binder content is plotted against the solid content in Figure 5.13b. The relationship between Δ_{UCS} and the solid content (%SC) is given by:

$$\Delta_{UCS,28} = 90.56\times\%SC - 6402.9 \quad \textbf{(5.11a)}$$

$$\Delta_{UCS,56} = 122.23\times\%SC - 8574.4 \quad \textbf{(5.11b)}$$

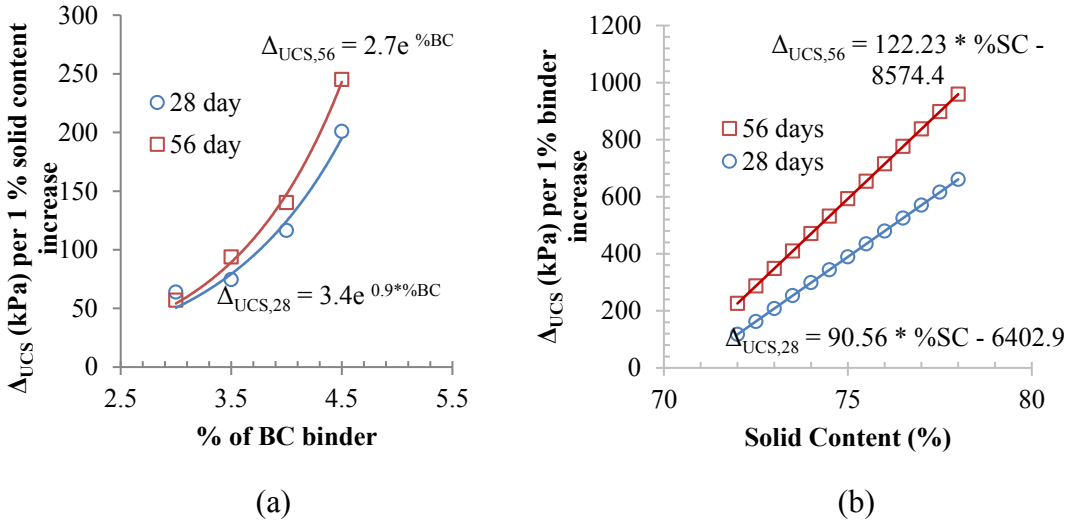

Fig. 5.13 UCS variation: **(a)** per unit solid content increment changes over binder increases; **(b)** per unit BC binder content increment changes over solid content increases

From Figure 5.13 or Equations 5.10 and 5.11, it is possible to estimate the increase in UCS based on the UCS value of a single mix. For example, a mix of 75% solid content and 3.5% binder content will show an increase in UCS_{28} of 79 kPa for an additional 1% increase in the solid content and 389 kPa for an additional 1% increase in binder content.

While the coefficients of the equations and the values reported herein are specific to the mine tailings used in the tests, the trends should be similar for other CPB tailings. Other mines may carry out a similar test program to establish their own parameters as these studies are often mine-specific.

5.7.1 Example

The UCS_{28} of a CBP mix with 73.78% solid content and 3.0% binder is 651.1 kPa (Data from Table 5.9). What would be the UCS_{28} of a CBP mix with 75.07% solid content and 4.5% binder?

5.7.2 Solution

The calculations are carried out in two steps as shown below.

The UCS_{28} of a CBP mix with 73.78% SC and 3.0% BC binder is 651.1 kPa (Given)

Step 1: UCS_{28} of a CBP mix with 73.78% SC and 4.5% BC binder is 1069.0 kPa [651.1 + (4.5-3.0) × (*278.6*)]

Step 2: UCS_{28} of a CBP mix with 75.07% SC and 4.5% BC binder is 1320.7 kPa [1069.0 + (75.07-73.78) × (*195.2*)]

Here, the values 278.6 kPa for 1% binder content increase and 195.2 kPa for 1% solid content increase were determined from Equations 5.11a and 5.10a, respectively. The measured value of UCS_{28} (from Table 5.9) is 1328.2 kPa, which is in close agreement with the predicted value.

Equations 5.10 and 5.11 can be comfortably used in simulating UCS data for solid content in the range of 73-77% and BC binder content in the range of 3.0-4.5%, for the specific mine tailings studied herein.

5.8 Summary

Cemented paste backfills (CPB) are one of the major types of backfills used in underground mining. They are placed in the form of thickened slurry that settles and gains strength both through consolidation and binder hydration. General Portland Cement (GPC) is the most common type of binder used in most mining operations. However, most mines are trying to reduce their GPC usage by partially replacing it with other cementitious material, such as fly ash or slag. The optimum mix design for a CPB stream involved determining what solid and binder contents generally give the ideal strength and rheology characteristics.

The first part of the chapter summarised the results from a laboratory test program to study the effect of binder content. This study used two different binders (GPC and BC)

to mix 10 different recipes. These mixes were then used to cast UCS cylinders for testing at 7, 14, 28 and 56 days. This study found that the mixes with BC binder gained approximately 83% of their long-term strength within 14 days whereas the GPC binder mixes only gained about 56% of their long-term strength. BC mixes with 2% binder had very low strength at all curing times, whereas the GPC mixes with 2% binder showed significant strength and stiffness.

All of the mixes (both GPC and BC) had very little gain in strength after 28 days, reaching the maximum value at 56 days. All the GPC binder mixes had higher stiffness at 56 days, whereas BC binder mixes had higher stiffness at 28 days. Furthermore, the BC binder mixes, except for the 2% mix, showed significantly higher strength and stiffness than the GPC mixes of the same dosage. In addition, the test data showed that for CPB, E/UCS was in the range of 150-350, with an average value of 250.

In the second part of this chapter, two simple expressions were proposed to express UCS in terms of UCS_{14} and curing time. It was shown that the expressions predict the UCS values with an error margin of less than 10%. Therefore, UCS can be estimated using the proposed two simple analytical equations and young's modulus can be estimated using proposed E/UCS value. Finally, UCS-solid content-binder dosage relationship was simulated for binder content in the range of 3.0-4.5 (%wt.), and solid content of 73-77 (%wt.), to assess their relative influences. Due to the popularity of BC binder, this exercise was limited to BC mixes only. In this section, two sets of simple equations were proposed to predict the UCS values at 28 and 56 days of curing by calculating the increase in UCS based on the UCS value of a single mix. Although these studies are often mine-specific, the trends remain quite similar and are valuable to all mines using cemented paste fills for backfilling.

6 Relevance of SEM to long-term Mechanical Properties of CPB

6.1 Introduction

Although research has been conducted on the development of new cemented paste backfill (CPB) around the world, little is known about the paste backfills made from the tailing from an Australian mine with environmental-friendly binders, such as fly ash-blended cement and geopolymers. In addition, the mechanical properties of CPB depend on not only the characteristics of tailings, binders and mixing water but also the chemical and microstructure properties of the materials used. Furthermore, the mechanical properties of CPBs may have a strong relationship with its microstructure.

Therefore, the purpose of this chapter was to study the long-term mechanical properties of the paste backfills made from the tailing from a mine in North Queensland, Australia, mixed with binders consisting of geopolymers, fly ash-blended cement and cement. In particular, the chapter focuses on the microstructure-property relations for these paste backfills consisting of tailings (94%) and binders (6%) in comparison with binder free tailings as control sample. The uniaxial compressive strength (UCS) test was performed on cylindrical paste backfill samples cured for 112 days. Scanning electron microscopy (SEM) was applied to analyse all microstructures of the paste backfill and their fractured samples. Finally, the microstructure-property relations for the paste backfills were established, which provides insights into the optimized design of stronger CPBs for the mining industry.

This chapter is published as "Niroshan, N., Yin, L., Sivakugan, N., and Veenstra, R. L. (2018)."Relevance of SEM to Long-Term Mechanical Properties of Cemented Paste Backfill." *Geotechnical and Geological Engineering*, doi: 10.1007/s10706-018-0455-5".

6.2 Materials

6.2.1 Tailing Material

The tailing used in this study was provided by George Fisher Mine in Mt Isa, North Queensland, Australia. Figure 6.1 shows the grain size distribution of the tailings and binders used in this study. The tailing particle size distribution shown in Figure 6.1 (dashed line) was determined using sieve and laser analysis following the ASTM C6913 (ASTM 2009). The tailing consisted of approximately 45 wt% of fine particles with sizes of less than 20 µm, which is significantly higher than 15%, the commonly accepted rule for operational activities at most mine sites (Sivakugan et al. 2006; Sivakugan et al. 2015).

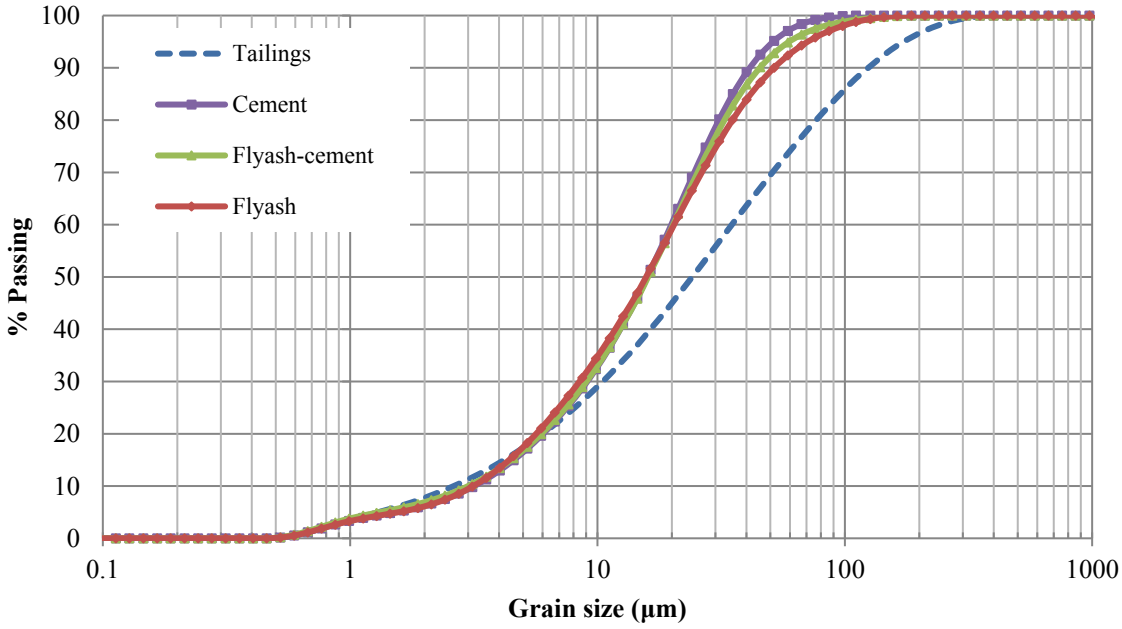

Fig. 6.1 Grain size distribution of tailing and binders

Table 6.1 shows the main physical properties of the tailing with the specific gravity (G_s) of 2.90, the particle size distributions (D_{10} to D_{60}) in the range of 2.98–35.2 µm, the uniformity coefficient (C_u) of 11.8, and the curvature coefficient (C_c) of 1.05. The tailing can be categorised as medium type tailing depending on the amount of 20 µm fractions in the total tailing (Fall et al. 2005; Landriault 2001). The initial moisture contents of the

received tailing were in the range of 9–12 %. In addition, liquid and plastic limits of the received tailing are 22% and 16%, respectively. These Atterberg limits clearly indicate that there is little (Plastic Index = 6%) or no plasticity in received mine tailing.

Table 6.1 Grain size distribution parameters of the tailing

	G_s	D_{10} (µm)	D_{30} (µm)	D_{50} (µm)	D_{60} (µm)	C_u	C_c
Tailings	2.90	2.98	10.5	27.4	35.2	11.81	1.05

A small amount of the tailing particles were gold-coated and examined using SEM (Jeol JSM5410LV, Tokyo, Japan). Figure 6.2 shows a series of SEM micrographs of the tailing microstructure and morphology at the different magnifications. Figure 6.2a shows the tailing particles with different sizes and shapes, with all grains in the figure well below 300 µm in size. This is also evident in Figure 6.1 which suggests that 86% of the grains are smaller than 100 µm. Figure 6.2b demonstrates some coarse and fine irregular shaped particles with a large particle of approximately 100 µm or larger and small particles with sizes of approximately 10 µm or less. Figure 6.2c shows that some ultrafine particles attached on a coarse particle surface. Figure 6.2d shows the ultrafine particles with complex shapes.

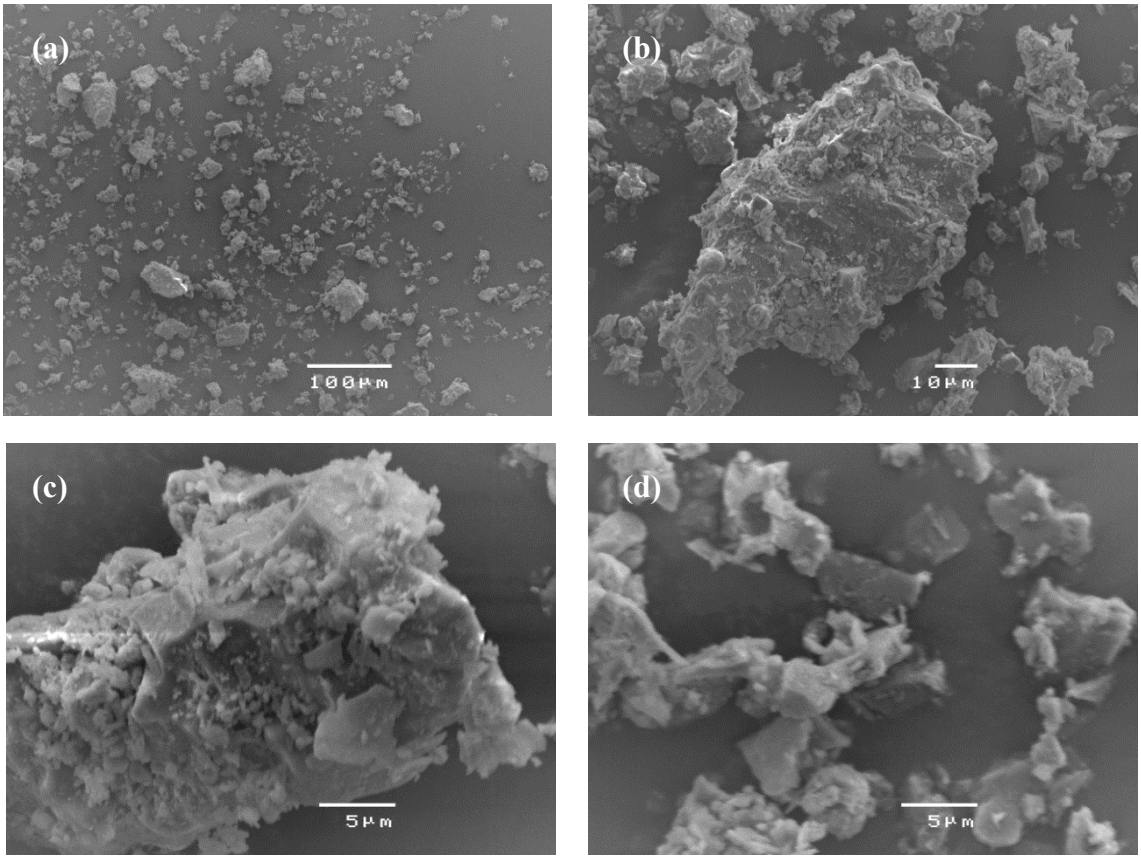

Fig. 6.2 SEM micrographs of the tailing at different magnifications

6.2.2 Binders

Three binders were selected for studying the mix design to optimize the mechanical properties of the paste backfill samples, including general purpose cement (Cement) or type I Portland cement according to ASTM C150 (ASTM 2007), fly ash-blended cement (fly ash-cement) containing 25% fly ash and 75% Cement, and fly ash-based geopolymer (Geopolymer), which contains no cement (i.e., cement free binder). Cement, fly ash-cement and pure fly ash were provided by Cement Australia. The fly ash-based geopolymer was prepared in laboratory by mixing pure fly ash with sodium hydroxide (NaOH) solution. In this study, 15M NaOH solution was used as an activator during geopolymer preparation. Since the reaction between NaOH and water is exothermic, utmost care was taken during the preparation of the solution. The solution shall be prepared at least 6 hours prior to the mixing

Chemical compositions and properties of the three binders are shown in Table 6.2. Cement contained 63.9% CaO, 19.2% SiO_2, 5% Al_2O_3, 3.2% Fe_2O_3, 2.4% SO_3, 1.1% MgO and 0.4% Na_2O. Fly ash-cement consisted of 48% CaO, 27.1% SiO_2, 10.6% Al_2O_3, 6.6% Fe_2O_3, 1.8% SO_3, 1% MgO and 0.7% Na_2O. The fly ash had a significantly high content of SiO_2 (48.1%), Al_2O_3 (26.7%) and Fe_2O_3 (15.2%) and a low amount of SO_3 (0.1%) and CaO (3.5%). The relative strength (i.e., activity index) of the fly ash was 119%. It is defined as the ratio between the average compressive strength of the fly ash-cement cubes and the average compressive strength of the general purpose (i.e., Ordinary Portland) cement cubes. It is sufficiently high for its qualification as the supplementary binding material according to ASTM C618 (ASTM 2015).

Table 6.2 Chemical compositions and properties of the binders

Constituents / Property	Cement	Fly ash-cement	Fly ash
CaO (%)	63.9	48.0	3.5
SiO_2 (%)	19.2	27.1	48.1
Al_2O_3 (%)	5	10.6	26.7
Fe_2O_3 (%)	3.2	6.6	15.2
SO_3 (%)	2.4	1.8	0.1
MgO (%)	1.1	1.0	1.4
Na_2O (%)	0.4	0.7	0.6
Total Chloride (%)	0.019	0.012	<0.001
Fineness Index (m^2/kg)	375	-	-
Residue @ 45μm sieve (%)	5.2	5.7	16
Specific gravity	3.16	-	2.39
Relative strength - 28 days (%)	-	-	119

A small amount of each binder was gold-coated and examined using the SEM. Figures 6.3 and 6.4 show the series of SEM micrographs of cement and fly ash-cement microstructures and morphologies at the different magnifications, respectively. Overall

particle size distributions of cement and fly ash-cement binders are shown in Figures 6.3a and 6.4a, respectively, and quantitatively in Figure 6.1. In the cement microstructure, there were elongated and angular shaped crystals (Figures 6.3c and 6.3d).

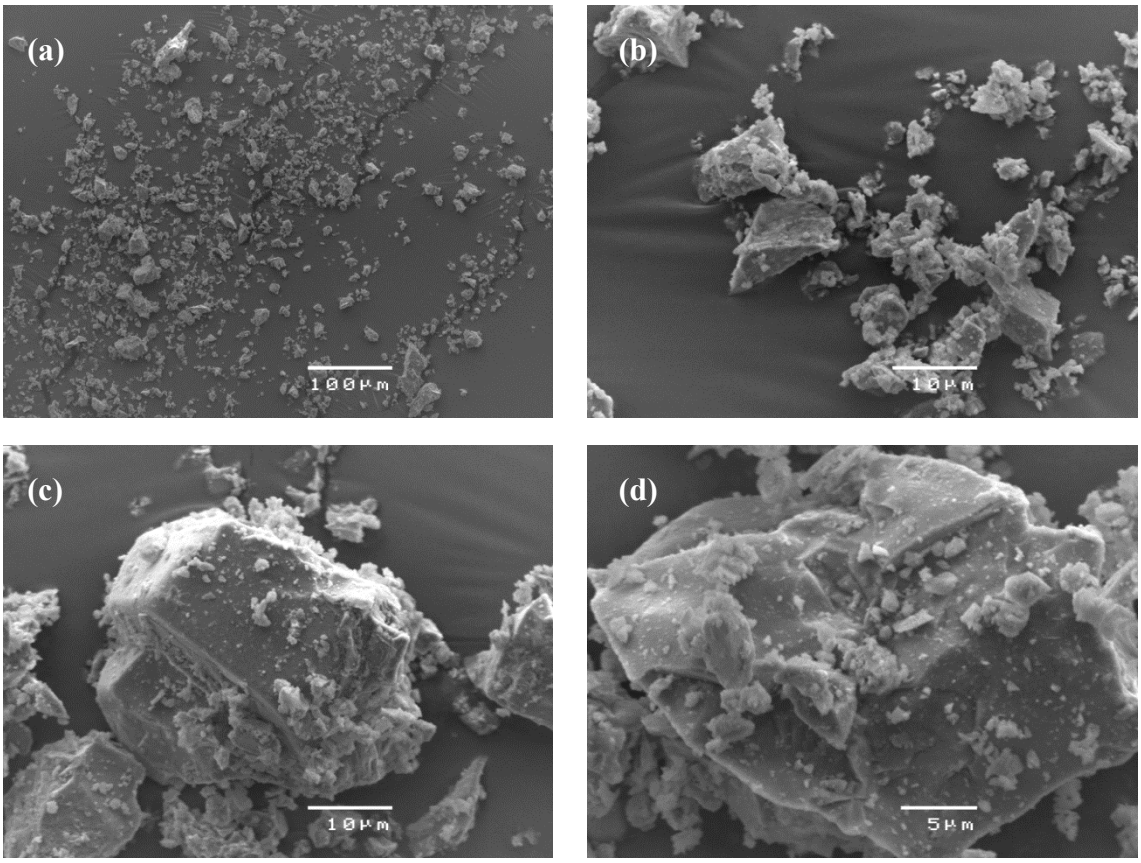

Fig. 6.3 SEM micrographs of general purpose cement (cement) at different magnifications

In the fly ash-cement microstructure, the needle-shaped particles are observed in Figure 6.4c. The spherical particles shown in Figures 6.4b, 6.4c and 6.4d are from fly ash, which was mixed with cement to produce the fly ash-cement binder.

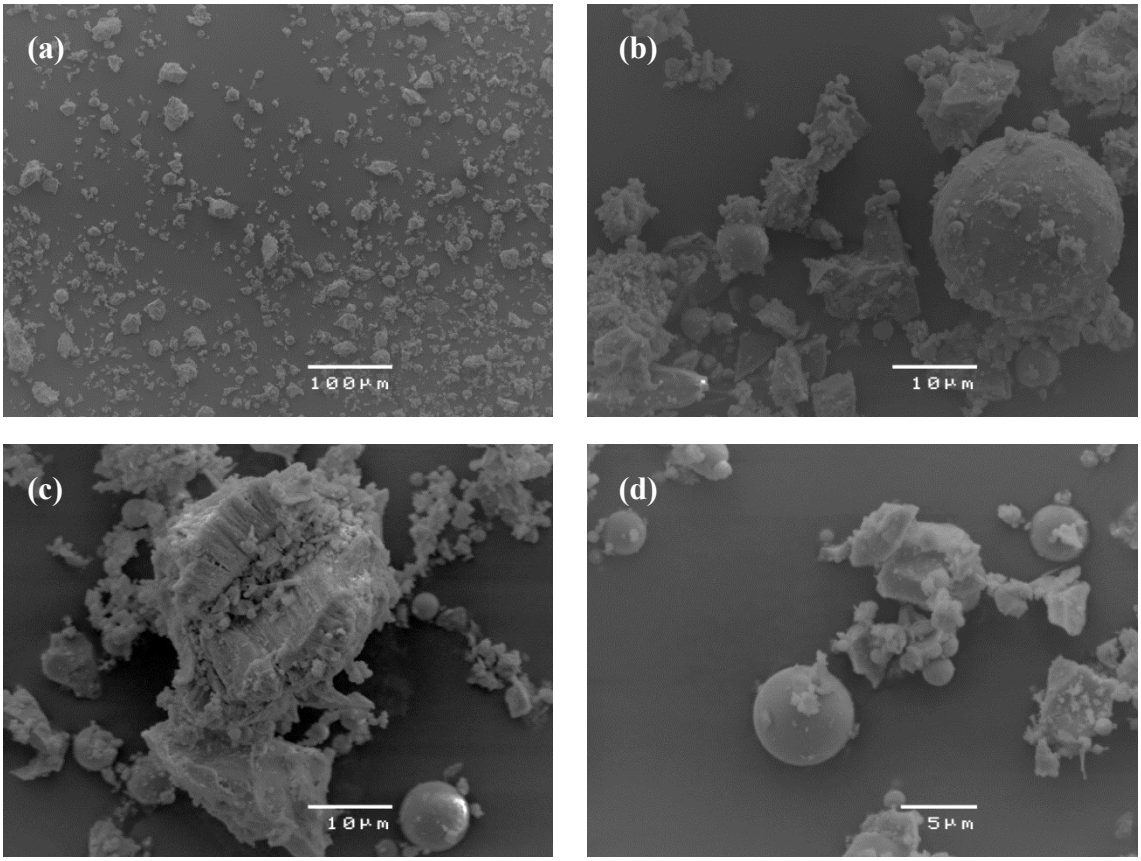

Fig. 6.4 SEM micrographs of fly ash-blended cement (fly ash-cement) at different magnifications

Geopolymer was synthesised from fly ash by using the alkaline-activated solution. The ratio between the alkaline activator and fly ash was found to have a great influence on the compressive strength of the geopolymer. The optimum ratio of 0.4 in the alkaline liquid was found to effectively activate the fly ash for the highest geopolymerization rate (Al Bakri et al. (2012). Using this ratio, 15-mol concentration sodium hydroxide (NaOH) solution was used as an activator in the geopolymer preparation.

Figure 6.5 shows the series of SEM micrographs of pure fly ash (i.e., before adding NaOH) microstructures and morphologies at the different magnifications. Figures 6.5a and 6.5b show the overall fly ash particle sizes and morphologies. At the higher magnifications in Figures 6.5c and 6.5d, some spherical shapes of fly ash with different

particle sizes smaller than 20 μm are observed. It is also observed that very fine powders were attached on the spherical particles.

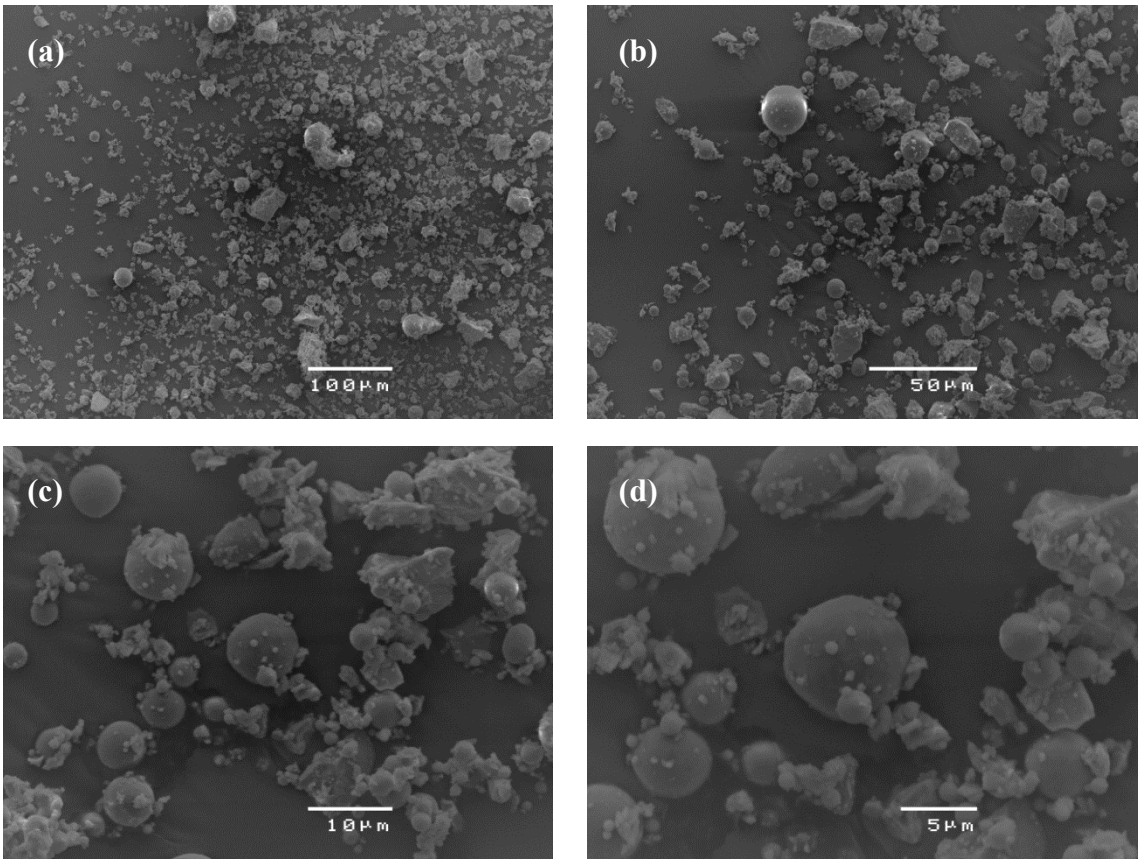

Fig. 6.5 SEM micrographs of fly ash at different magnifications

6.3 Fabrication of CPB Samples

Tap water (pH ≈ 7) was used to prepare the paste backfill mixes. All initial tailing moisture contents and particle densities were determined in accordance with ASTM D2216 (ASTM 2010) and ASTM D854 (ASTM 2014). Table 6.3 summarises the binder types and contents, curing time and the sample numbers for the four different paste backfill mixes.

Table 6.3 Mix proportions in CPB samples

Mix No.	Binder type	% Binder in solids	% Tailing in solids	% solids in CPB mix	Curing Time	No. of Samples
Mix 1	No binder	0.0%	100.0%	74.0%	112 days	3
Mix 2	Geopolymer	6.0%	94.0%			3
Mix 3	Fly ash-cement	6.0%				3
Mix 4	Cement	6.0%				3

Each mix contained solids and water in 74:26 proportion, which corresponded to the average standard conical slump height of 260 mm (ASTM 2015). Mix 1 contained 100% tailings (no binder) with 74% solids and 26% tap water as controls. All other mix samples were prepared by mixing 94% tailing and one of the three different binders at 6%. The three binders were geopolymer in Mix 2, fly ash-cement (75% Cement and 25% fly ash) in Mix 3 and cement in Mix 4, with tap water used in all mixes. The water to binder ratio (by weight) of each mix, except Mix 1 (no binder), was 5.85. All mixing processes were assisted by an electrical drill rotating at 2500 rpm, which was attached to a paint stirrer to stir the mix for 3 min to 5 min, for making a homogeneous paste. All mixes were cast within plastic tubes of inner dimensions of 50 mm diameter and 125 mm height on a vibrating table to reduce air voids within the samples. Then, all cast samples were placed in a closed bucket with approximately 3-cm height of water in the bottom to maintain a constant humidity and cured for 112 days at room temperature. All cured samples were extruded from the plastic tubes and cut to obtain 100 mm in length to meet the general requirement of the height to diameter ratio (2:1) for the UCS testing. The top and bottom surfaces were manually smoothened using knife edges to ensure their flatness and *parallelity*. The initial mass of each sample was measured for calculation of its bulk density.

6.4 Mechanical Properties and Statistical Analysis

UCS tests were performed on all paste backfill mix samples to measure their mechanical properties, including the UCS, failure strains and Young's moduli. Each sample was placed in a uniaxial compression strength test apparatus and loaded at a strain rate of 0.8 mm/min. Figure 6.6 shows a mix sample in the UCS test setup in accordance with ASTM 7012 (ASTM 2014). After the UCS testing, specimens from all tested samples were placed in an oven at the temperature of 100 °C for 24 hours to determine their moisture contents.

Fig. 6.6 A cemented paste backfill (CPB) sample in UCS test setup

A two-way factorial analysis of variance (ANOVA) and a paired t-test without replica at 5% significance were applied for statistical analyses. ANOVA was used to analyse the difference among all CPB mixes with respect to their strength, failure strains, and Young's moduli. The paired t-test test was used for two selected mixes to compare the influence of the binders on their mechanical properties.

Figure 6.7 shows the photographs of the compression-tested paste backfill mix samples. Figure 6.7a shows the immediate collapse of Mix 1 once extruded from the plastic tube. The sample was unable to stand alone unsupported. Figures 6.7b–6.7d reveal shear failures for Mixes 2–4, respectively. This result indicates that Mix 1 did not have any load bearing capacity due to the absence of any binders in comparison with other mixes.

(a)

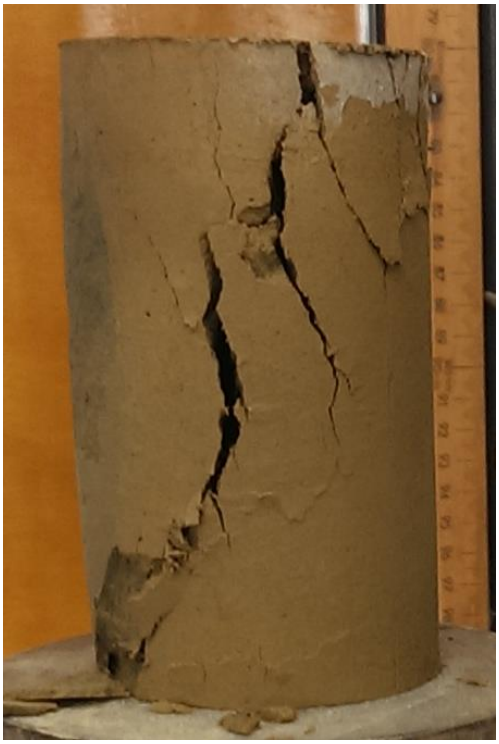

(b)

(c)

(d)

Fig. 6.7 Photographs showing **(a)** the immediate collapse in a Mix 1 sample once extruded from the plastic tube, and the compression-tested **(b)** Mix 2, **(c)** Mix 3 and **(d)** Mix 4 samples

Figure 6.8 shows the axial compression stress–strain plots on triplicate samples for Mixes 2–4. It shows good repeatability but very different mechanical behaviour of each mix. Figure 6.8a reveals that the strain hardening and then necking occurred before fracture in Mix 2. Figure 6.8b demonstrates the strain softening with possible plastic deformation prior to fracture in Mix 3. Figure 6.8c displays straining softening prior to fracture in Mix 4.

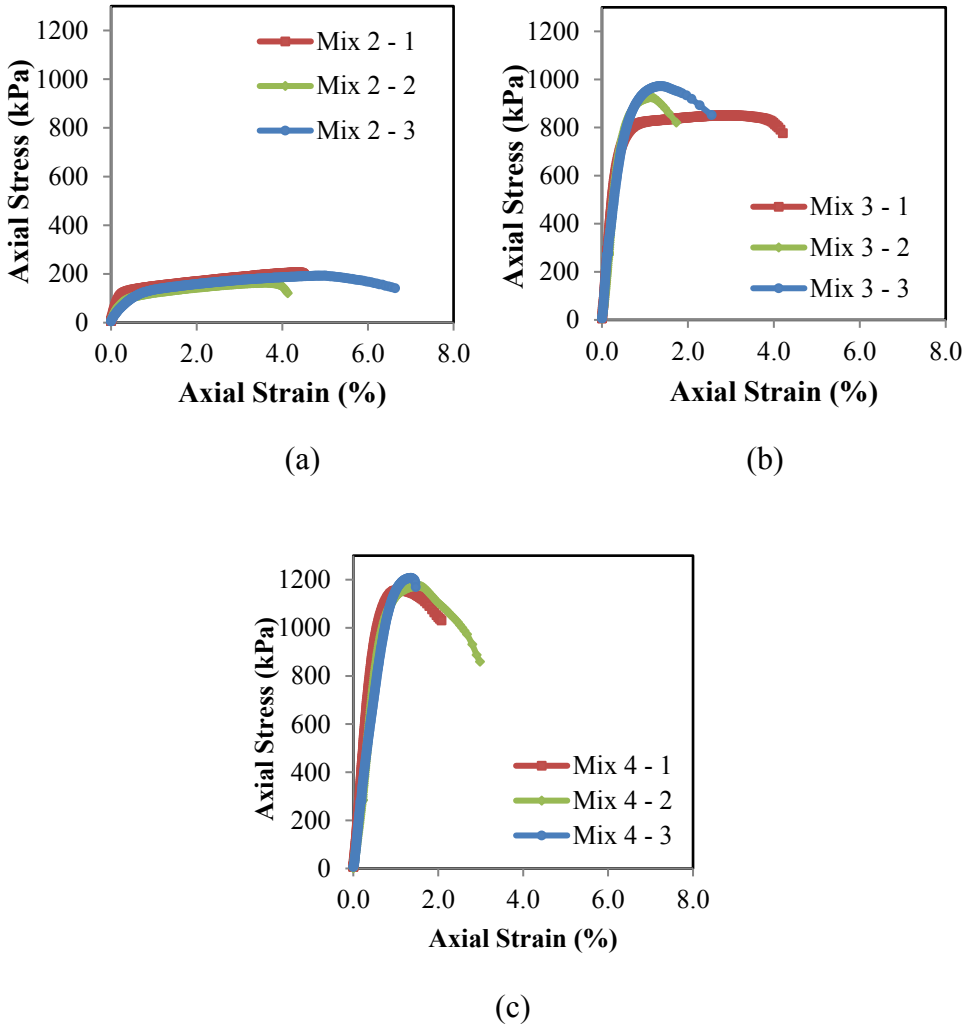

Fig. 6.8 Axial stress - axial strain plots of CPB mixes: **(a)** Mix 2, **(b)** Mix 3, and **(c)** Mix 4

Table 6.4 summarises all measured UCS values, failure strains and Young's moduli for all samples. Figure 6.9 displays the plots of these properties. Figure 6.9a shows the highest average USC of 1179 kPa for Mix 4, followed by Mix 3 with 916 kPa and then Mix 2 with 187 kPa. In Figure 6.9b, Mix 2, with intermediate average UCS value had the highest average failure strain of 4.29%, in comparison with the strain values of 1.80% and 1.31% for Mix 3 and Mix 4, respectively. Figure 6.9c demonstrates the highest average Young's modulus of 216.56 MPa for Mix 3, following by 199.47 MPa for Mix 4 and 33.77 MPa for Mix 2.

Table 6.4 Strength, failure strains and Young's moduli of CPB mixes after 112-day curing

Mix	Sample	Strength, UCS (kPa)	Failure Strain, ε_f (%)	Young's modulus, E (MPa)	Average values ± Std. deviation		
					Strength, UCS (kPa)	Failure Strain, ε_f (%)	Young's modulus, E (MPa)
Mix 1	Mix 1 - 1	0	0	0	0	0	0
	Mix 1 - 2	0	0	0			
	Mix 1 - 3	0	0	0			
Mix 2	Mix 2 - 1	205.98	4.30	49.90	187.70 ±21.88	4.29 ±0.72	33.77 ±15.09
	Mix 2 - 2	164.06	3.57	31.42			
	Mix 2 - 3	193.05	5.00	20.00			
Mix 3	Mix 3 - 1	850.26	2.92	221.78	916.12 ±62.78	1.80 ±0.98	216.56 ±7.01
	Mix 3 - 2	926.11	1.12	208.59			
	Mix 3 - 3	971.99	1.35	219.31			
Mix 4	Mix 4 - 1	1156.05	1.09	231.28	1179.17 ±26.37	1.31 ±0.21	199.47 ±28.12
	Mix 4 - 2	1174.36	1.50	189.18			
	Mix 4 - 3	1207.09	1.34	177.94			

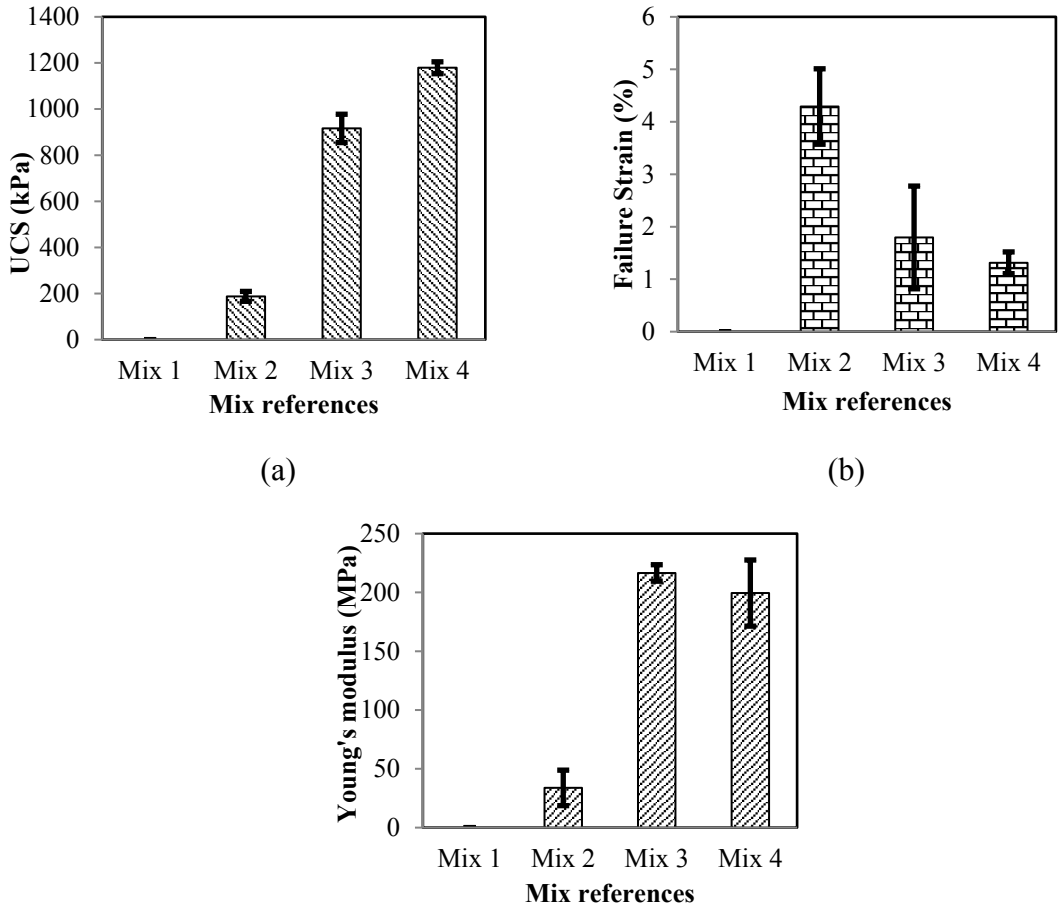

Fig. 6.9 (a) UCS versus mix samples, **(b)** failure strain versus mix samples, and **(c)** Young's modulus versus mix samples

Tables 6.5–6.7 summarise the ANOVA analyses of the mechanical properties of all mixes. They indicate that different binders in the four mixes significantly affected their UCS values ($p < 0.05$), failure strains ($p < 0.05$) and Young's moduli ($p < 0.05$), respectively. In comparison of the mechanical properties for Mix 3 (Fly ash-cement binder mixes) and Mix 4 (Cement binder mixes) using the t-test, Tables 6.8–6.10 reveal significant difference in their UCS values ($p < 0.05$), but insignificant differences in their failure strains ($p > 0.05$) and Young's moduli ($p > 0.05$), respectively. These respective *P* values are highlighted in bold relevant Tables 6.5-6.10.

Table 6.5 One-way analysis of variance (ANOVA) of the strength for all CPB mixes

Source of Variation	Sum of squares (*SS*)	Degrees of freedom (*df*)	Mean square (MS)	F-ratio (*F*)	*p-Value*	*F crit*
Between Groups	2885810.8	3	961936.946	783.808	**3.2482E-10**	4.066
Within Groups	9818.089	8	1227.261			
Total	2895628.9	11				

Table 6.6 One-way analysis of variance (ANOVA) of the failure strains for all CPB mixes

Source of Variation	Sum of squares (*SS*)	Degrees of freedom (*df*)	Mean square (MS)	F-ratio (*F*)	*p-Value*	*F crit*
Between Groups	29.012	3	9.671	25.556	**0.000189**	4.066
Within Groups	3.027	8	0.378			
Total	32.039	11				

Table 6.7 One-way analysis of variance (ANOVA) of the Young's moduli for all CPB mixes

Source of Variation	Sum of squares (*SS*)	Degrees of freedom (*df*)	Mean square (MS)	F-ratio (*F*)	*p-Value*	*F crit*
Between Groups	111738.07	3	37246.023	139.578	**3.0168E-07**	4.0662
Within Groups	2134.779	8	266.847			
Total	113872.85	11				

Table 6.8 Paired t-test for comparison of the strength for Mix 3 and Mix 4

	Mix 3	**Mix 4**
Mean	916.120	1179.167
Variance	3779.450	668.793
Observations	3	3
Hypothesized Mean Difference	0	
df	3	
t Stat	-6.831	
P(T<=t) one-tail	**0.00321**	
t Critical one-tail	2.353	
P(T<=t) two-tail	0.00642	
t Critical two-tail	3.182	

Table 6.9 Paired t-test for comparison of the failure strains for Mix 3 and Mix 4

	Mix 3	**Mix 4**
Mean	1.80	1.31
Variance	0.960	0.0427
Observations	3	3
Hypothesized Mean Difference	0	
df	2	
t Stat	0.842	
P(T<=t) one-tail	**0.244**	
t Critical one-tail	2.920	
P(T<=t) two-tail	0.488	
t Critical two-tail	4.303	

Table 6.10 Paired t-test for comparison of the Young's moduli for Mix 3 and Mix 4

	Mix 3	**Mix 4**
Mean	216.56	199.466
Variance	49.165	790.650
Observations	3	3
Hypothesized Mean Difference	0	
df	2	
t Stat	1.021	
P(T<=t) one-tail	**0.207**	
t Critical one-tail	2.919	
P(T<=t) two-tail	0.414	
t Critical two-tail	4.302	

6.5 SEM Analysis of Fractured Samples

Macroscale optical images of all failed samples after the UCS testing were taken using a camera. Failure analyses for each sample were also conducted at the microstructural scale. All selected fractured samples were gold-coated and viewed using the SEM. Multiple SEM micrographs have been taken at different magnifications to get the essential failure information from each sample.

Failure analyses for each mix at the microstructural scale are shown in Figures 6.10–6.13. Figure 6.10 shows a series of SEM micrographs of the collapsed morphology for Mix 1 at different magnifications. Figure 6.10a gives overall texture of the collapsed surface morphology. Figure 6.10b shows clay-like and crystallized particles in the structure of

Mix 1. Figure 6.10c reveals the loose linkages of particles. Figure 6.10d shows the collapsed particles at the particle boundaries.

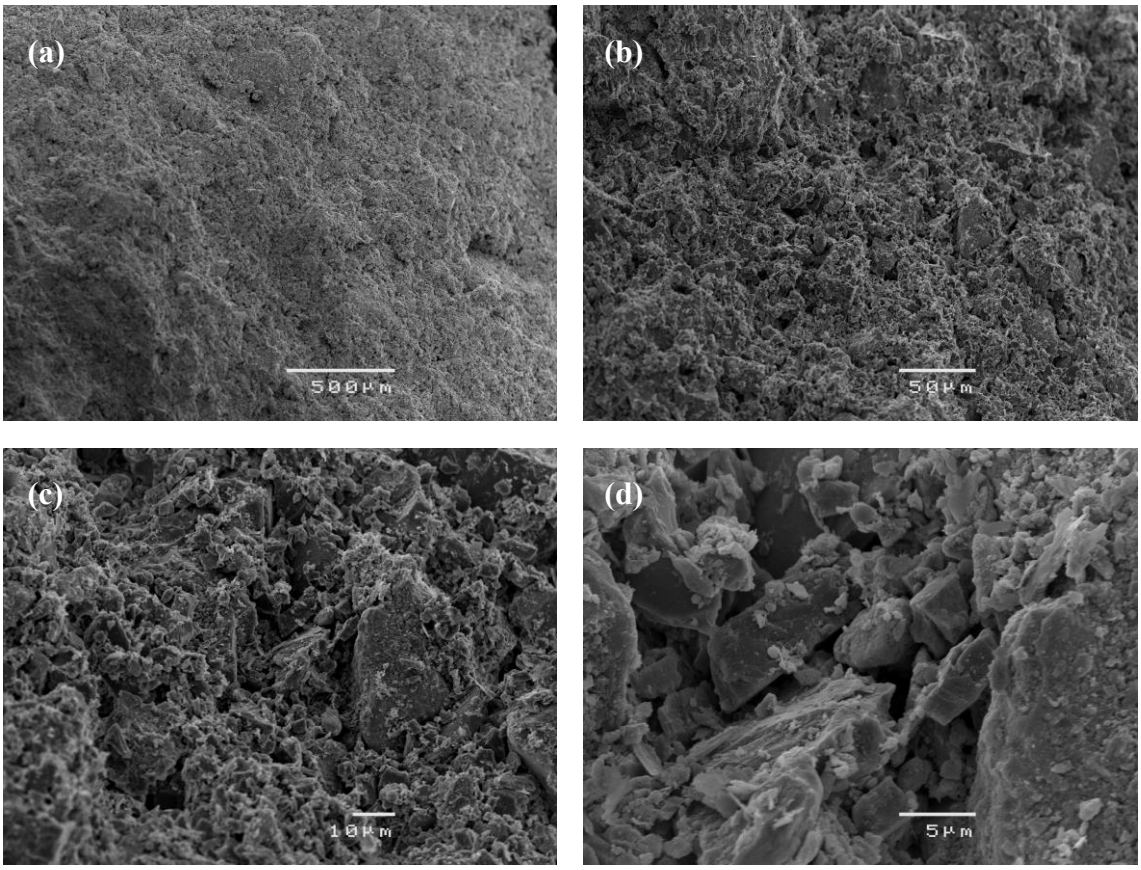

Fig. 6.10 SEM micrographs of the collapsed Mix 1 sample (no binder)

Figure 6.11 shows a series of SEM micrographs of the fractured surface morphology in Mix 2. Figure 6.11a displays the general fractured texture. Figure 6.11b reveals cracks up to 300 µm in the fractured area. Figure 6.11c shows the cracks around particle boundaries. Figure 6.11d reveals the voids and trans-particle fractures.

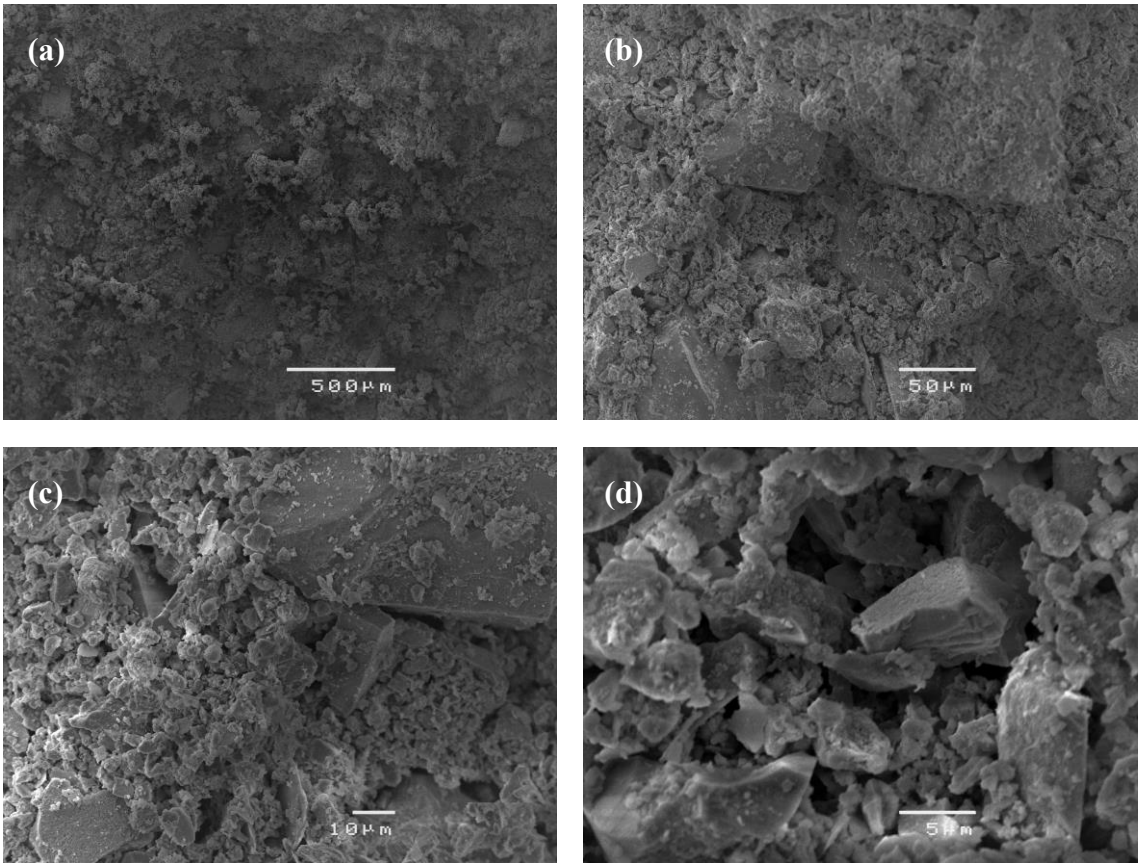

Fig. 6.11 SEM micrographs of the fractured Mix 2 sample (geopolymer)

Figure 6.12 shows a series of SEM micrographs of the fractured surface morphology in Mix 3. Figures 6.12a and 6.12b reveal the overall texture of fractured samples at the different magnifications. Figure 6.12c shows that cracks around the boundaries of fine and coarse particles. Figure 6.12d clearly shows the fracture bridges built by the needle-shaped particles in the fractured areas.

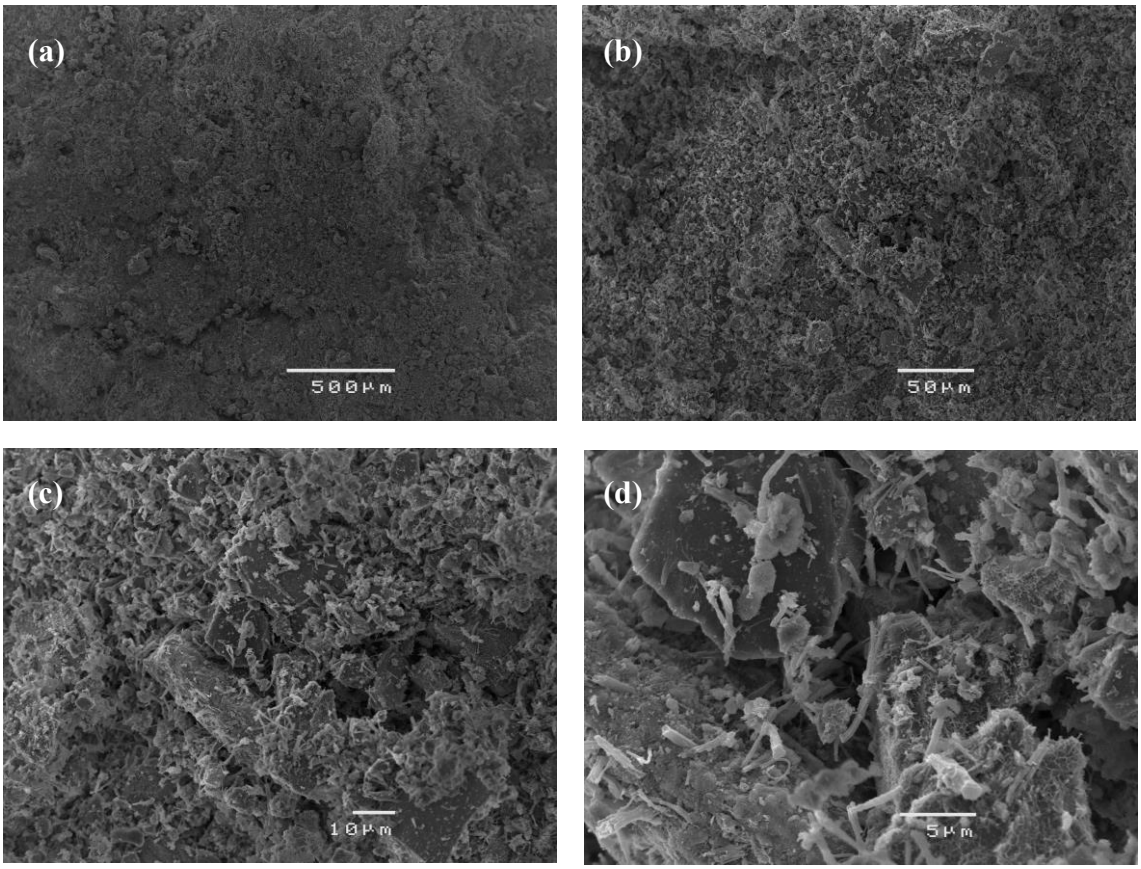

Fig. 6.12 SEM micrographs of the fractured Mix 3 sample (Fly ash-cement)

Figure 6.13 shows a series of SEM micrographs of the fractured morphology in Mix 4. Figures 6.13a and 6.13b reveal the overall fractured textures. Figures 6.13c and 6.13d reveal clearly that the needle-shaped particles were spread densely in Mix 4 and functioned as bridges in the fracture areas. This demonstrates the needle-shaped particles from cement binder as they were identified only in Mixes 3 and 4, where the cement was the common binder used in 75% and 100%, respectively.

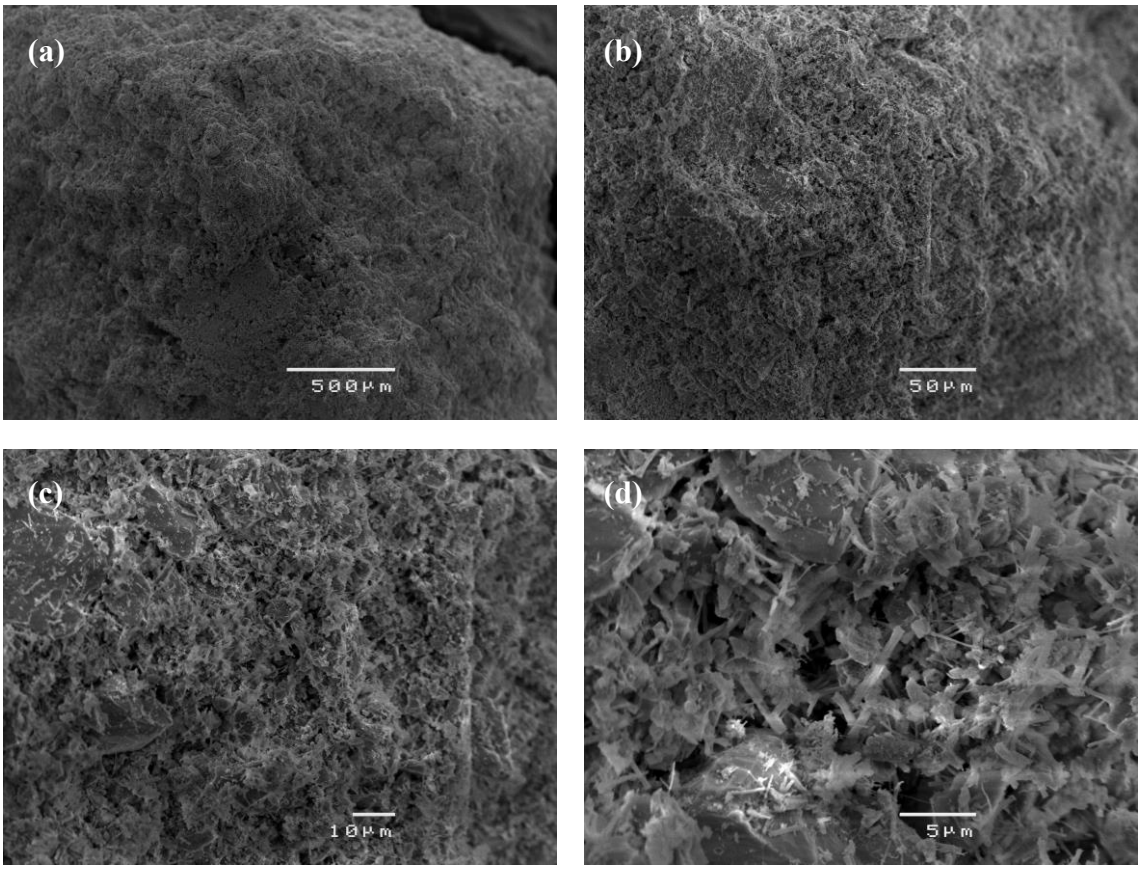

Fig. 6.13 SEM micrographs of the fractured Mix 4 sample (cement)

6.6 Discussion

This study investigated the relationship between the long-term mechanical properties and their microstructures in the paste backfill materials. The mechanical properties of these paste backfill samples were measured using UCS tests on specimens cured for 112 days. The fractured surface morphology of the UCS tested samples was examined using SEM at different microscales to understand the influence of the tailings and binders on the mechanical behaviour of these paste backfills.

Fly ash-cement binder significantly modifies paste backfill's mechanical properties, whereas the cement-free geopolymer binder slightly modifies the mechanical properties of paste backfill mix. The behaviour of paste backfills with similar binders, especially in early ages, has been discussed by Niroshan et al. (2016). Therefore, if the mine's

objective is to achieve UCS strength of 700 kPa at 28 days, the fly ash-cement is adequate in terms of short and long term mechanical properties as well as environmental considerations, as this fly ash-cement binder consists of less cement, which is one of the main source of carbon emission to the environment. This 25% reduction of cement in binders could save millions of dollars to the mine and can reduce the required land for the disposal of large amount of fly ash, which is a waste by-product of coal power plants. In addition, it is well documented that the strengths measured using the laboratory specimens are much lower than those from the specimens obtained from coring of in situ CPB, mainly due to the influence of the effective overburden stress during curing on the strength of CPB in the mine (Fahey et al. 2011).

Further, the coefficient of variation (COV, the ratio of standard deviation to mean value) of mechanical properties of CPB mixes are within the acceptable limit (less than 15%) except COV of Young's modulus of mix - 2 (Geopolymer binder) which is about 45%. Mix 3 (Fly ash-cement binder) and Mix 4 (Cement binder) samples had much higher strength values with significant difference ($p < 0.05$) than Mix 2 (Geopolymer binder) samples, as shown in Table 6.4 and Figure 6.9a. This indicates that both fly ash-cement and cement binders had much stronger reinforcements in CPBs than geopolymer. However, higher Young's moduli are displayed by CPB mixes with fly ash-cement and cement binder, with no significant differences between the two ($p > 0.05$).

In our studies, 6% fly ash-cement mix shows relatively higher UCS strength than the laboratory tests by Kesimal et al. (2005) in sulphide-rich tailings, which also contained significantly higher fine contents (about 80%). In their studies, two different pozzolanic based composite cements (7 wt.%), in which type of pozzolan and ratio between pozzolan and Portland cement were unknown, were used and solid content of CPB mixes is relatively higher (about 82%) than the our current studies (74%). Similarly, in this study, 6% cement binder mix shows slightly higher UCS value than the sulphide-rich tailing based CPB mix studied by Cihangir et al. (2012). It is well known that even 1% change in solid content could lead to a substantial change in slump value or yield stress of CPB

mixes in addition to the changes in the mechanical properties. In addition, coefficient of uniformity (C_u) of tailing used in our studies is 11.8 and classified as medium type of tailing for the paste fill samples, which type of tailing would generally yield higher mechanical strength (Benzaazoua et al. 2004).

Relatively similar strength was shown for CPB with 7% binder consisting 60% Portland cement and 40% fly ash tested by Benzaazoua et al. (1999) in 28 days. Relatively higher solids (about 80%) and higher binder content (7%) in CPB would lead to a higher strength in the short term compared to this study. However, this strength may be reduced after certain period due to the presence of high sulphide content in the tailings used this test. Moreover, relatively low strengths (650 kPa) were obtained by Ercikdi et al. (2009) due to the presence of sulphide-rich tailing in CPB, though the solid content of studied mix was 77 wt.%. Once again, 4.5 wt. % Portland cement binder used to prepare CPB showed relatively similar strength due to the higher solid content (76%) even though at slightly less binder dosage compared to our current study. Also, relatively low strength (700 kPa) was shown in tests conducted by Benzaazoua et al. (2002) due to the higher proportion of fly ash in binder and slightly lower curing period (91 days) though similar sulphide content (5 wt.%) and binder content (6 wt.%) to current study.

As suggested by Niroshan et al. (2015), geopolymer binder has been tried in this study as an alternative binder in order to evaluate its effectiveness in strength improvement of CPB. It appears that the effectiveness of the geopolymer binder in terms of strength is relatively low when compared to the other two binders. Furthermore, in this study, NaOH is used as an alkaline activator to activate fly ash in order to prepare geopolymer. It would have given better results for geopolymer binder mixes if alkaline activator is prepared as suggested by Al Bakri et al. (2012) with mixture of NaOH and water glass in certain percentage. However, geopolymer binders may be used instead of cement binder in other geotechnical applications like soft soil stabilization (ground improvement) as these geopolymers are environmentally friendly (cement-free) binder and especially, the

treated tailing mix using geopolymer (Mix 2) is classified as stiff clay based on UCS or q_u (≈ 100 to150 kPa) (Sivakugan and Das 2010).

Needle-shaped particles can be observed at microscopic level for CPB mixes with fly ash-cement and cement binders (Figures 6.12d and 6.13d, respectively). The binders in the two mixes contain 75 wt. % and 100 wt. % cement, respectively, and these mixes show relatively high strength and Young's modulus among the four mixes studied herein. These needle-shaped particles are found in raw cement binders (Figure 6.4c). Therefore, it can be concluded that the needle-shaped structure is from cement binder which contributes significantly in alteration of mechanical properties of CPB mixes. Although cement binder mix gives higher mechanical properties than fly ash-cement binder mix, some mines may prefer to use fly ash-cement binder for the early strength gain and environmental concerns, provided the target strength requirements are met. This fly ash-cement binder consists of 25% fly ash, which is also a by-product of the coal combustion products, and 75% cement. Therefore, carbon emission to the environment due to the cement production would be significantly reduced due to the 25% cement replacement by fly ash in a traditional binder (100% cement). In addition, land requirement for waste (fly ash) storage will be dramatically reduced. It is clearly observed that there is a relatively small size of micro-pore network and cracks as well as more dense packing between tailing particles in cement based CPB mixes (Figure 6.13d) with SEM analysis than the three other investigated mixes in this study. Compared to the geopolymer binder based CPB mixes, the fly ash-cement and cement binder based CPB mixes had denser and less porous matrix at micro level. These observations confirm that the mechanical properties of each CPB mix can be correlated with their microstructure.

6.7 Summary

Among the four paste backfill mixes studied, CPB mix with cement binder shows highest strength, whereas CPB mix with fly ash-cement binder gives highest Young's modulus. However, there was no significant difference ($p > 0.05$) in the Young's modulus of CPB mixes with cement or fly ash-cement binders, UCS strength of CPB mix with cement binder is slightly higher than the mix with fly ash-cement. Those two binders are well suited in CPB preparation, in long-term basis in accordance with the mine specific target strength. Since geopolymer slightly improved mechanical properties of CPB and is a cement-free (CaO-free) as well as eco-friendly binder, it can be used to backfill the secondary stopes when there are no more free standing or exposed wall afterwards. Alternatively, it is recommended to use NaOH with water glass (Na_2O:SiO_2) in different concentration as an activator in the process of producing geopolymer for the better results as suggested by other researchers. SEM analyses revealed needle-shaped structure clearly observed in fly ash-cement and cement binder CPB mixes, which acted as bridging components among tailings and binders and also significantly enhanced mechanical properties of CPB. These specific observations for the microstructure of each CPB mix were consistent with their mechanical performances. In addition, SEM images illustrate CPB's structures and bonding which forms poorly and have loose structure for geopolymer binder. Smaller pore sizes and crack lines are clearly identified in cement, fly ash-cement mixes than the geopolymer and no binder mixes.

7 Rheological characteristic of CPB

7.1 Introduction

Density, binder content, and binder type determine the mechanical and rheological properties of a CPB material, which is categorised as a pumpable non-Newtonian fluid in terms of flow properties. The optimum dosage with the right binder is expected to enhance strength and stiffness characteristics in the long term, while ensuring that the CPB has the desired short-term rheological characteristics to ensure laminar pipe flow from the mixing plant to the underground stope.

In an attempt to dispose of more tailings into underground voids, the mines prefer increasing the solid content to the maximum possible limit, as dense CPB needs less binder to achieve a target strength. On the other hand, a high solids content slurry has both increased yield stress and viscosity, which increases the likelihood of blocking the reticulation pipeline. Therefore, it is necessary to establish a balance to optimize the solid content and flow properties of CPB. To determine the subsequent rheological effects arising from the modification of CPB mixture composition, numerous tests must be carried out in order to gain insight into the response of each specific flow and strength based parameter.

As the *strength* based parameters of CPB are already explained in chapter 5 and some published articles (Niroshan et al. 2016; Niroshan et al. 2017), this chapter aims to study the *flow* parameters of CPB and the effects of different types and dosages of binders on flow characteristic of CPB. In addition, this chapter discusses the interrelationship among the solid content, slump, saturated density and the yield stress of the paste, measured through an extensive laboratory test program.

This chapter was submitted as major part of a journal article and published as Niroshan, N., Sivakugan, N., and Veenstra, R. L. (2018)."Flow characteristics of Cemented Paste Backfills." *Geological and Geotechnical Engineering,* doi: 10.1007/s10706-018-0460-8.

7.2 Materials

7.2.1 Mine tailing

George Fisher Mine (GFM) tailings were used to prepare CPB for this laboratory test program. GFM, which is a hard rock underground mine, is located in the north Queensland, Australia. The index properties, such as specific gravity, in-situ moisture content, bulk density, grain size distribution and Atterberg limits, of GFM tailing used in this project are briefly explained in chapter 3. Based on the Atterberg limit test and the grain size distribution, the mine tailings used shows low plasticity index with the significant fines and can be classified as silty clay (ML or CL) according the unified soil classification system ASTM D2487 (ASTM 2011). Based on the SEM image, shapes of most grains are angular, which would enhance greater strength and stiffness due to the high friction angle and interlocking ability between them. In addition, it is revealed through a XRF analysis that GFM tailing has relatively low sulfide content. Appropriate range of solid content of CPB mix, reflecting what is used in practice at the mine, were chosen in order to understand the flow characters, (i.e. rheological behaviour) of CPB with solid content changes. For this series of laboratory tests, the solid content of CPB was between 72 and 78%, approximately.

7.2.2 Binders

Two type of binders, namely a general purpose (GP) and slag blend cement, were examined over a range of binder dosages between 0 and 6% (M_{binder}/M_{solids}). GP cement is a normal type I Portland cement according to ASTM C150 standard (ASTM 2007), and slag blend cement contained 60% slag and 40% GP Cement. These two (cement) binders were received from Cement Australia.

7.2.3 Water

Mine water is used to prepare samples for the laboratory testing as because the mine uses the same water in the preparation of paste fill. As the properties of water may influence much in the rheology testing, the water analysis of mine water used is shown in table 7.1.

Table 7.1 Water analysis of the mine water used

Water Types	pH	Total Dissolved Solids (mg/l)	Chloride (mg/l)	Sulphate (mg/l)
Mine Water	7.51	4600	467	2200

7.3 Sample preparation and testing program

Prior to testing the GFM tailings were sieved to achieve a relatively homogeneous mix with a maximum particle size of 4.75 mm. The water content of the sieved tailings was also determined 24 hours prior to testing by drying a small sample. Once the required materials have been added to the raw tailings, a rotary drill equipped with a paint mixer was used to mix the sample. This was done to ensure the hard packed tailings were separated, with the constituents effectively blended with binder throughout the mix into a homogeneous slurry. This process was carried out for approximately 5 minutes for each batch in order to get a homogeneous paste.

The highest solid content was tested first after which pre-determined quantity of water was added to the mix in order to reduce the solids content from 79% to 74% in approximately 0.5% steps. This procedure is continued for each mix until the highest slump height of CPB was reached. In addition, prior to each testing, the mix was effectively mixed to ensure homogeneity.

Laboratory tests were carried out on five different CPB mixes as shown in Table 7.2. The five mixes include one with no binder, and four other the mixes with GP or slag cement at dosage of 4% or 6%.

Table 7.2 CPB mix design

Mix No.	Binder Type	% Binder
Mix 1	No binder	0.0
Mix 2	GP Cement	4.0
Mix 3	GP Cement	6.0
Mix 4	Slag Cement	4.0
Mix 5	Slag Cement	6.0

7.4 Slump Measurement

The slump tests are carried out using two different devices. One is the standard cone as per ASTM C 143 standard (ASTM 2015), which is normally used in concrete testing, and the other one is relatively smaller cylinder with 110 mm (diameter) × 110 mm (height). The cylinder appears to give reproducible results and enables more and quicker tests even with its smaller volume. It may better suit these high moisture content slurries. Moreover, using small cylinder for slump test is a faster, with a smaller volume of material used in the test.

The slump cylinder was filled with remoulded paste fill with and without cement in different percentage at various solid concentrations. The water contents were varied to obtain different consistencies of CPB materials ranging from 30% to 40% (M_{water}/M_{solids}) in order to get solid contents of approximately 72% to 78% (M_{solids}/M_{total}). For each CPB sample, the slump test was conducted as quickly as possible to avoid hydration effects in the binder mixes. The devices used for the standard and cylindrical slump test are shown in Figure 7.1.

(a) (b)

Fig. 7.1 Slump test devices; **(a)** Standard cone slump, **(b)** Cylindrical slump

While both standard and cylindrical slump tests were carried out in the same mixes, only the standard slump test is critically analysed in this section because of the similarity of test results. The purpose of doing both tests in similar samples is to demonstrate the viability of using the cylinders for slump tests of CPB as well as to suggest a correlation between standard and cylindrical slump. This cylindrical slump method may well suit fine-grained types of materials where small amount of material is available for the tests.

Standard slump height changes with solid content of CPB mixes are shown in Figure 7.2. As expected, slump height decreases with increasing solid content for all CPB mixes. As expected, the CPB mixes without binder exhibit higher slump values than the CPB mixes with binders, at all solid contents. Especially in high slump mixes, the solid contents of all the mixes are converging compared to low slump mixes. This trend clearly shows that there is an effect of binder content and binder type on slump height of CPB, especially in higher solid content mixes (above 76% solids).

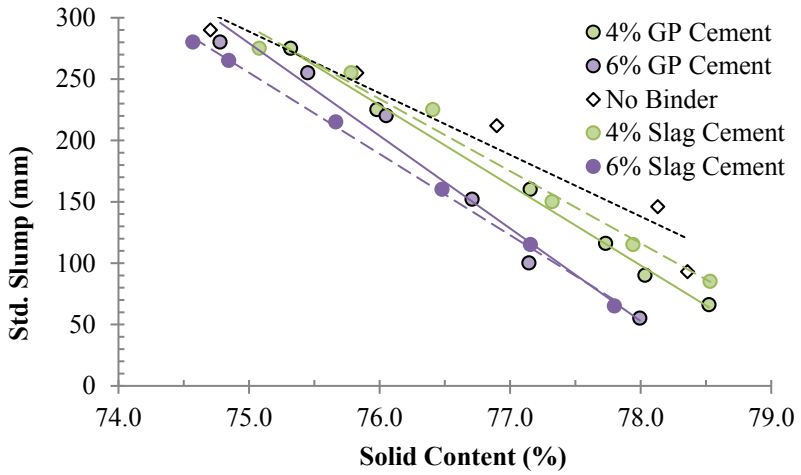

Fig. 7.2 Standard slump height changes with solid content of CPB mixes

7.4.1 Effect of Binder Content on Slump

Slump height changes with solid content of CPB mixes with GP cement and slag cement are shown in Figures 7.3(a) and 7.3(b), respectively. It can be seen that the slump height decreases with increasing binder content at specific solid content. In GP cement binder mixes, slump height decreases gradually with increasing binder dosages whereas in slag cement binder mixes, slump height of no binder and 4% mixes are approximately same and slump height of 6% CPB mix is much lower for all solid contents, with the difference increasing with the solid content.

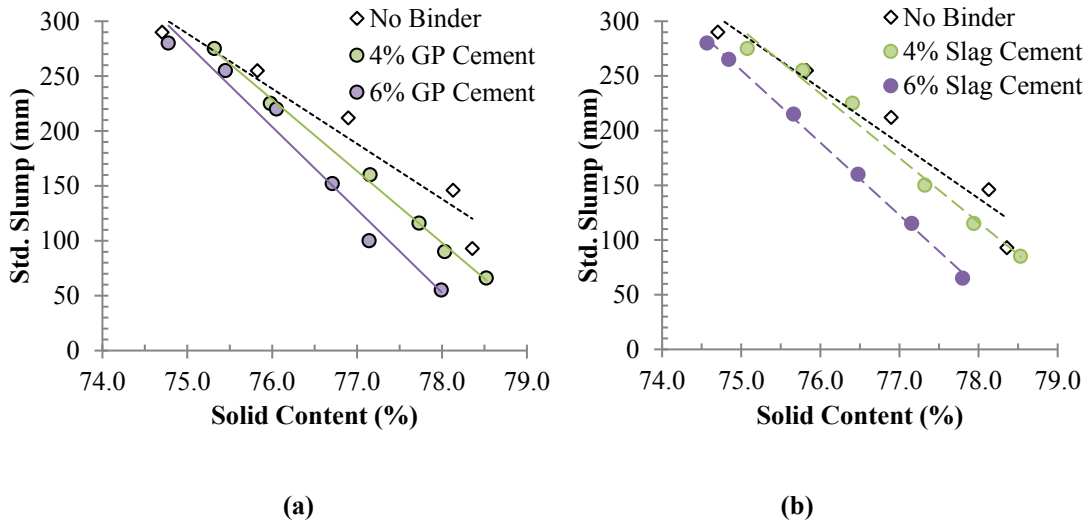

Fig. 7.3 Standard slump height changes with solid content of binder CPB mixes **(a)** GP cement, **(b)** Slag cement

7.4.2 Effect of Binder Type on Slump

Slump heights change with solid contents for 4% and 6% binder CPB mixes are shown in Figures 7.4(a) and 7.4(b), respectively. The changes clearly indicate that there is no major effect of binder type in slump height. However, the similar trends may possibly be due to the low dosages of binders. Finally, these extensive slump tests on CPB mixes show the binder type does not affect the slump height whereas the binder content is affecting the slump height and the deviation of slump height between the mixes with no binder and those with binder increases with increasing solid content and binder content.

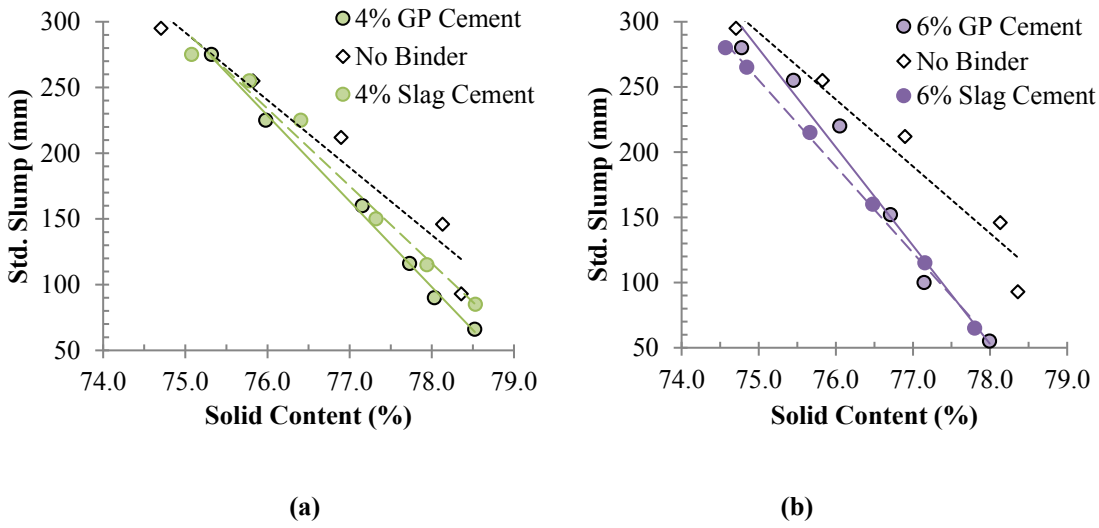

Fig. 7.4 Standard slump height changes with solid content of **(a)** 4% binder **(b)** 6% binder, CPB mixes

7.4.3 Correlation between Standard and Cylindrical Slump of CPB Mixes

As indicated in the methodology, the standard (conical) and cylindrical slump tests are carried out in same mixes of CPB in order to propose the simpler cylindrical mould as an alternative to the conical counterpart. Cylindrical slump changes with standard slump of correspondent CPB mixes regardless to the binder types is shown in Figure 7.5. The data include tests with and without binder. There is good correlation between the two slumps ($R^2 = 0.9655$) as shown in Equation 7.1. The unit of the both slumps is mm.

$$S_C = 9.3446 \times e^{0.0076 \times S_S} \quad \textbf{(7.1)}$$

where, S_C is cylindrical slump and S_S is standard slump.

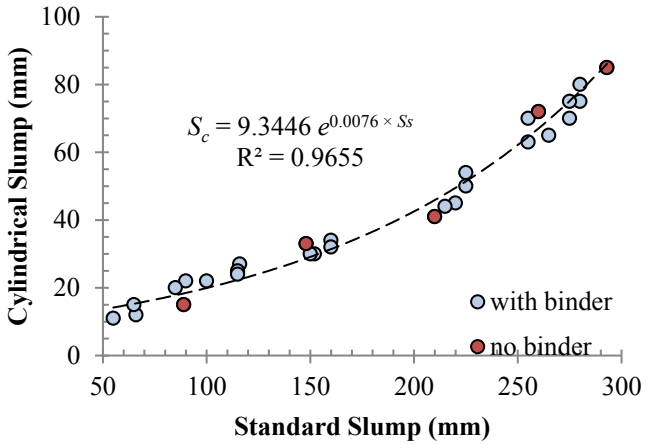

Fig. 7.5 Correlation between cylindrical slump and standard slump of CPB mixes

As the correlation is based on data spread over of wide range of slump and solid contents, with an excellent fit, it is expected that the Equation 7.1 may be applicable to tailings from other mines.

7.4.4 Correlation between Bulk Density and Solid Content

Bulk density of each mix was measured by filling a bucket and weighing. The bulk density of CPB changes with corresponding solid content is shown in Figure 7.6. The data presented here include the two binder types and different dosages.

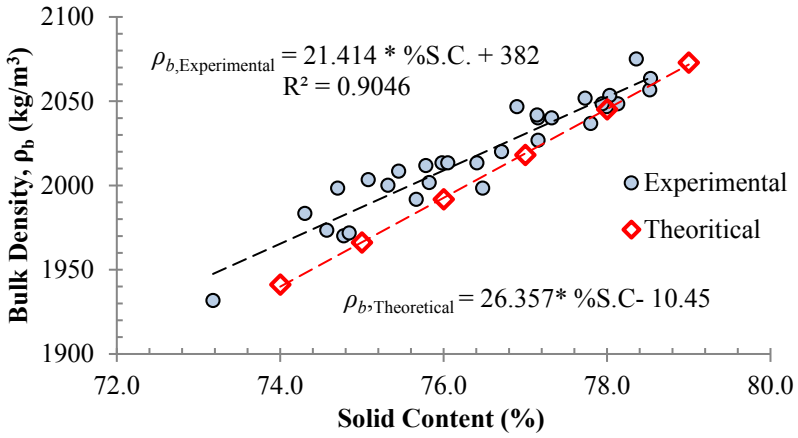

Fig. 7.6 Experimental and theoretical curves of bulk density changes with solid contents

The theoretical line shown in Figure 7.6 was calculated using Equation 7.2 where, the values 2.90 and 1000 kg/m^3 are used for specific gravity (G_S) and density or of water (ρ_w), respectively. As prepared CPB samples were assumed as fully saturated, the degree of saturation (S) is considered as 1.

$$\rho_{bulk} = \frac{(1+w).G_s.\rho_w}{(1+e)} \quad \textbf{(7.2)}$$

where, the ρ_{bulk} is bulk density and e is the void ratio defined as the ratio of void volume to solids volume.

The measured bulk densities are slightly higher than what is derived theoretically. The slight deviation between the experimental and theoretical line is possibly due to the site water, and different types and dosages of binders used in this experimental study that can affect the value of G_s. In addition, the calculated (theoretical) values may vary possibly due to the assumed saturation, which may not be exactly 100% and may be slightly less in practical. Mix with 100% saturation would be the densest possible. It is more likely due to the different tailings or specific gravity (G_s) of binder used. Note that the slag binders typically have a lower G_s than the 100% GP binders. However, there is a good agreement between experimental and theoretical curves as shown in Figure 7.6.

7.5 Yield Stress Measurement

Pumping out the CPB requires good understanding of the yield stress and the viscosity of the slurry. In Newtonian fluids, the ratio of the shear stress (τ) to the shear rate ($\dot{\gamma}$) is defined as viscosity (μ), known as dynamic viscosity, and it is given in Equation 7.3

$$\mu = \frac{\tau}{\dot{\gamma}} \quad \textbf{(7.3)}$$

where, $\dot{\gamma}$ is the rate of shear strain (i.e., $\frac{d\gamma}{dt}$). Here, the viscosity remains the same at all shear rates. In non-Newtonian fluids (e.g., Bingham), there is a yield stress (τ_y) that has to be overcome before the slurry can flow. Typical flow curves are shown in Figure 7.7.

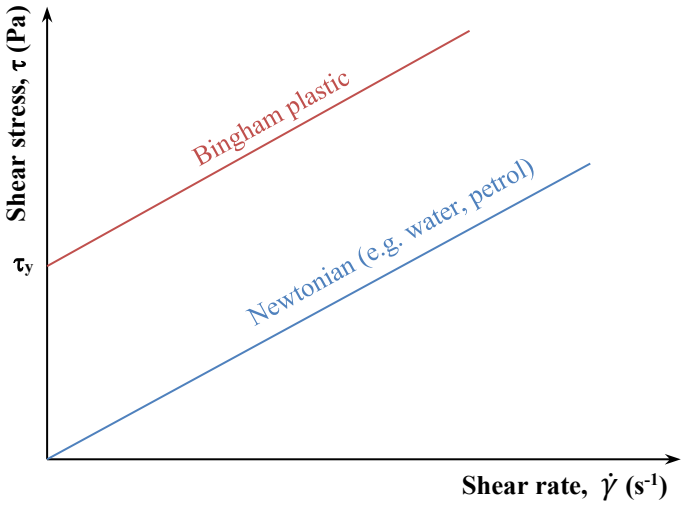

Fig. 7.7 Typical flow curves

CPB exhibits non-Newtonian behaviour that is similar to Bingham plastics, where the shear stress, viscosity and shear strain rate are related as shown in Equation 7.4

$$\tau = \tau_y + \mu\dot{\gamma} \quad \textbf{(7.4)}$$

where, μ is the Bingham plastic viscosity, and τ_y is the Bingham yield stress. Typical yield stress values are listed in Table 7.3

Table 7.3 Typical yield stress values (adopted from Boger et al. (2006))

Substance	Yield stress (Pa)
Tomato sauce	15
Yoghurt	80
Toothpaste	110
Peanut butter	1900
Thicken Tailings disposal	30-100
Mine stope fill	250-800

The yield stress of the CPB is measured using shear vane technique, which is commonly known as cup and vane method. Generally, the vane is inserted into the CPB slurry sample and rotated at a very low speed where the torque is changing with time. The torque increases until it reaches a maximum value (T_m), when the material starts to flow freely. Using this technique, T_m is measured of each prepared CPB mix. The measured T_m is converted to yield stress (τ_y) using Equations 7.5 and 7.6.

$$\tau_y = Q \times T_m \times K \quad \textbf{(7.5)}$$

$$K = \frac{2}{\pi D^3 \left[\frac{L}{D} + \frac{1}{3}\right]} \quad \textbf{(7.6)}$$

where, Q is spring constant of Viscometer, T_m is maximum torque, L and D are length and diameter, respectively, of shear vane used to measure the maximum torque of CPB. The spring constant (Q), which is a constant of Viscometer used per full-scale readings of torque, is 5.7496×10^{-3} N·m. Torque (T_m) is the percentage reading (%) from the full scale vane viscometer reading. The length and diameter of shear vane is 12.67 mm and 25.35 mm, respectively. The experimental setup for the yield stress measurement and the vane used for the yield stress measurements are shown in Figure 7.8. The methodology of this cup and vane method is very similar to the vane shear test used by geotechnical engineers in soft clays in the laboratory and field for determining the undrained shear strength. The Equations 7.5 and 7.6 are also the same. Only the size of the vane is different.

(a) (b)

Fig. 7.8 Apparatus for measuring yield stress of CPB; **(a)** Viscometer, spindle, and beaker, **(b)** Vane

This vane shear test is generally carried out as an in-situ testing method for clay soils as it is quick, easy and cost effective. However, under special conditions, this test can be performed in laboratory using a Brookfield Viscometer. The Brookfield DV-II+ Pro model viscometer with vane spindle (model V-73) was used for the entire series of tests. This is a popular method as there is minimal slippage between the spindle and the paste, and only a small amount of paste disruption in submersion of the spindle. The Brookfield viscometer manual suggests that a V-73 spindle operated on a HBV Model viscometer is suitable for shear stress in a range of 80-800 Pa. This is considered a suitable for the testing of CPB used in this study. The 250 ml beaker was used as the cup in this method. It is important to ensure any adverse effects arising from the contact between the beaker and the fill material is minimised during the vane rotation for the yield stress

measurement. This test performed by inserting a four-blade vane into a sample and then the vane is rotated at a set speed with the torque being measured at regular time intervals.

The vane and cup method is an effective method for measuring the yield stress of the slurry as a function of solid content (%). This method is used to measure the short-term (i.e., immediately upon mixing) yield stress of the CPB in this study. Tests were carried out on CPB mixes at different solid content, binder type and binder dosage.

7.5.1 Effect of Solid Content on Yield Stress

The variation of yield stress of CPB mixes with solid content is shown in Figure 7.9. As expected, the yield stress of the particular CPB mix increases with solids content. The yield stress is increasing exponentially while slump is inversely proportional to solid content. The trend clearly shows the effect of binder content on changes in yield stress. In other word, the binder contributes more than the tailings to the yield stress. However, it is hard to see the effect of the binder types on yield stress changes as observed in slump changes (see Figure 7.2).

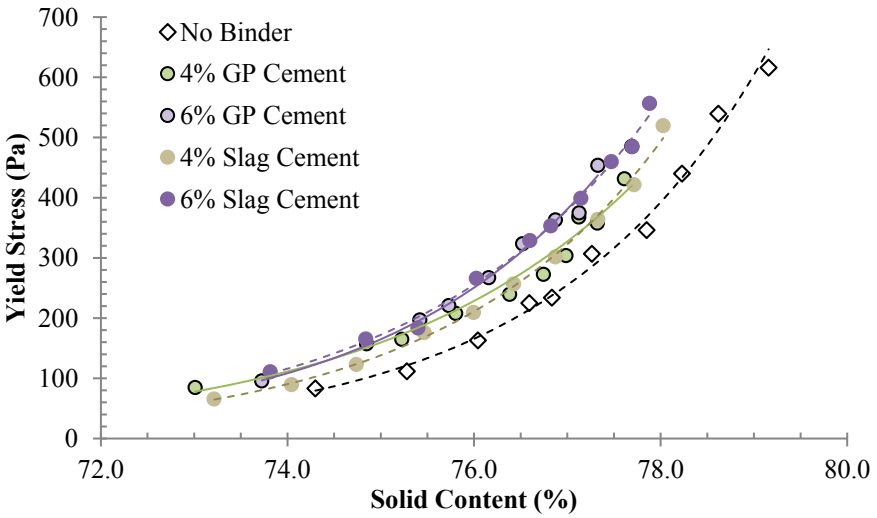

Fig. 7.9 Yield stress changes with solid content of CPB binder mixes

The relationship between yield stress and solid content for all five mixes in Table 7.2 is shown in Figure 7.10. There are two distinct trend lines for the mixes with and without binder, with R^2 of 0.9678 and 0.9931, respectively. There is clear indication that the binder content increases the yield stress and reduces slump, even at the same solid content.

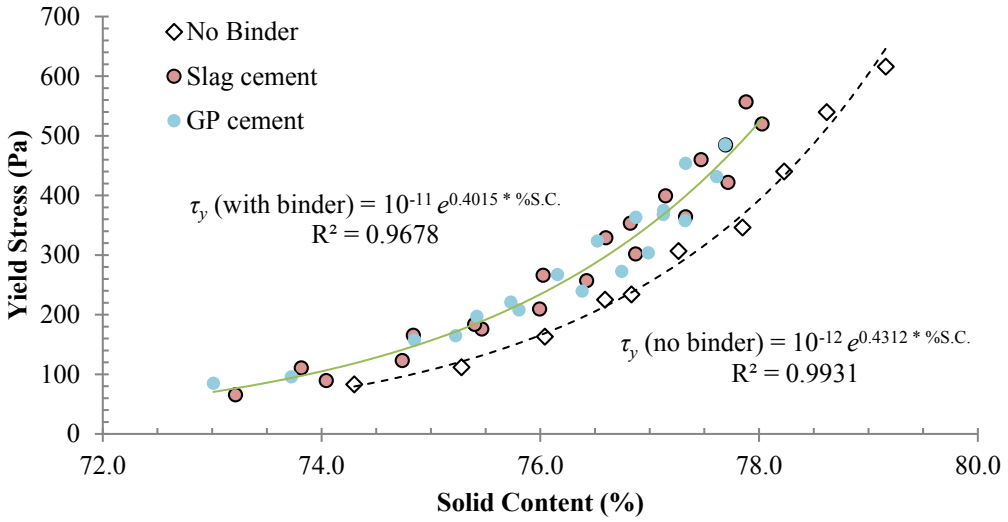

Fig. 7.10 Correlation between yield stress and solid content of mixes with and without binder

The proposed analytical correlations for the mixes without and with the binder are shown in Equations 7.7 and 7.8, respectively.

$$\tau_{y\ (no\ binder)} = 10^{-12} \times e^{0.4312 \times \%S.C.} \quad \textbf{(7.7)}$$

$$\tau_{y\ (with\ binder)} = 10^{-11} \times e^{0.4015 \times \%S.C.} \quad \textbf{(7.8)}$$

where, τ_y is the yield stress in Pa and *%S.C.* is solid content in % by weight.

Equation 7.7 does not separate the cases with 4% or 6% binder. To incorporate the binder content in the estimation of yield stress, the regression analysis was performed using MS Excel in-built function. Simple correlation among yield stress, solid content and binder content are shown in Equation 7.9. The estimated values using the Equation 7.9 show good agreement (R^2= 0.9744) with experimental data and the R^2 value reveals that there

was a slight improvement in estimation of yield stress by incorporation binder content as well.

$$\tau_y = 3.6686 \times 10^{-12} \times e^{(\%S.C. \times (0.4117 + 0.001177 \times \%B)} \quad \textbf{(7.9)}$$

where, τ_y is yield Stress in Pa, *%S.C.* is solid content in %, and *%B* is the binder content in % by weight.

The Equation 7.9 may be valid for the binder content range from 2% to 6%. The experimental and estimated values of yield stress against the solid content changes are shown in Figure 7.11.

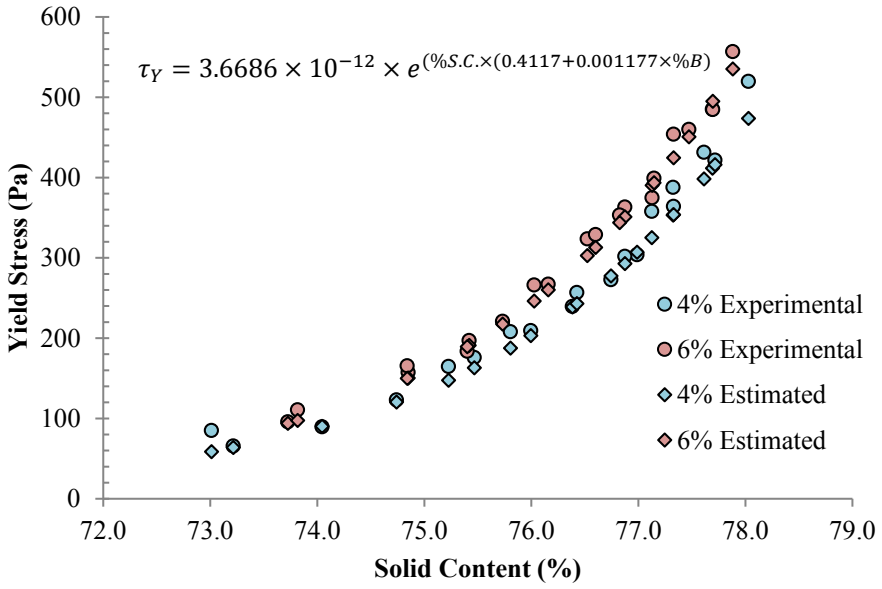

Fig. 7.11 Experimental and estimated yield stress changes with solid content

In Figure 7.11, almost all the experimental data of yield stress are within the estimated values. Moreover, two separate trend lines can be identified for the two different binder contents 4% and 6%.

7.5.2 Correlation between Cylindrical Slump and Yield Stress

Variation between the yield stress and the cylindrical slump of CPB mixes is shown in Figure 7.12. Obviously, the yield stress decreases with increasing slump height. Mixes with lower solid content always exhibit lower yield stress and higher slump height and vice versa. As can be seen, binder influence is more pronounced in higher solid content mixes. Also, it is clearly identified (from Figures 7.2 and 7.9) that the binder type has an effect on slump and yield stress of CPB. As noted previously from the slump test results, the yield stress values also converge into a narrow band for low solid content (i.e., high slump and low yield stress), and the band widens for higher solid content.

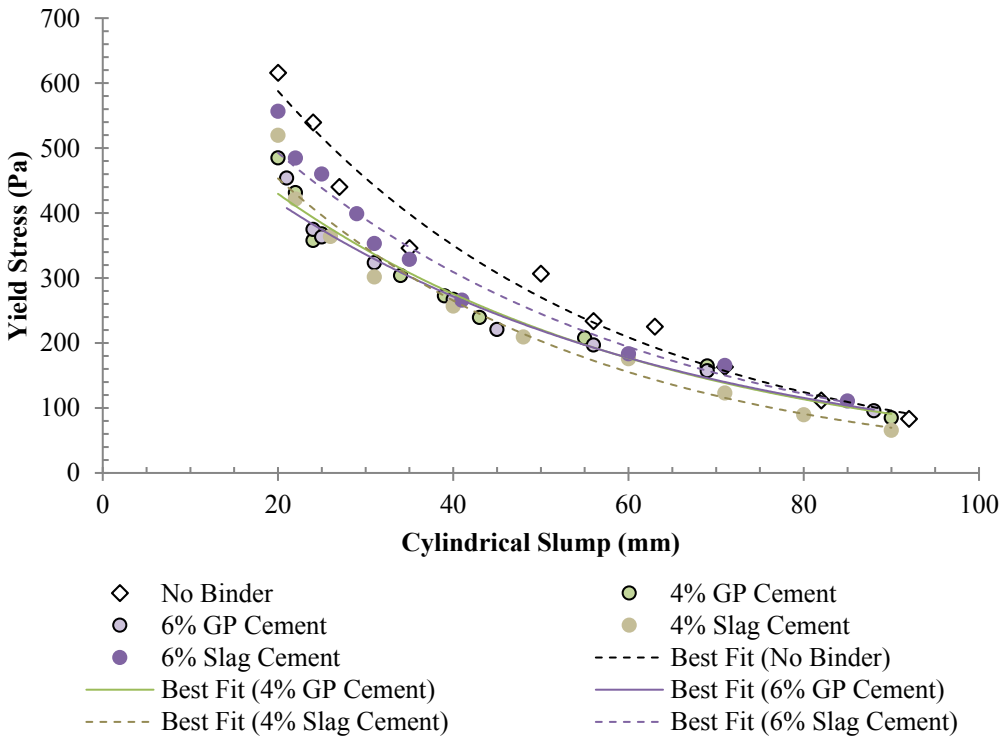

Fig. 7.12 Yield stress changes with cylindrical slump of CPB binder mixes

Relation between yield stress and cylindrical slump for mixes with and without binder are shown in Figure 7.13. Both proposed correlations show a good agreement (R^2=

0.9604 and 0.9780). Yield stress of the mix with and without binder can be calculated using proposed Equations 7.10 and 7.11, respectively.

$$\tau_{y\ (with\ binder)}=728.2\times e^{-0.024\times S_C} \quad \textbf{(7.10)}$$

$$\tau_{y\ (no\ binder)} = 986.24\times e^{-0.026\times S_C} \quad \textbf{(7.11)}$$

where, τ_y yield Stress in Pa and S_C is cylindrical slump in mm

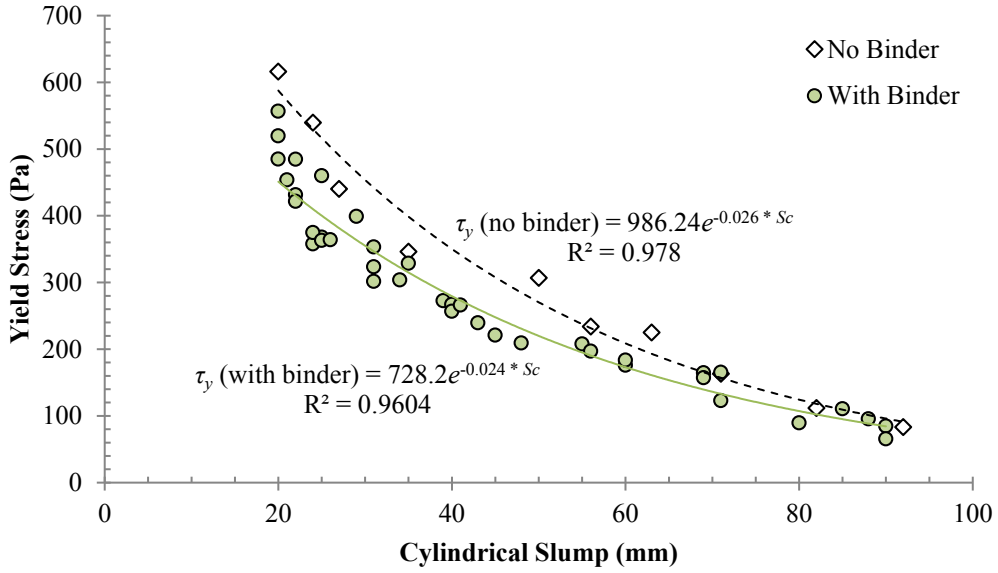

Fig. 7.13 Correlation between yield stress and cylindrical slump of mixes with and without binder

7.5.3 Effect of Bulk Density on Cylindrical Slump and Yield Stress

Bulk density is a direct measure of the solid content. Therefore, this can also be correlated to the slump or yield stress. Relationship of cylindrical slump and yield stress of CPB mixes with bulk density are shown in Figures 7.14a and 7.14b, respectively. In this relationship, the mixes without binder were discarded since most of the time CPBs include at least a small amount of binder in order to avoid liquefaction effect. Using these relationships (Figures 7.14a and 7.14b), Equations 7.12 and 7.13 and are proposed to estimate the cylindrical slump and yield stress of CPB, respectively using bulk density.

The unit of the bulk density must be in kg/m^3 in order to get slump value and yield stress in mm and Pa, respectively.

$$S_C = -0.8062 \times \rho_b + 1671.3 \quad \textbf{(7.12)}$$

$$\tau_y = 10^{-15} \times e^{-0.0198 * \rho_b} \quad \textbf{(7.13)}$$

where, S_C is cylindrical slump in mm, τ_y yield Stress in Pa and ρ_b is bulk density in kg/m^3

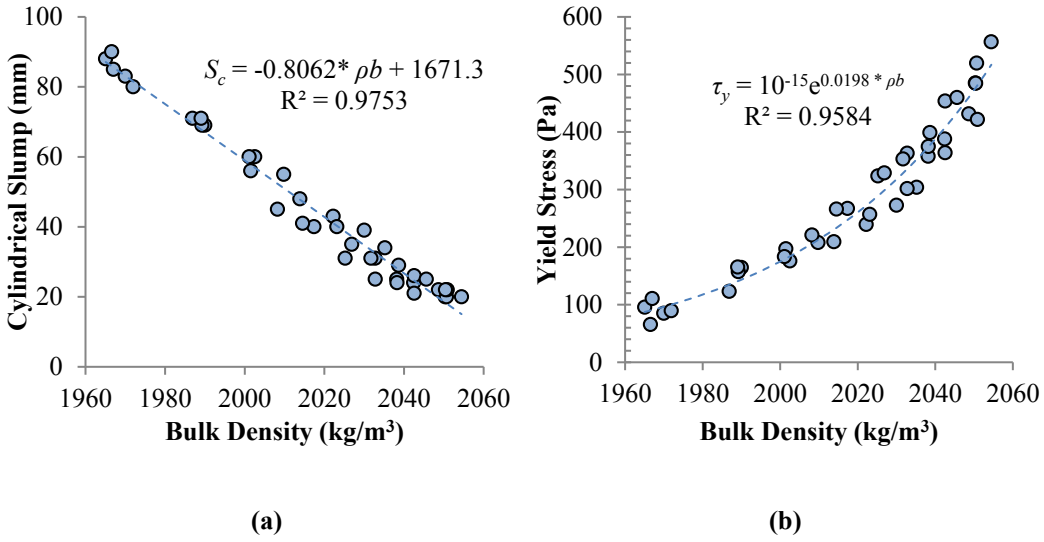

Fig. 7.14 Relationship between **(a)** cylindrical slump, **(b)** yield stress and bulk density of CPB with 4% and 6% binder

Since bulk density of CPB mix is easily measured in field, these two proposed correlations will be more useful to calculate or cross check the slump height and yield stress

By using Equations 7.10 and 7.13, the yield stress of CPB can be estimated on-site by measuring cylindrical slump height and bulk density, respectively for eliminating the need for sophisticated equipment and allowing easy.

7.6 Summary

The flow characteristics (i.e. rheological properties) of CPB were investigated using slump tests and yield stress test. Five different CPB mixes were prepared using GFM tailings and two different binders, namely GP cement and slag cement (40% GP Cement + 60% Slag) over a range of dosages between 0-6% and the solids content of CPB were between 72% and 78%, approximately including control mix (no binder). The mine tailing used for this experiment shows low plasticity index is categorised as silty clay (CL). The present study is an attempt to understand whether the different types or dosages of binders were influenced in flow characteristic of CPB in addition to the establishment of some correlations among standard slump, cylindrical slump, solid content, yield stress, bulk (i.e. saturated) density. As expected, the slump height is decreasing with increasing solid content while yield stress is increasing.

It was found that the flow characteristics of CPB were affected by the binder dosage but not the types of binder used in this study. However, the binder dosages also show less impact in low solid content (i.e. less than 75%) CPB mixes. It may be due to the lower binder content in higher water content mixes (i.e., highly flowable mixes). The relationship determined between the slump devices (refer to Equation 7.1) can be used to estimate one slump using other one for any mixes approximately. This cylindrical slump test, which is a faster and more efficient method, may be performed for any fine grain soil slurry such as dredged mud.

In addition, the yield stress can be estimated using known solid content and binder content (refer to Equation 7.9) or cylindrical slump (refer to Equation 7.10) of CPB mixes. In those, Equation 7.9 may be used in testing plan and design stage where as Equation 7.10 (i.e. correlation between cylindrical slump and yield stress) may be used during the testing stage on any type of CPB for comparison.

Finally the cylindrical slump height (refer to Equation 7.12) and yield stress (refer to Equation 7.13) of the unknown CPB mixes can be estimated by known bulk density (ρ_b)

of the corresponding CPB mix. It is a simplest method to estimate and crosscheck the flow properties (i.e. slump and yield stress) of CPB in the paste backfill plant or paste delivering points at stope. It may be necessary to carry out the tests in some other tailings from other mines, to validate the relationships developed in this project.

8 Determination of c and φ of CPB: Experimental, Analytical and Numerical Modelling

8.1 Introduction

The shear strength parameters, such as cohesion (c) and the angle of internal friction angle (φ), are important, especially during the design and modelling the stability of the backfilled underground voids. Shear strength parameters of geomaterials such as soils and rocks are often determined by Mohr-Coulomb theory. Generally, these properties are determined through complex laboratory CD/CU/UU triaxial tests. However, the triaxial test requires very expensive sophisticated equipment and consumes too much run time for the sample preparation and testing, which may not suitable for routine field or laboratory test. The objective of this chapter is to determine these two shear strength parameters using the uniaxial compressive strength (UCS) and indirect tensile (IDT) strength of the cemented paste backfill (CPB) specimens. No attempt is made to distinguish between the drained and undrained parameters. The paste fill is treated as a Mohr-Coulomb material with specific values of c and φ. The alternative approach was proposed to determine these properties for asphalt concrete using IDT strength testing and UCS testing by Christensen and Bonaquist (2002). This approach is used in this chapter to determine the shear strength parameters of CPB. In addition, these determined shear strength parameters were validated and correlated through a series of triaxial test. Furthermore, simple correlations are proposed to determine the shear strength parameters of CPB using UCS, IDT and relationships between the experimental values and the estimates. Finally, the predicted shear strength parameters were used for numerical simulation of the laboratory tests in FLAC^{3D} (ITASCA 2017) to check whether they give realistic predictions of IDT and UCS comparable to the experimental values.

8.2 Sample Preparation

The tailing materials used in this study also were provided by George Fisher Mine, Australia. Geotechnical characteristics of this mine tailings were already explained in

Chapter 03. Two types of binders were selected for studying the mix design to optimize the mechanical properties of the paste backfill samples are: (a) GP cement or type I Portland cement according to ASTM C150 (ASTM 2007), and (b) slag blended cement containing 60% slag and 40% GP Cement. These two binders were provided by Cement Australia. The characteristics of these two binders were well illustrated in Chapter 05. The water (i.e., LC80 Water) used in this experiment was from the Mine site. The water analysis is given in Table 8.1, where the similar analysis of tap water is also included for comparison. The LC80 water shows significantly higher total dissolved solids (TDS), chloride and sulphate when compare to tap water.

Table 8.1 Water analysis

Analysis	Unit	Tap Water	LC80 Water
pH		7.67	7.51
Total Dissolved Solids (TDS)	mg/L	160	4,600
Chloride	mg/L	42	467
Sulphate	mg/L	3	2,200

Table 8.2 summarises the laboratory testing program, where 72 CPB samples were cast in total with two different binders and three different dosages including the control mixes, where no binder was added. The solid content of each CPB mix were maintained around 75%. The samples were cured up to 56 days for three different testings, namely UCS, IDT and triaxial. For triaxial test, only 6% binder CPB samples were used.

Table 8.2 Testing Program

Mix Ref.	Binder	% Binder	% Solids	curing time	No. of samples per test		
					UCS	IDT	Triaxial
C0		0	75.0	7, 14, 28, & 56	3	3	-
C2	GP Cement	2.0					-
C4		4.0					-
C6		6.0					3
S2	Slag-cement	2.0					-
S4		4.0					-
S6		6.0					3

All these CPB mixes were mixed using an electrical drill rotating at 2500 rpm, which was attached to a paint stirrer to stir the mix for 3 min to 5 min, for making a homogeneous paste. All mixes were cast within plastic tubes of inner dimensions of 50 mm diameter and 120 mm height on a vibrating table to reduce air pockets within the samples. Then, all cast samples with plastic mould were placed in a closed bucket with approximately 2 cm height of water in the bottom to maintain a constant humidity and cured up to 56 days at room temperature. All cured samples were extruded from the plastic tubes and trimmed to obtain 100 mm in length to meet the general requirement of the height to diameter ratio of 2 (2:1) for the UCS and triaxial testing and 0.5 for IDT testing. The top and bottom surfaces were manually smoothened using knife-edges to ensure their flatness and parallelity. Triplicate samples were tested from each mix in UCS apparatus, once they were prepared.

8.3 Analytical Approach

The analytical approach to estimate the shear strength parameters (c and φ) using UCS and IDT values derived from laboratory experiments was initially proposed by Christensen Jr and Bonaquist (2002) on asphalt concrete base material. Further research by Piratheepan et al. (2012) and Sivakugan et al. (2014) utilised the correlation for lightly stabilised granular material, and rocks samples respectively. The theoretical framework of this alternate method for determining c and φ assumes Mohr-Coulomb failure criterion. The derivation was described in detail by Piratheepan et al. (2012). The equations presented in the paper by Piratheepan et al. (2012) were presented in a simple form by Sivakugan et al. (2014) and can be seen in Equations 8.1 and 8.2.

$$c = \frac{0.5\sigma_c\sigma_t}{\sqrt{\sigma_t(\sigma_c - 3\sigma_t)}} \quad \textbf{(8.1)}$$

$$\varphi = sin^{-1}\left(\frac{\sigma_c - 4\sigma_t}{\sigma_c - 2\sigma_t}\right) \quad \textbf{(8.2)}$$

Therefore, in order to estimate the shear strength parameters c and φ of cemented paste backfill using the analytical correlative equations 8.1 and 8.2, the UCS (σ_c) and IDT (σ_t) values of respective CPB samples are necessary.

8.3.1 Uniaxial Compression Strength Test

Uniaxial compression strength (UCS) test is a popular method of determining the compressive strength of cohesive soil due to its speed and ease. A cylindrical sample of soil or rock is trimmed so that its length to diameter (L:D) ratio is between two to three. The sample is assumed to be saturated, and undrained during testing. The sample is axially crushed with the applied load and strain recorded. The experimental setup for the UCS test of CPB sample is shown in Fig. 8.1. The applied load and adjusted cross sectional area, dependant on strain (using Equation 8.3), are used to determine the axial stress using Equations 8.4. Assuming volume of sample is constant throughout the test.

$$A = \frac{A_0}{1-\varepsilon} \tag{8.3}$$

$$\sigma_c = \frac{Applied\ Load}{A} \tag{8.4}$$

where, A_0 is the initial cross-sectional area of the sample, ε is the strain, A is the corrected cross-sectional area of the sample, and σ_c is the compressive stress applied to the sample. The relationship between σ_c and ε can be used to determine the Young's modulus (E) while the sample remains in the elastic deformation stage, identifiable when the data is graphed. The UCS (q_u) is the maximum value of σ_c. If the tested sample is fully saturated the undrained shear strength (c_u) can be calculated using Equation 8.5.

$$c_u = 0.5q_u \tag{8.5}$$

Fig. 8.1 Experimental setup for UCS test of CPB sample

8.3.2 Indirect Tensile (IDT) Strength Test

Unlike materials such as steel, the tensile strength of a geomaterials such as rocks, clays and cemented soils is quite difficult to determine by direct tensile strength test. The Brazilian test, also known as the indirect tensile (IDT) test, is a commonly used practical alternative to derive tensile strength of a material (Sivakugan et al. 2014). The test uses a cylindrical sample with diameter (D), with a metal loading strip at the top and bottom to apply a uniformly distributed compressive load (P) across the thickness (t) of the cylinder. Fig. 8.2 shows a schematic of the loading situation of an IDT test. The lateral deformation generates tensile stresses acting horizontally throughout the test cylinder, generally splitting the test sample vertically along the end faces.

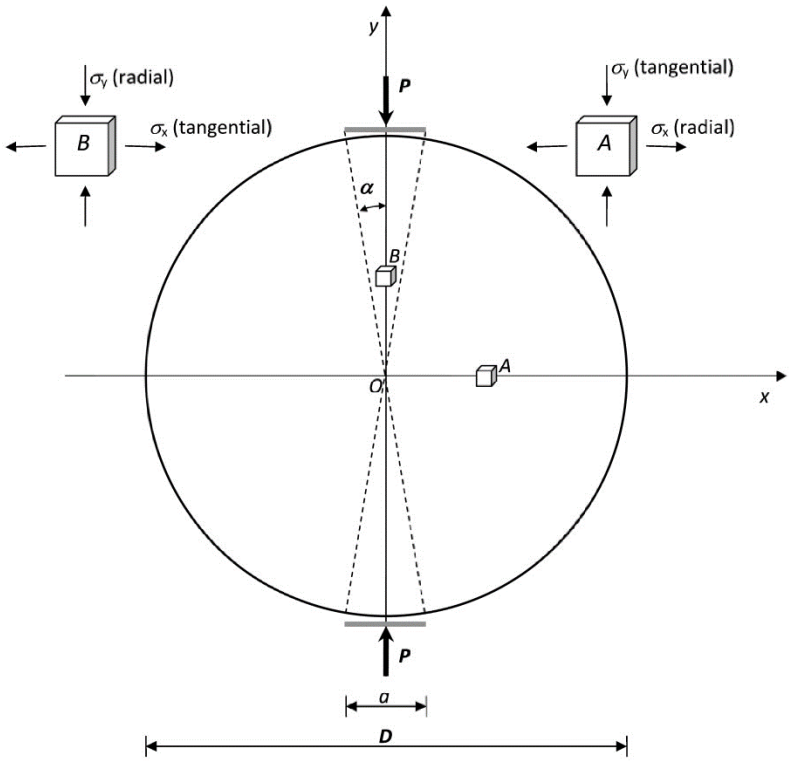

Fig. 8.2 Schematic loading situation of cylindrical sample of IDT strength test (Sivakugan et al. 2014)

This test is common for determining the tensile properties of both concrete and rocks, however literature surrounding the successful use on cemented sands (Clough et al. 1981; Das et al. 1995) is also present. Based on existing literature, the CPB should present a

strength between that of cemented sands and rock. Das et al. (1995) found that as the binder content increased, so too did the tensile strength, whilst the strain to failure decreased. A similar result is expected for CPB. Equation 8.6 is used to determine the IDT strength of the cylindrical sample.

$$\sigma_t = 2P/\pi Dt \quad \textbf{(8.6)}$$

where, σ_t is the splitting tensile strength in MPa, P is the maximum applied load indicated by the testing machine in N, t is the thickness of the specimen in mm, and D is the diameter of the specimen in mm. Experimental setup of an IDT strength test for cylindrical CPB sample is shown in Fig. 8.3.

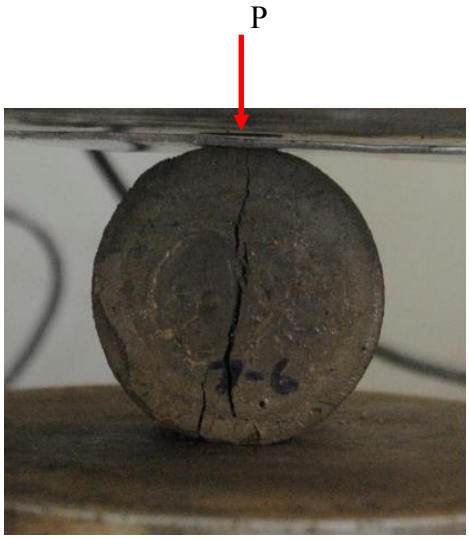

Fig. 8.3 Experimental setup for an IDT strength test of cylindrical CBP sample

The tensile strength determined through other two forms of tensile strength tests, including both bending test and direct tensile strength test, have been considered inappropriate for use in this studies due to the determination of shear strength properties for the analytical correlation being reliant on data collected using the Brazilian test (i.e., indirect tensile strength).

To investigate the L:D ratio effect on IDT strength of CPB samples, separately, 16 CPB samples were cast in two different L:D ratios (0.5 and 2) with two different dosages (4 and 6 %) and two different binders (cement and slag-cement blend). Figure 8.4 shows the correlation of mean IDT strength between the two different sizes for four different mixes.

It is shown that the IDT strength for CPB samples with L/D = 2 was lower than the sample with L/D =0.5, and which is around 0.7 times of IDT strength of CPB sample having L/D = 0.5 with good coefficient of correlation (R^2 = 0.9729).

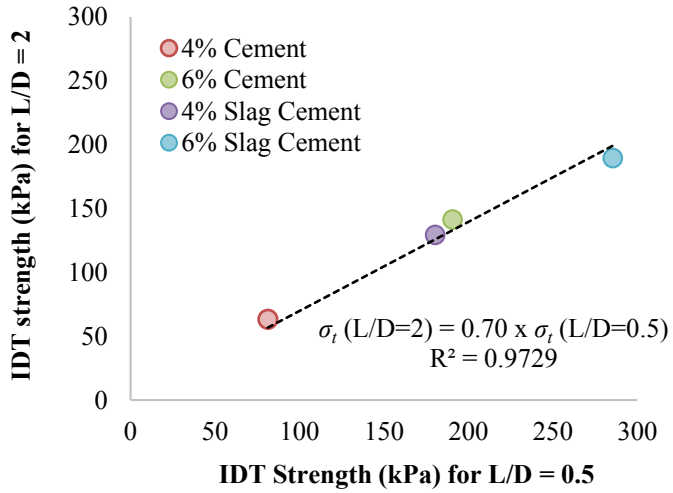

Fig. 8.4 Correlation for IDT strength of CPB prepared in two different sizes

As expected, the zero binder mix did not gain any form of strength as time progressed, failing when the confinement provided by plastic mould was removed. The mean value with standard deviation for σ_c, σ_t and E of each CPB mix from the experimental results (i.e., UCS and IDT tests) and for c and φ from the analytical correlations (i.e., Equations 8.1 and 8.2) are tabulated in Table 8.3. CPB mixes with low binder content (~2%) exhibit lower E/σ_c ratio, while mixes with higher binder content (≥ 4%) display higher E/σ_c ratio, which were between 116 and 195 when excluding early strength (i.e., 7 days strength) data. The σ_c/σ_t ratios were relatively constant and were between 3.8 and 6.6, when excluding 7 day results.

Table 8.3 Experimental results with analytical outcome

Curing time (days)	Mix Ref.	Experimental (UCS and IDT test results)			Analysis of experimental results		From analytical correlation (Eqs. 8.1 & 8.2)	
		σ_t (KPa)	σ_c (KPa)	E (GPa)	σ_c/σ_t	E/σ_c	c (kPa)	φ (°)
7	C2	8.3 ±0.96	131.9 ±10.11	1.2 ±0.18	15.9 ±1.15	8.9 ±0.67	18.4 ±1.79	58.9 ±1.30
	C4	29.0 ±4.80	318.1 ±22.41	40.3 ±2.38	11.0 ±1.20	126.5 ±11.65	56.3 ±7.64	51.2 ±2.51
	C6	122.6 ±12.30	593.7 ±15.63	96.1 ±58.85	4.8 ±0.39	161.9 ±67.95	230.1 ±32.83	14.7 ±6.47
	S2	4.0 ±0.50	24.5 ±3.43	0.3 ±0.04	6.2 ±0.52	13.1 ±1.60	6.9 ±0.86	31.1 ±3.89
	S4	164.8 ±4.31	846.9 ±35.47	279.4 ±33.98	5.1 ±0.09	329.9 ±34.67	289.5 ±6.83	21.3 ±1.15
	S6	250.6 ±22.50	1349.3 ±6.32	592.6 ±112.69	5.4 ±0.49	439.2 ±82.09	438.4 ±42.98	24.1 ±4.99
14	C2	26.2 ±1.35	142.0 ±22.12	1.3 ±0.10	5.4 ±0.56	9.3 ±1.03	45.9 ±1.91	23.8 ±5.75
	C4	68.1 ±11.91	381.2 ±31.12	52.7 ±2.24	5.6 ±0.51	138.4 ±9.53	118.7 ±22.03	26.5 ±5.34
	C6	140.0 ±4.26	749.0 ±33.47	146.2 ±13.01	5.4 ±0.09	195.2 ±24.20	244.3 ±7.04	23.7 ±0.99
	S2	19.2 ±0.53	73.5 ±8.36	0.6 ±0.02	3.8 ±0.37	7.9 ±0.80	42.7 ±7.27	0.8 ±0.56
	S4	166.5 ±16.24	968.5 ±17.20	185.6 ±18.52	5.8 ±0.47	191.7 ±19.75	289.3 ±29.39	28.4 ±4.32
	S6	276.1 ±32.27	1560.4 ±39.11	304.8 ±91.81	5.7 ±0.49	195.3 ±58.07	481.0 ±60.40	26.9 ±5.02
28	C2	25.0 ±2.38	171.6 ±11.14	1.4 ±0.03	6.9 ±0.50	8.4 ±0.37	43.6 ±3.93	36.1 ±2.90
	C4	78.6 ±7.16	381.0 ±53.96	54.3 ±19.48	4.8 ±0.34	142.6 ±63.36	140.8 ±12.04	16.8 ±5.25
	C6	175.9 ±16.63	869.6 ±107.08	159.8 ±71.29	4.9 ±0.36	183.8 ±111.21	313.1 ±28.33	18.3 ±5.06
	S2	20.0 ±0.87	103.9 ±38.08	5.6 ±1.22	5.2 ±1.73	53.5 ±17.37	47.9 ±21.73	31.0 ±2.90
	S4	198.6 ±9.65	952.7 ±30.64	116.1 ±19.50	4.8 ±0.08	121.9 ±24.15	355.3 ±19.23	16.6 ±1.21
	S6	313.2 ±9.47	1541.0 ±107.71	220.9 ±50.96	4.9 ±0.19	143.4 ±23.99	556.7 ±11.08	18.2 ±2.65
56	C2	12.9 ±0.62	85.3 ±3.37	4.2 ±1.57	6.6 ±0.06	49.3 ±16.75	22.5 ±1.06	34.4 ±0.36
	C4	58.3 ±4.46	384.6 ±42.24	44.9 ±12.99	6.6 ±0.23	116.7 ±24.81	101.5 ±8.03	34.3 ±1.51
	C6	176.9 ±21.76	1155.6 ±32.41	212.4 ±54.58	6.5 ±0.61	183.8 ±42.39	308.1 ±36.10	34.0 ±4.30
	S2	12.6 ±0.10	58.2 ±3.41	5.1 ±1.23	4.6 ±0.23	88.5 ±26.40	22.9 ±0.30	13.6 ±3.99
	S4	136.7 ±12.05	883.8 ±44.21	155.6 ±27.75	6.5 ±0.30	176.1 ±27.22	237.5 ±20.23	33.5 ±1.98
	S6	275.2 ±20.60	1511.4 ±156.54	212.6 ±114.77	5.5 ±0.17	140.7 ±62.68	479.0 ±34.27	25.2 ±1.79

Figure 8.5 shows the relation between the UCS and IDT strength of CPB samples. There is a good correlation between UCS and IDT for CPB samples (R^2=0.9649) as shown in Equation 8.7. Most of the samples were within 15% deviation lines.

$$\sigma_c = 5.4\sigma_t \quad \textbf{(8.7)}$$

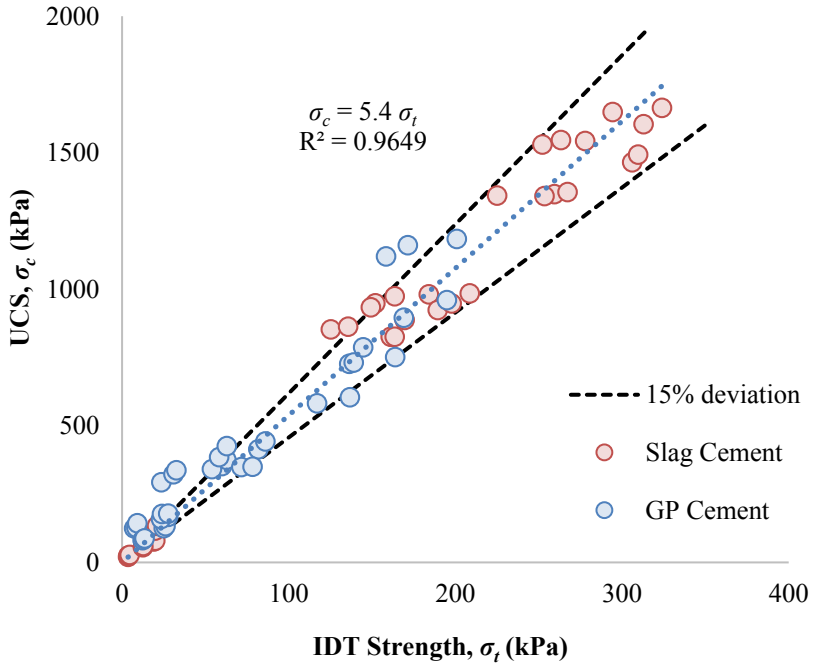

Fig. 8.5 Correlation between UCS and IDT of CPB

Correlation between determined cohesion using analytical correlation and, IDT and UCS strength are shown in Figures 8.6 and 8.7, respectively. These Figures 8.6 and 8.7 indicate that the cohesion can be estimated with minimal error (i.e., R^2 = 0.9994 and 0.9612, respectively) using the Equation 8.8 and 8.9, if the IDT and UCS strength of any CPB samples are known.

$$c = 1.76\sigma_t \quad \textbf{(8.8)}$$

$$c = 0.32\sigma_c \quad \textbf{(8.9)}$$

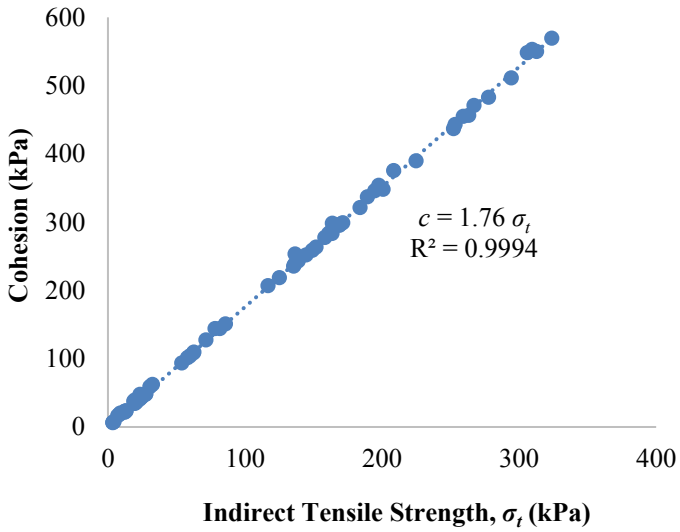

Fig. 8.6 Estimated cohesion (c) changes with indirect tensile strength of CPBs

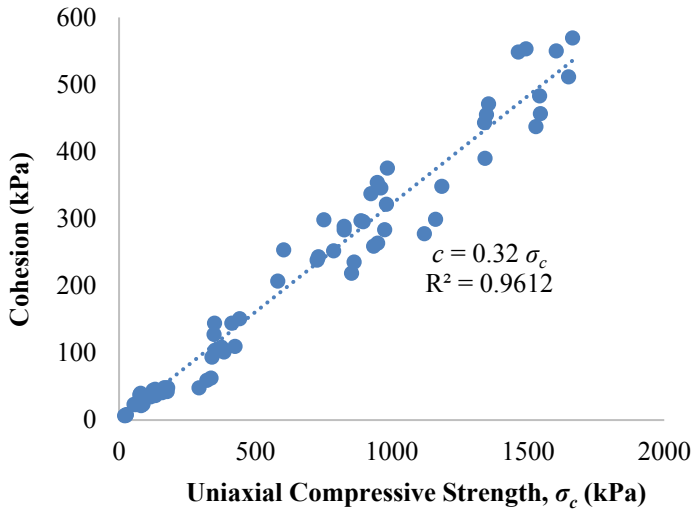

Fig. 8.7 Estimated cohesion (c) changes with uniaxial compressive strength of CPBs

Cohesion determined using analytical correlation changes with binder dosage of CPB sample prepared using cement and slag-cement binders are shown in Figures 8.8 and 8.9, respectively. The slag-cement binder CPB mixes show higher rate of increment of cohesion with dosage increment than the cement binder mixes. In addition, slag-cement binder mix shows higher cohesion than the cement binder mix in a particular binder dosage.

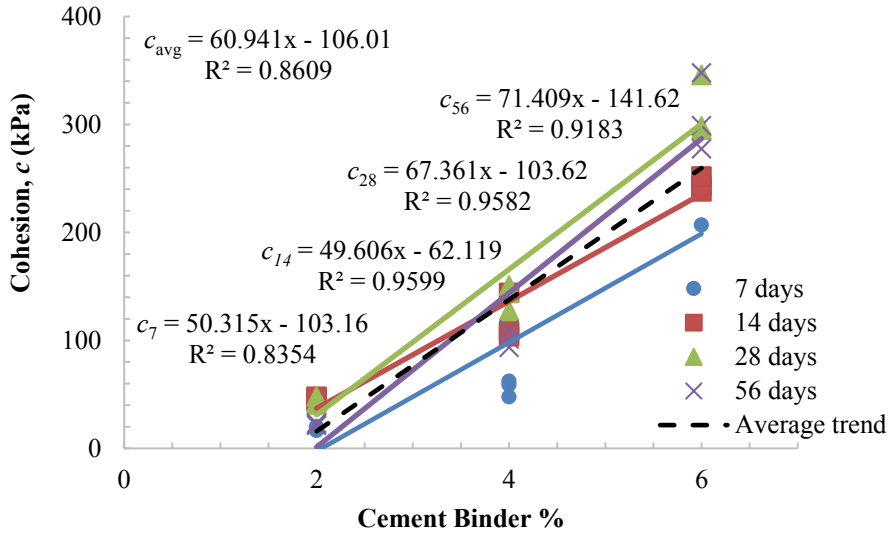

Fig. 8.8 Estimated cohesion (*c*) versus binder dosage for CPB prepared with cement binder

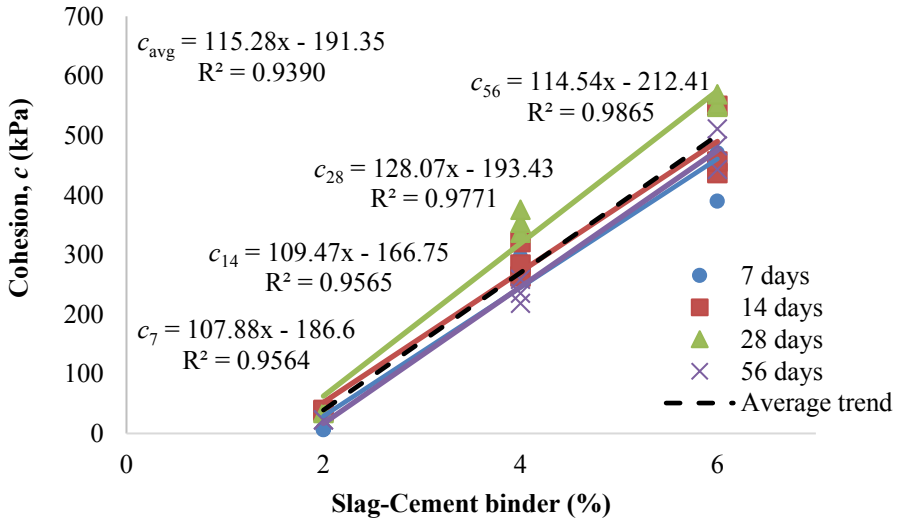

Fig. 8.9 Estimated cohesion (*c*) changes with dosage for CPB prepared with slag-cement binder

Finally, the findings on different geomaterials by the past researchers and current findings studies on CPB materials by this research are tabulated in Table 8.4 for comparison. It is also revealed from this comparison that the *c*/IDT ratios were between 1.75 and 1.85 with good coefficient of correlation for most of geomaterials, while *c*/UCS ratios were between 0.20 and 0.34 with relatively low coefficient of correlation.

Table 8.4 Comparison between current and past studies of the ratio of, *c*/UCS and *c*/IDT for different geomaterials

Researcher	Material	Curing days	*c*/IDT ratio	*h/D* ratio	R^2	*c*/UCS ratio	*h/D* ratio	R^2
White (2006)	Granular base materials stabilized cementitiously with slag lime	28	1.80	2.0	0.9823	0.31	2.0	0.1971
Khattak and Alrashidi (2006)	Four different fiber-reinforced soils stabilized with 10% Type 1 Portland cement	7,	1.79	0.625	0.9933	0.33	1.14	0.7579
		28	1.77		0.9942	0.33		0.9006
Kolias et al. (2005)	Three fine-grained clayey soils stabilized with high calcium fly ash and cement	7, 28, 90	1.76	2.0	0.999	0.25	2.0	0.9383
Consoli et al. (2002)	Polyethylene terephthalate fiber-reinforced sand stabilized with rapid hardening Portland cement varying from 0–7% by weight	3	1.83	2.0	0.9687	0.20	2.0	0.6724
Arabani and Karami (2007)	Five different clayey sands stabilized with 3, 6, and 9% lime	3	1.81	2.0	0.994	0.34	2.0	0.7919
Sobhan and Mashnad (2002)	Granular base materials stabilized cementitiously with slag lime soil chemically stabilized with cement and fly ash, and mechanically reinforced with recycled plastic strips [high-density polyethylene (HDPE)]. The specimens were prepared with maximum of 12% cement and 10% fly ash by dry weight of the mix and contained an additional 0.25–0.80 % fiber of recycled plastic waste	28	1.75	1.875	0.9992	0.28	1.875	0.9462
Piratheepan et al. (2012)	Two granular materials lightly stabilized with slag lime (3 - 5%) and general blend (GB) cement–fly ash (1.5%)	7, 28	1.85	0.6	0.998	0.20	2.0	0.9574
(Sivakugan et al. 2014)	35 rock specimens	-	1.82	-	0.9244	-	-	-
Niroshan et al. (2018)	72 CPB samples with 2 to 6% of Slag-BC and GP Cement binder	7, 14, 28, 56	1.76	0.5	0.9994	0.32	2.0	0.9612

8.4 Experimental Approach

In order to experimentally validate the proposed analytical correlative equations to estimate the shear strength parameters of CPB, extensive triaxial tests were carried out on different CPB samples cured in different days (see Table 8.2).

8.4.1 Triaxial Test

Triaxial test involves subjecting a cylindrical sample, contained within a thin rubber membrane, to a radial stress known as the confining pressure (σ_c). Generally, a deviatoric stress ($\Delta\sigma$) is then applied to the sample until failure. The relationship between the radial and axial stress is used to construct a Mohr circle and derive the c and φ values of the sample and hence the failure envelope.

The triaxial tests were carried out using the triaxial apparatus (Wykeham Farrance Tritech) located in the JCU Soils Laboratory. The testing was conducted based on the method of an Unconsolidated Undrained (UU) triaxial test detailed in ASTM D2850 (ASTM 2015), with the exception of full saturation. Considering the relatively fast loading in the UCS and IDT, UU appears to be more realistic in the triaxial testing. The UU triaxial samples were not subjected to further saturation to ensure they are at the same state (e.g., water content, saturation) as the UCS and IDT samples. The saturation levels were close to full saturation with the average saturation level of 95%. A UU test was chosen with a displacement rate of 2 mm/min, equating to a strain rate of 2 %/min; this was used to ensure a failure time comparable to the UCS, and IDT tests. The average failure time was about 6 minutes. The samples were trimmed to a length of 100 mm producing a L:D ratio of 2:1 as specified in ASTM D2850 (ASTM 2015). The confining pressures of 100, 200 and 300 kPa were used to allow for the stress paths to be drawn, and the shear strength parameters, c and φ, deduced for each mix on each test day. The UU Triaxial test setup can be seen in Figure 8.10(a) and typical cracked CPB sample after tested is shown in Figure 8.10(b).

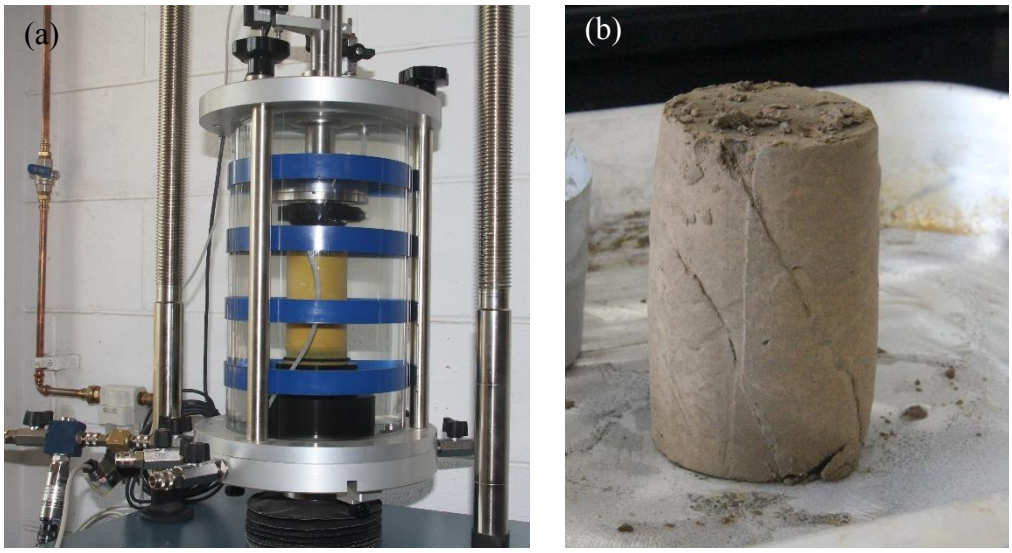

Fig. 8.10 (a) Triaxial test setup and **(b)** CPB sample after test

Figure 8.11 shows the comparison for cohesion of CPB derived from experimental and analytical methods. Although almost all the mixes are roughly along the line of equality, slag-cement CPB mixes show slightly better matching than the cement CPB mixes.

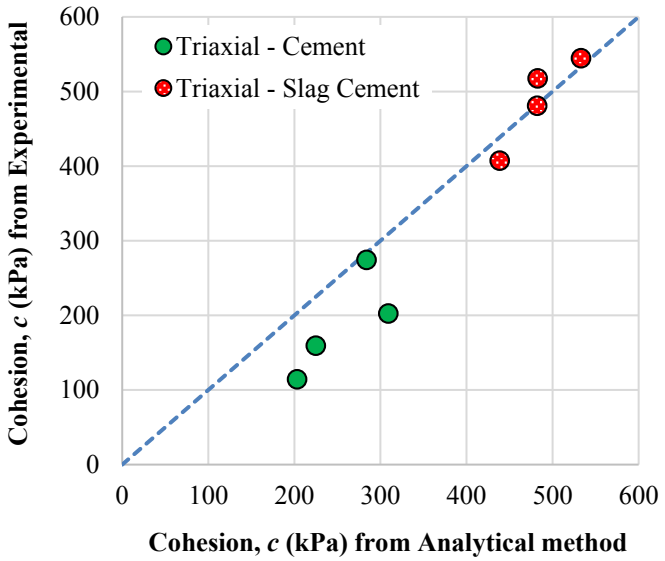

Fig. 8.11 Comparison for cohesion of CPB from experimental and analytical outcome

Comparison for friction angle of CPB mixes determined from experimental and analytical approaches are shown in Figure 8.12. Friction angle of most of the CPB mixes are along the line of equality regardless to the binder type used.

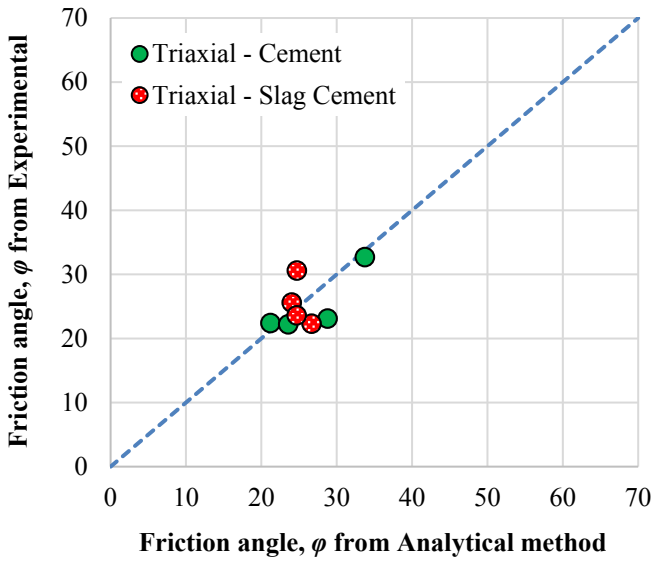

Fig. 8.12 Comparison for friction angle of CPB from experimental and analytical outcome

For further comparison, the analytical and experimental values for shear strength parameters are tabulated in Table 8.5. The R^2 values, which were from the triaxial test data correlation when finding the shear strength parameters, clearly indicate that the cement binder mix exhibits low coefficient of correlation than the slag-cement mixes. Because of the low R^2 values, the error percentages for shear strength parameters are high for cement binder CPB mixes.

It is worth to note that the CPB samples were cast separately for the experiments in analytical and experimental approaches. Therefore, there may be slight difference in the final CPB mix during sample preparation for both approaches, which could lead the higher variation of R^2 values as shown in the table 8.5.

Table 8.5 Comparison between the analytical and experimental results for shear strength parameters

Curing time (days)	Binder	*c* (kPa)		*φ* (°)		R^2	Error % for '*c*'	Error % for '*φ*'
		Analytical correlation	Triaxial	Analytical correlation	Triaxial	Triaxial		
7	cement	203.1	114.4	21.2	22.4	0.6099	-77.55	5.26
	Slag-cement	438.6	407.3	24.0	25.6	0.9732	-7.69	6.08
14	cement	224.9	159.4	23.6	22.2	0.4145	-41.10	-6.23
	Slag-cement	482.6	517.6	26.7	22.3	0.9817	6.77	-19.58
28	cement	283.8	274.4	28.8	23.1	0.9579	-3.43	-24.68
	Slag-cement	533.0	544.7	24.7	23.6	0.9680	2.15	-4.66
56	cement	309.1	202.4	33.7	32.7	0.7480	-52.72	-3.19
	Slag-cement	482.1	481.0	24.7	30.6	0.9732	-0.22	19.2

The triaxial tests results were obtained by Rankine and Sivakugan (2007) on CPB samples prepared in two different solid content using tailings from BHP's Cannington mine can be seen in Table 8.6.

Table 8.6 Triaxial test results obtained by Rankine and Sivakugan (2007) of CPB samples cured at 28 days

% cement	% solid	φ_u (kPa)	c_u (kPa)
2	74	5.7	49
2	78	6	95
6	74	12.7	158
6	78	15.8	264

The cohesion and friction angle of CPB prepared using 6% cement binder and 75% solid content were 274.4 kPa and 23.1°, respectively (see Table 8.5). The triaxial findings of this study may be comparable to experiments conducted by Rankine and Sivakugan (2007) who found that the effect of cementation reduced under higher confining pressures and frictional factors dominate the response. This would indicate that cement provides additional stiffness in the vicinity of 10 times that which is provided by the friction of the tailings (Rankine and Sivakugan 2007).

Finally, from this experimental approach, it can be concluded that the determined shear strength parameters using analytical correlation closely match the experimental results. In addition, it is recommended to cast all samples from same batch or mix for all laboratory test to avoid or minimise the human error.

8.5 Numerical Approach

A series of numerical runs were carried out using FLAC^{3D} (ITASCA 2017) finite difference software in order to numerically assess the validity and applicability of the proposed estimation method for shear strength parameters (c and φ) of CPB materials. The calculated c and φ, in addition to the experimental Young's modulus (E) and assumed Poisson's ratio (v), were used as inputs for Mohr coulomb built-in model in FLAC^{3D} (ITASCA 2017) finite difference software and the respective numerical outputs were compared with the actual experimental results.

Our simulation using FLAC^{3D} will never converge to the equilibrium state. Instead, we can step through the simulation process one timestep at a time and plot and print the results of the collapse as it occurs. This is the real power of the explicit method. The model is not required to converge to equilibrium at each calculation cycle, because we never have to solve a set of linear algebraic equations simultaneously, as is the case for implicit codes, with which many engineers are familiar.

8.5.1 FLAC^{3D} Simulation

UCS and IDT tests were simulated using FLAC^{3D}, for specific c and φ values determined experimentally, in order to know the compressive and tensile strength, respectively, of CPB. Then these numerical results were compared with experimental (UCS and IDT) results for verification.

In FLAC, unbalanced force indicates when a mechanical equilibrium state (or the onset of plastic flow) is reached for a static analysis. A model is in exact equilibrium if the net nodal-force vector (the resultant force) at each gridpoint is zero. The maximum nodal-

force vector is monitored in FLAC^{3D}, and printed to the screen when the STEP or SOLVE command is invoked. The maximum nodal force vector is also called as the unbalanced or out-of-balance force. The maximum unbalanced force will never exactly reach zero for a numerical analysis, but the model is considered to be in equilibrium when the maximum unbalanced force is small compared to the total applied forces in the problem. If the unbalanced force approaches a constant non-zero value, this probably indicates that failure and plastic flow is occurring within the model. When a gridpoint is fixed in a given direction, the component of the unbalanced force in that direction is equivalent to the reaction force.

12 × 18 × 24 and 10 × 20 × 10 size grids were generated to represent the FLAC^{3D} model for the IDT and UCS specimens, respectively. The models were created and run using code input using FISH programme language. In this investigation, full cylindrical specimen was modelled, because of the three dimensional simulation using FLAC^{3D}. The boundary conditions were applied to the model such that the model was fixed in all three directions at top and bottom of the sample, to replicate the actual experiments.

The input parameters for the built – in Mohr – Coulomb model in FLAC^{3D} are stiffness modulus, Poisson's ratio, cohesion, internal angle of friction and density. Table 8.7 shows the input parameters of FLAC^{3D}. The c and φ parameters were derived from analytical correlation method using UCS and IDT were used in numerical simulation. These UCS IDT values were from the individual CPB sample cured in 28 days, whereas the values previously mentioned in Table 8.3 are mean value of triplicate samples tested. In addition, the shear modulus and bulk modulus were calculated based on Young's modulus from UCS test and the assume Poisson's ratio, which is equal to 0.3.

Table 8.7 FLAC^{3D} input parameters

Materials		FLAC^{3D} Inputs		
CPB Ref.	**% Binder**	***E* (MPa)**	***c* (kPa)**	**φ (°)**
C2	2	1.5	48.1	33.4
C4	4	44.6	150.8	21.5
C6	6	133.2	345.7	18.5
S2	2	5.3	36.3	33.1
S4	4	103.2	375.3	15.4
S6	6	272.5	569.2	21.3

Figure 8.13 shows output of UCS simulation from FLAC^{3D}. Typical stress-strain plot with relevant 3-D UCS model for 6% slag-cement binder CPB Mix before and after reaching the peak strength are shown in Figures 8.13 (a) and (b), respectively. In numerical simulation, 6% slag-cement binder mix reaches around 1675 kPa of stress, where similar mix in laboratory experiment reached 1664.3 kPa of stress, and thus determined *c* and φ using analytical correlation can be realistic due to the close matching of experimental and numerical simulation of UCS experiment.

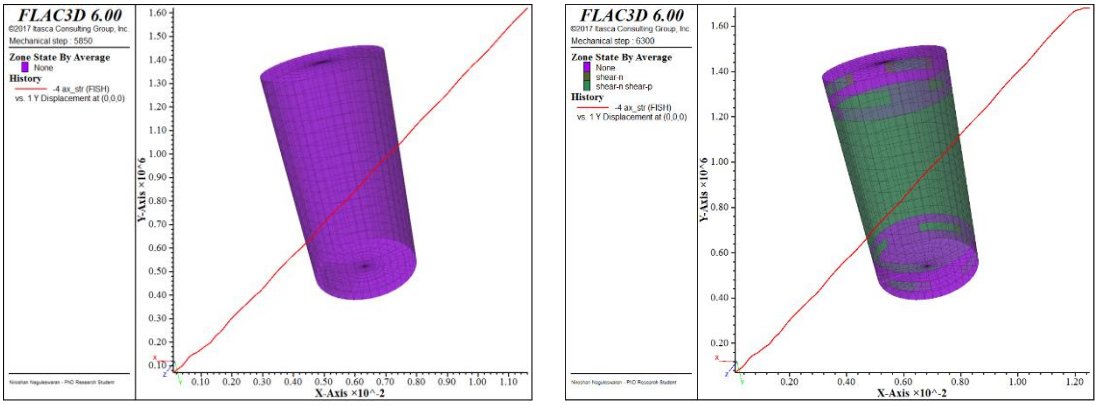

(a) (b)

Fig. 8.13 Simulation of UCS test of slag-cement binder CPB mix, **(a)** just before reach peak strength **(b)** After reached peak strength

On the other hand, the IDT simulation of CPB prepared using cement binder is shown in Figure 8.14, where the stresses in three directions of midpoint of cylindrical specimen changes with step increment during the simulation are graphically shown.

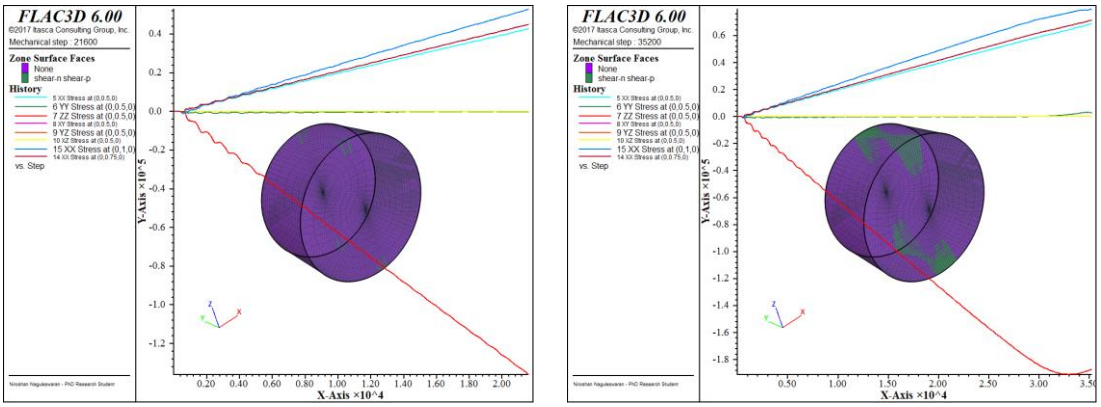

(a) (b)

Fig. 8.14 Simulation of IDT test of cement binder CPB mix, **(a)** before reached peak strength **(b)** After reached peak strength

Finally, selective individual experimental results of CPB samples cured at 28 days were used as inputs values in numerical simulation. Comparison of the results obtained by numerical simulation and experimental approach is presented in Table 8.8. The UCS simulation shows a good fitting with experimental results, whereas the IDT simulation shows relatively low values when compared to experimental values.

Table 8.8 Comparison of numerical outputs with experimental results

Materials		**Experimental output**		**Numerical Output**	
CPB Ref.	**% Binder**	σ_t **(kPa)**	σ_c **(kPa)**	σ_t **(kPa)**	σ_c **(kPa)**
C2	2	27.7	178.6	17.0	180.0
C4	4	85.9	443.3	32.5	446.0
C6	6	194.9	960.8	71.2	978.0
S2	2	20.9	134.1	15.5	139.0
S4	4	208.6	985.3	72.3	982.0
S6	6	324.0	1664.3	136.0	1675.0

In order to, defined a correlation between the experimental and numerical simulation, the data from both analysis are graphically plotted separately as shown in Figures 8.15 and 8.16. When comparing experimental results with numerical analysis, Figure 8.15 shows a best fitting with R^2 = 0.9999, while the Figure 8.16 also shows a good fitting with R^2=0.9738.

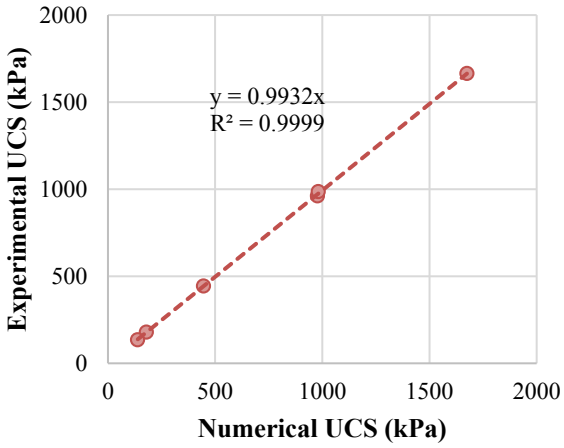

Fig. 8.15 Comparison between experimental results with numerical simulation of UCS test

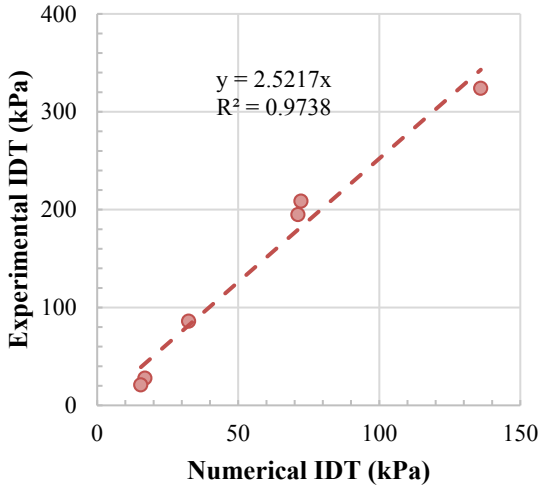

Fig. 8.16 Comparison between experimental results with numerical simulation of IDT test

However, the difference in IDT strengths derived from numerical and experimental approaches could be due to the assumed loading area, which may be smaller or larger either in experimental or in numerical studies.

Therefore, since the experimental and numerical approaches show a good agreement with estimated values, the analytical correlation can be used to estimate the shear strength parameters (c and φ) of CPB based on relevant UCS and IDT strengths.

8.6 Summary

Cemented paste backfills (CPB) are used to backfill the large underground voids created during the ore removal, and are placed in the form of slurry for the ease of transportation. The slurry settles, cures due to hydration, and the strength and stiffness develop with time. In modelling the stability of backfilled voids, the shear strength parameters c and φ are important. However, their determination requires complex triaxial tests. Due to their expensive and time-consuming nature, the need for other simpler methods to determine the same values as triaxial tests is evident. In this chapter, an alternative method is used for checking the applicability in determining the shear strength parameters of CPB using the uniaxial compressive strength (UCS) and indirect tensile strength of the CPB specimens. This method was already used in different geomaterials in past years.

The specimens for the tests were cast at 75% solid content with 0-6% binder (cement or slag-cement blend), and tested after 7, 14, 28 and 56 days of curing. Relationship between the tensile and compressive strengths was also studied. Some triaxial tests were also carried out to determine c and φ to validate our predictions. In addition, model for UCS and IDT strength tests were created for numerical simulation in FLAC^{3D} to evaluate the predicted shear strength parameters.

The experimental study shows better matching for shear strength parameters of CPB with which were derived using analytical correlation. Furthermore, UCS simulation shows good agreement with the experimental values while the accuracy for IDT simulation being poorer. Finally, it can be concluded that the shear strength parameters (c and φ) of CPB can be estimated easily using the analytical correlation based on the relevant UCS and IDT strengths.

9 Summary, Conclusions and Recommendations for Future Research

9.1 Summary

Cemented Paste Backfill (CPB) is one of the many backfill materials used to fill the large underground mine voids that are created by the mining activities around the world, including Australia. CPB, which is primarily used for backfilling underground voids at George Fisher Mine (Mount Isa, Australia), is produced by mixing the mine tailings, binder (2 to 10 wt.%) and required amount of water as per the consistency of CPB materials required for the flow through pipes. In terms of production benefits, the use of CPB, compared to the hydraulic fill, results in significant time saving in stope filling. As a result, the usage of CPB results in almost 50% reduction in mining cycle time, barricade preparation requirements, and capacity to fill stope voids with higher solid contents.

Ordinary Portland cement is the common binder, which is currently being used in most of the mines in Australia. The cost of the cement in CPBs is around half of the overall backfill cost. Due to the increasing environmental problems around the world and increasing backfill cost, the possibilities of replacing the cement by alternate environmental friendly binders, i.e., large percentage of supplementary cementitious materials along with relatively small percentage of cement, in CPB are being extensively assessed by researchers world-wide. However, the results of these investigations cannot be easily generalised, since the physical and chemical behaviour of a certain batch of tailings is related to its origin. In addition, there is no typical backfill type or mix design for all applications as the backfill system is mine oriented. Therefore, a thorough study to quantify the effects of additives, such as blast furnace slag and fly ash with ordinary Portland cement in certain percentages on CPB is necessary and which could save large sums of money for Australian mining companies, if the required cement percentage is reduced in binder for CPB. On the other hand, the majority of alternative binders are waste products from other industries. Therefore, the usage of this by products in underground mine offers environmental benefits while increasing revenues to the waste

providers. In addition to the cost savings and technical benefits that can be realised by using alternative binders at appropriate dosage, there are environmental benefits.

In addition, a proper curing method of Cemented paste backfill (CPB) samples is one of the essential parts in laboratory uniaxial compressive strength (UCS) testing procedure in order to define its mechanical properties. However, there is no standardised process for curing for the paste backfill materials in laboratory. Even though the test results of in situ samples from the underground are often different from the laboratory experiment in many cases, standardised procedure, as for concrete or soil, for sampling, curing, and testing is necessary to minimise the error and variation between the lab and in situ samples. Furthermore, a detailed statistical and probabilistic analysis is quite necessary to define the variabilities of mechanical properties.

In a challenge to dispose more tailings underground, the mines prefer increasing the solid content to the maximum possible limit, as dense CPB needs less binder to achieve a target strength. On the other hand, a high solids content slurry has both increased yield stress and viscosity, which increase the possibility of blocking the reticulation pipeline. As CPB is transported from paste fill plant through a pipe system, the flow characteristics of the CPB are governed by its rheological parameters, such as slump and yield stress. These flow characteristics play a key role as the CPB more commonly flows by gravity down a mineshaft to fill the void. Therefore, it is essential to establish a balance to optimise the solid content and flow properties of CPB.

The shear strength parameters, such as cohesion (c) and the angle of internal friction angle (φ), are important, especially during the design and modelling the stability of the backfilled underground voids. Shear strength parameters of geomaterials such as soils and rocks are often determined by Mohr-Coulomb theory. Generally, these properties are determined through complex laboratory CD/CU/UU triaxial tests. However, the triaxial test requires very expensive and sophisticated equipment and consumes too much run time for the sample preparation and testing. Therefore, it is better having alternative

approach with experimental or numerical validation to estimate these shear strength parameters.

In chapter 03, the geotechnical characterisation of the tailings and the rheological properties of the CPB are summarised as determined from a laboratory testing program undertaken at James Cook University. Two binders were examined [a General Purpose (GP) cement and a slag blend cement] over a range of dosages 0-6% and CPB mix solids content in the range of 72-78%. The slump tests were carried out using the standard cone (ASTM C 143) used for concrete and a cylinder with 110 mm (diameter) × 110 mm (height), whereas the yield stress was measured using a shear vane. The index properties of the tailings including the grain size distribution, liquid limit, plastic limit, specific gravity were determined as per ASTM standards. Finally, the interrelationships among the solid content, slump, saturated density and the yield stress of the CPB were discussed.

In chapter 04, different curing methods are evaluated in order to find the proper curing method for UCS samples made by CPB. Five different curing methods are evaluated using UCS of 28 and 56 days cured duplicate CPB samples in terms of their mechanical properties and the moisture and saturation changes with curing time. In addition, the variability and reliability of mechanical properties of CPB are evaluated. Separately, 25 identical CPB specimens from each mix were tested to assess the variability and reliability of UCS and Young's modulus of CPBs.

In Chapter 05, the findings from an extensive laboratory test program carried out to understand the effects of binder dosage and solid content on the strength development over 56 days of curing are summarised. Ten different mixes were studied using 80 specimens, and it was shown that the blended cement mixes give an early gain in strength and stiffness, along with higher long-term values compared to the GPC mixes.

In chapter 06, the relationship between microstructure and mechanical property of cemented paste backfill (CPB) produced from a hard rock mine tailing from North Queensland in Australia bound with flyash-based geopolymer, flyash-blended cement,

and cement were studied. A relatively high slump (260 mm) paste backfill mix with 74 wt.% solids has been used to prepare cylindrical paste backfill samples with a diameter of 50 mm and a height of 100 mm. The uniaxial compressive strength (UCS) tests were conducted on all samples after curing for 112 days to obtain their strength, failure strain and Young's modulus. Fractured samples were examined under scanning electron microscope (SEM) to understand the failure mechanisms at the microstructural scale.

In chapter 07, flow parameters of CPB and the effects of different types and dosages of binders on flow characteristic of CPB were studied. In addition, the interrelationship among the solid content, slump, saturated density, and the yield stress of the paste, measured through an extensive laboratory test program are discussed.

In chapter 08, shear strength parameters (c and φ) are determined using a simple correlation in addition to the uniaxial compressive strength (UCS) and indirect tensile (IDT) strength of the cemented paste backfill (CPB) specimens. Moreover, these determined shear strength parameters were validated and correlated through a series of triaxial test. Furthermore, simplified correlations are proposed to determine the shear strength parameters of CPB using UCS, IDT and correlations between the experimental and estimations. Finally, the predicted shear strength parameters were used for numerical simulation of the laboratory tests in FLAC^{3D} to check the prediction.

9.2 Conclusions

The conclusions drawn from this dissertation are divided into the sections corresponding to the chapters of the thesis.

9.2.1 Geotechnical Characterisation of Mine Tailings

- The grain shapes of GFM tailings used for this experiment are mostly angular with 28% finer than 20 μm and the mine tailings are categorised as low plasticity Sandy Silty Clay (ML-CL) as the plasticity index of 7% with liquid limit of 15%.

9.2.2 Specimen Preparation – Casting and Curing Methods

- Out of the five different ways of curing, Method 1 works the best. Here, it is required to place the sample with the casing (i.e., plastic mould) and bottom cap in a bucket filled with water only for 2 cm (i.e., slightly below the top of the bottom cap to make sure the sample is not in direct contact with water) and covered with a lid to ensure humid environment. This method is the simplest and provides satisfactory results.
- It was shown that the specimens can be trimmed after 7 days (when they are soft), in order to prepare required length to height ratio for testing, and continued to be cured without the casing, but with the 2 cm water at the bottom of the bucket. This was referred to as Method 5.
- It was shown that the samples cured using Method 1 follow a normal distribution when it comes to UCS and Young's modulus, with relatively small coefficients of variations (COV) of less than 10% and 25%, respectively. It is validated the consistency of sample casting, curing, and testing methods in laboratory. In addition, the probability density plot reveals the spreading of mechanical properties increases with curing time.

9.2.3 Effect of Different Types of Binders on Strength and Stiffness

- The CPB mixes with slag blended cement binder gained approximately 83% of their long-term strength within 14 days whereas the Portland cement binder mixes only gained about 56% of their long-term strength.
- Slag blended cement mixes with 2% binder had very low strength at all curing times, whereas the Portland cement mixes with 2% binder showed significant strength and stiffness. The slag blended cement binder mixes, except for the 2%

mix, showed significantly higher strength and stiffness than the Portland cement mixes of the same dosage.

- Slag blended cement can be used as replacement of cement binder in CPB with less dosage to achieve the same strength and stiffness like cement binder with shorter curing time. This significant reduction in Portland cement usage will contribute to sustainable development in Australia in addition to the huge cost savings.
- It was also shown that the *E*/UCS, which is the ratio of Young's modulus (*E*) to Uniaxial Compressive Strength (UCS), values for the CPB throughout the curing period were in the range of 150-350, with an average value of 250. Young's modulus, *E* can be crudely estimated for preliminary studies using proposed *E*/UCS values.
- Two simple mathematical expressions were developed to express UCS as a function of time and the 14-day UCS value (UCS_{14}) and these expressions predict the UCS values with an error margin of less than 10%.
- Finally, two sets of simple equations were proposed to predict the UCS values at 28 and 56 days of curing by calculating the increase in UCS based on the UCS value of a single mix.

9.2.4 Relevance of SEM to Long-term Mechanical Properties of CPB

- Flyash-based Geopolymer binder slightly improved mechanical properties of CPB and is a cement-free (CaO-free) as well as eco-friendly binder. It can be used to backfill the secondary stopes when there are no more free standing or exposed wall afterwards.
- SEM analyses revealed needle-shaped structure clearly observed in fly ash blended cement and GPC binder CPB mixes, which acted as bridging components

among tailings and binders and also significantly enhanced mechanical properties of CPB.

- SEM images illustrate CPB's structures and bonding which forms poorly and have loose structure for geopolymer binder. Smaller pore sizes and crack lines are clearly identified in cement, fly ash blended cement mixes than the geopolymer and no binder mixes.

9.2.5 Rheological Characteristics of CPB

- It is shown that there is strong correlation between the two different slump test devices used in this study. The smaller cylindrical device appears to have good potential for slurries like mine tailings or dredged mud that have high water content.
- There is also strong inter-relationships among solid content, slump, yield stress, and bulk density. Increasing the solid content increases the bulk density and yield stress, but reduces the slump.
- While there is hardly any difference between the two binder types in terms of flow parameters, namely the yield stress and slump, the binder dosage has an effect.
- At any specific solid content, higher binder dosages lead to a drop in the slump and increase in the yield stress. The difference is more pronounced in dense slurries.

9.2.6 Determination of c and φ of CPB

- It is shown that the, indirect tensile (IDT) strength for CPB samples having L:D ratio = 2 was 0.7 times lower than the sample having L/D =0.5 with good coefficient of correlation ($R^2 = 0.9729$)

- CPB mixes with higher binder content (≥ 4%) display higher E/σ_c (i.e., E/UCS) ratio, which were between 116 and 195 when excluding early strength (i.e., 7 days strength).
- The σ_c/σ_t (i.e., UCS/IDT) ratio of CPB were relatively constant and were between 3.8 and 6.6, when excluding 7 day results. The average σ_c/σ_t ratio of CPB was 5.4 with good agreement (R^2 = 0.9649) for around 70 samples tested. Most of the samples were within 15% deviation lines.
- The c/σ_t (i.e., c/IDT) ratio for CPB was 1.76 with coefficient of correlation, R^2 of 0.9994. However, this ratio were between 1.75 and 1.85 for most of the geomaterials from past researches with good coefficient of correlation.
- The c/σ_c (i.e., c/UCS) ratio for CPB was 0.32 with coefficient of correlation, R^2 of 0.9612. However, this ratio were between 0.20 and 0.34 for most of the geomaterials from past researches with relatively low coefficient of correlation.
- The slag blended cement binder CPB mixes show higher rate of increment of cohesion with dosage increment than the Portland cement binder mixes. In addition, slag blended cement binder mix shows higher cohesion than the cement binder mix in a same binder dosage.
- In numerical simulation of laboratory experiments, the UCS test simulation shows a good fitting with experimental results, whereas the IDT strength test simulation shows relatively low values when compared to experimental values, which may be due to the numerical modelling error in IDT simulation.
- Since the experimental and numerical approaches show a good agreement with estimated values, the analytical correlation can be used to estimate the shear strength parameters (c and φ) of CPB based on relevant UCS and IDT strengths.

9.3 Recommendations for Future Research

Although there have been considerable achievements through this dissertation in understanding the effect of different types binders on mechanical and flow properties of CPB, relevance of micro structure to mechanical properties of CPB and the numerical modelling tools to simulate the laboratory experiments, there are many areas that deserve further study. There are three sets of recommendations. The first set deals with the recommendations for mechanical and flow properties of CPB, the second deals with the structure-property relationship, while the third deals with shear strength parameters of CPB. These recommendations are outlined below.

9.3.1 Mechanical and Flow Properties of CPB

- Laboratory testing can be conducted on CPB prepared using mine tailings from different sources and different types of binders, which may be more environmental friendly, and this may include cement-free binders.
- Long term both strength and stiffness investigation can be carried out beyond 112 days of curing for better understanding of CPB behaviour.
- Validation of laboratory test results can be performed with *in-situ* tests results on underground mine backfilled samples.
- The use of different types of additives on improvement of CPB's flowability while considering changes on strength characteristics, as these two are interconnected.

9.3.2 Relevance of SEM to Mechanical Properties of CPB

- To study further the *microstructure-process-property relations* SEM images from different tailings (having different mineral properties) and binder mixes can be compared.
- SEM analysis can be used to observe the mechanical properties of CPB mix at different stages of mixing, during hydration and hardening process.

- SEM images can also be used to study the permeability, strength development rate, binder distribution and identify the aggregated/dispersed bonds, bond structure of CPB.
- Finally, it is recommended to use NaOH with water glass (Na_2O:SiO_2) in different concentrations as an activator in the process of producing geopolymer binder for the better results as suggested by other researchers on geopolymer concrete research. The alteration of Geopolymer may give better performance in CPB production.

9.3.3 Shear Strength Parameter (*c* and *φ*) of CPB

- Triaxial test can be done on CPB prepared using different types and dosages of binder to compare the experimental results with estimates from analytical correlation. In addition, CU/CD triaxial tests may be performed on CPB for comparison.
- Direct shear test also can be performed on CPB samples prepared using different types of binders and dosages in laboratory to derive the shear strength parameters to compare with analytical correlation.
- Numerical simulation for laboratory experiments (UCS and IDT strength tests) can be carried out using experimental (i.e., *c*, *φ* and E from triaxial experiments) results as input values.

References

ACI Committee 116 (1988). "Cement and Concrete Terminology." *ACI 116R-85, ACI Manual of Concrete Practice*, American Concrete Institute.

ACI Committee 209 (1971). "Predicition of Creep, Shrinkage, and Temperature Effects in Concrete Structure." *ACI 209-71*, American concrete Institute, Detroit, Michigan, 258-269.

ACI Committee 233 (2003). "Slag Cement in Mortar and Concrete." *ACI 233R-03, ACI Manual of Concrete Practice*, American Concrete Institute.

Ahmari, S., and Zhang, L. (2013). "Utilization of cement kiln dust (CKD) to enhance mine tailings-based geopolymer bricks." *Construction and Building Materials*, 40, 1002-1011.

Al Bakri, A. M. M., Kareem, O. A. A., and Myint, S. (2012). "Optimization Of Alkaline Activator/Fly Ash Ratio On The Compressive Strength Of Fly Ash-Based Geopolymer."

Al Bakri, M., Kamarudin, H., karem, O. A. K. A., Ruzaidi, C. M., Rafiza, A. R., and Norazian, M. N. (2012). "Optimization of alkaline activator/fly ash ratio on the compressive strength of manufacturing fly ash-based geopolymer." *Applied Mechanics and Materials*, 110, 734-739.

Arabani, M., and Karami, M. V. (2007). "Geomechanical Properties of Lime Stabilized Clayey Sands." *Arabian Journal for Science & Engineering (Springer Science & Business Media BV)*, 32.

Archibald, J. F., Chew, J. L., and Lausch, P. (1999). "Use of ground waste glass and normal Portland cement mixtures for improving slurry and paste backfill support performance." *CIM bulletin*, 92(1030), 74-80.

ASTM (2003). "Standard Test Methods for Measurement of Hydraulic Conductivity of Saturated Porous Materials Using a Flexible Wall Permeameter." *ASTM D5084* ASTM International, West Conshohocken, PA.

ASTM (2005). "Standard Test Method for Compressive Strength of Cylindrical Concrete Specimens." *ASTM C39-05* ASTM International, West Conshohocken, PA.

ASTM (2007). "Standard Specification for Portland Cement." *ASTM C150-07* ASTM International, West Conshohocken, PA.

ASTM (2009). "Standard Test Methods for Particle-Size Distribution (Gradation) of Soils Using Sieve Analysis." *ASTM D6913-04* ASTM International, West Conshohocken, PA.

ASTM (2010). "Standard Test Methods for Laboratory Determination of Water (Moisture) Content of Soil and Rock by Mass." *ASTM D2216 - 10* ASTM International, West Conshohocken, PA.

ASTM (2010). "Standard Test Methods for Liquid Limit, Plastic Limit, and Plasticity Index of Soils." *ASTM D4318-10*, ASTM International, West Conshohocken, PA.

ASTM (2011). "Standard Practice for Classification of Soils for Engineering Purposes (Unified Soil Classification System)." *ASTM D2487-11*, ASTM International, West Conshohocken, PA.

ASTM (2011). "Standard Test Methods for One-Dimensional Consolidation Properties of Soils Using Incremental Loading." *ASTM D2435 / D2435M-11*ASTM International, West Conshohocken, PA.

ASTM (2014). "Standard Specification for Slag Cement for Use in Concrete and Mortars." *ASTM C989 / C989M - 14* ASTM International, West Conshohocken, PA.

ASTM (2014). "Standard Test Methods for Compressive Strength and Elastic Moduli of Intact Rock Core Specimens under Varying States of Stress and Temperatures " *ASTM D7012-14* ASTM International, West Conshohocken, PA.

ASTM (2014). "Standard Test Methods for Specific Gravity of Soil Solids by Water Pycnometer." *ASTM D854-14* ASTM International, West Conshohocken, PA.

ASTM (2015). "Standard Specification for Coal Fly Ash and Raw or Calcined Natural Pozzolan for Use in Concrete " *ASTM C618 - 15* ASTM International, West Conshohocken, PA,.

ASTM (2015). "Standard Test Method for Slump of Hydraulic-Cement Concrete." *ASTM C143 / C143M-15* ASTM International, West Conshohocken, PA.

ASTM (2015). "Standard Test Method for Unconsolidated-Undrained Triaxial Compression Test on Cohesive Soils." *ASTM D2850 - 15* ASTM International, West Conshohocken, PA,.

Baecher, G. B., and Christian, J. T. (2005). *Reliability and statistics in geotechnical engineering*, John Wiley & Sons.

Bagheri, A., and Nazari, A. (2014). "Compressive strength of high strength class C fly ash-based geopolymers with reactive granulated blast furnace slag aggregates designed by Taguchi method." *Materials & Design*, 54, 483-490.

Beer, F. P., Johnston, E. R., DeWolf, J. T., and Mazurek, D. F. (2012). "Mechanics of Materials, McGraw-Hill." *New York*.

Belem, T., and Benzaazoua, M. (2004). "An overview on the use of paste backfill technology as a ground support method in cut-and-fill mines." *Proc., Proceedings of the 5th Int. Symp. on Ground support in Mining and Underground Construction. Villaescusa & Potvin (eds.)*, Tayler & Francis Group, London, 637 – 650.

Belem, T., and Benzaazoua, M. (2008). "Design and Application of Underground Mine Paste Backfill Technology." *Geotechnical and Geological Engineering*, 26(2), 147-174.

Belem, T., Benzaazoua, M., and Bussière, B. "Mechanical behaviour of cemented paste backfill." *Proc., 53rd Candadian Geotechnical Conference*, 373-380.

Benzaazoua, M., Belem, T., and Bussiere, B. (2002). "Chemical factors that influence the performance of mine sulphidic paste backfill." *Cement and Concrete Research*, 32(7), 1133-1144.

Benzaazoua, M., Fall, M., and Belem, T. (2004). "A contribution to understanding the hardening process of cemented pastefill." *Minerals engineering*, 17(2), 141-152.

Benzaazoua, M., Ouellet, J., Servant, S., Newman, P., and Verburg, R. (1999). "Cementitious backfill with high sulfur content Physical, chemical, and mineralogical characterization." *Cement and Concrete Research*, 29(5), 719-725.

Bieniawski, Z. (1989). "Engineering Rock Mass Classifications, ." *Numerical modelling of subsidence induced by underground coal mining*, 251.

Boger, D., Scales, P., and Sofra, F. (2006). "Rheological concepts." *Paste and Thickened Tailings-A Guide (Second Edition), Jewell and Fourie (eds), Australian Centre for Geomechanics, Perth, Australia*, 25.

Boger, D. V. (1998). "Environmental rheology and the mining industry." *Proc., Proceedings of the 6th International Symposium on Mining with Backfill: Minefill 98*, Australasian Institute of Mining and Metallurgy Publication Series, 15-17.

Boldyrev, V. V., Pavlov, S. V., and Goldberg, E. L. (1996). "Interrelation between fine grinding and mechanical activation." *International Journal of Mineral Processing*, 44-5, 181-185.

Brackebusch, F. W. "Basics of paste backfill systems." *Proc., International Journal of Rock Mechanics and Mining Sciences and Geomechanics Abstracts*, 122A.

Chindaprasirt, P., and Rukzon, S. (2009). "Pore structure changes of blended cement pastes containing fly ash, rice husk ash, and palm oil fuel ash caused by carbonation." *Journal of Materials in Civil Engineering*, 21(11), 666-671.

Christensen, D., and Bonaquist, R. (2002). "Use of strength tests for evaluating the rut resistance of asphalt concrete." *Journal of the Association of Asphalt Paving Technologists*, 71.

Christensen Jr, D., and Bonaquist, R. (2002). "Use of strength tests for evaluating the rut resistance of asphalt concrete." *Journal of the Association of Asphalt Paving Technologists*, 71.

Cihangir, F., Ercikdi, B., Kesimal, A., Turan, A., and Deveci, H. (2012). "Utilisation of alkali-activated blast furnace slag in paste backfill of high-sulphide mill tailings: Effect of binder type and dosage." *Minerals Engineering*, 30, 33-43.

Clough, G. W., Sitar, N., Bachus, R. C., and Rad, N. S. (1981). "Cemented sands under static loading." *Journal of Geotechnical and Geoenvironmental Engineering*, 107(6), Pg. 799-817.

Consoli, N. C., Montardo, J. P., Prietto, P. D. M., and Pasa, G. S. (2002). "Engineering behavior of a sand reinforced with plastic waste." *Journal of Geotechnical and Geoenvironmental Engineering*, 128(6), 462-472.

Coulthard, M. A. (1999). "Applications of numerical modelling in underground mining and construction." *Geotech Geol Eng*, 17(3-4), 373-385.

Das, B. M., and Sivakugan, N. (2017). *Fundamentals of geotechnical engineering*, Cengage Learning.

Das, B. M., Yen, S. C., and Dass, R. N. (1995). "Brazilian tensile strength test of lightly cemented sand." *Canadian Geotechnical Journal*, 32(1), 166-171.

Davidovits, J. (1991). "Geopolymers." *J Therm Anal Calorim*, 37(8), 1633-1656.

Davidovits, J., Davidovits, M., and Davidovits, N. (1994). "Process for obtaining a geopolymeric alumino-silicate and products thus obtained." Google Patents, U.S. Patent 5,342,595.

De Souza, E., Archibald, J. F., and Dirige, A. P. "Economics and perspectives of underground backfill practices in Canadian mines." *Proc., Proceedings of the 105th Annual General Meeting of the Canadian Institute of Mining, Metallurgy and Petroleum. Montreal*.

Detwiler, R. J., Bhatty, J. I., and Battacharja, S. (1996). *Supplementary cementing materials for use in blended cements*, Portland Cement Association, Skokie, Illinois, U.S.A.

Doven, A. G., and Pekrioglu, A. (2005). "Material properties of high volume fly ash cement paste structural fill." *Journal of materials in civil engineering*, 17(6), 686-693.

Ercikdi, B., Cihangir, F., Kesimal, A., Deveci, H., and Alp, İ. (2009). "Utilization of industrial waste products as pozzolanic material in cemented paste backfill of high sulphide mill tailings." *Journal of hazardous materials*, 168(2–3), 848-856.

Ercikdi, B., Kesimal, A., Cihangir, F., Deveci, H., and Alp, İ. (2009). "Cemented paste backfill of sulphide-rich tailings: Importance of binder type and dosage." *Cement and Concrete Composites*, 31(4), 268-274.

Ercikdi, B., Yılmaz, T., and Külekci, G. (2014). "Strength and ultrasonic properties of cemented paste backfill." *Ultrasonics*, 54(1), 195-204.

Fahey, M., Helinski, M., and Fourie, A. (2011). "Development of Specimen Curing Procedures that Account for the Influence of Effective Stress During Curing on the Strength of Cemented Mine Backfill." *Geotechnical and Geological Engineering*, 29(5), 709-723.

Fall, M., Belem, T., Samb, S., and Benzaazoua, M. (2007). "Experimental characterization of the stress–strain behaviour of cemented paste backfill in compression." *Journal of materials science*, 42(11), 3914-3922.

Fall, M., Benzaazoua, M., and Ouellet, S. (2005). "Experimental characterization of the influence of tailings fineness and density on the quality of cemented paste backfill." *Minerals Engineering*, 18(1), 41-44.

Fall, M., Benzaazoua, M., and Saa, E. G. (2008). "Mix proportioning of underground cemented tailings backfill." *Tunnelling and Underground Space Technology*, 23(1), 80-90.

Fredlund, D., and Dahlman, A. (1972). "Statistical geotechnical properties of glacial lake Edmonton sediments." *Statistics and Probability in Civil Engineering*.

Grice, A. G. "Fill Research at Mount Isa Mines Limited." *Proc., the 4th International Symposium on Mining with Backfill*.

Harr, M. E. (1977). *Mechanics of Particulate Media: A Probability Approach*, McGraw Hill, New York.

Heidrich, C., Feuerborn, H.-J., and Weir, A. "Coal combustion products: a global perspective." *Proc., Proceedings of the World of Coal Ash Conference*, 22-25.

Helinski, M., Fahey, M., and Fourie, A. (2011). "Behavior of Cemented Paste Backfill in Two Mine Stopes: Measurements and Modeling." *Journal of Geotechnical and Geoenvironmental Engineering*, 137(2), 171-182.

Hibbeler, R. C. (2016). *Mechanics of materials*, Pearson.

ITASCA. 2017. FLAC 3D, Version 6.0, Fast Lagrangian Analysis of Continua in 3 Dimensions ITASCA Consulting Group Inc.

Kesimal, A., Ercikdi, B., and Yilmaz, E. (2003). "The effect of desliming by sedimentation on paste backfill performance." *Minerals Engineering*, 16(10), 1009-1011.

Kesimal, A., Yilmaz, E., Ercikdi, B., Alp, I., and Deveci, H. (2005). "Effect of properties of tailings and binder on the short-and long-term strength and stability of cemented paste backfill." *Materials Letters*, 59(28), 3703-3709.

Khattak, M. J., and Alrashidi, M. (2006). "Durability and mechanistic characteristics of fiber reinforced soil–cement mixtures." *The International Journal of Pavement Engineering*, 7(1), 53-62.

Kolias, S., Kasselouri-Rigopoulou, V., and Karahalios, A. (2005). "Stabilisation of clayey soils with high calcium fly ash and cement." *Cement and Concrete Composites*, 27(2), 301-313.

Kumar, S., Bandopadhyay, A., Rajinikanth, V., Alex, T. C., and Kumar, R. (2004). "Improved processing of blended slag cement through mechanical activation." *Journal of Materials Science*, 39(10), 3449-3452.

Lambe, T., and Whitman, R. (1969). "Soil Mechanics." John Wiley, New York.

Landriault, D. (2001). "Backfill in underground mining." *Proc., Underground mining methods: Engineering Fundamentals and International Case Studies*, Society for Mining, Metallurgy, and Exploration, Inc. (SME) New York, 601-614.

Li, L. (2013). "Generalized solution for mining backfill design." *International Journal of Geomechanics*, 14(3), 04014006.

Li, L., Aubertin, M., Simon, R., Bussière, B., and Belem, T. "Modeling arching effects in narrow backfilled stopes with FLAC." *Proc., Proceedings of the 3rd international symposium on FLAC & FLAC 3D numerical modelling in Geomechanics, Ontario, Canada*, 211-219.

Manca, P., Massaci, G., Massidda, L., and Rossi, G. "Mill tailings and analysis of properties related to mining problems." *Proc., Proceedings of the International Symposium on Mining with Backfill*, 39-47.

Matsuo, M., and Kuroda, K. (1974). "Probabilistic approach to design of embankments." *Soils and Foundations*, 14(2), 1-17.

Mehta, P. K. (1989). "Pozzolanic and cementitious by-Products in Concrete - Another Look." *ACI Special Publication*, 114, 1-44.

Montgomery, D. C., and Runger, G. C. (2010). *Applied statistics and probability for engineers*, John Wiley & Sons.

Morse, R. (1971). "Importance of proper soil units for statistical analysis." *Proc., Proccedings of the 1st International Conference On applications of Statistics and Probability to Soil and Structural Engineering, Hong Kong*.

Nguyen, Q. D., Akroyd, T., De Kee, D. C., and Zhu, L. (2006). "Yield stress measurements in suspensions: an inter-laboratory study." *Korea-Australia Rheology Journal*, 18(1), 15-24.

Nguyen, Q. D., and Boger, D. V. (1983). "Yield stress measurement for concentrated suspensions." *Journal of Rheology*, 27(4), 321-349.

Niroshan, N., Sivakugan, N., and Lovisa, J. (2015). "A Review on Use of Pozzolanic Materials and Geopolymers in Stabilizing Mine Tailings and Dredged Mud." *Proc., International Conference on Geotechnical Engineering* Sri Lankan Geotechnical Society (SLGS), Colombo, Sri Lanka 375-378.

Niroshan, N., Sivakugan, N., and Veenstra, R. (2016). "Effects of Different Binders on the Strength and Stiffness of Paste Fills." *Proc., Geo-China 2016*, American Society of Civil Engineers, Shandong, China, 197-205.

Niroshan, N., Sivakugan, N., and Veenstra, R. L. (2017). "Laboratory Study on Strength Development in Cemented Paste Backfills." *Journal of Materials in Civil Engineering, ASCE*, 29(7), 04017027.

Öner, M., Erdoğdu, K., and Günlü, A. (2003). "Effect of components fineness on strength of blast furnace slag cement." *Cement and Concrete Research*, 33(4), 463-469.

Ouellet, J., Bidwell, T., and Servant, S. "Physical and mechanical characterisation of paste backfill by laboratory and in-situ testing." *Proc., Proceedings of minefill*, 249-254.

Patzelt, N. (1993). "Finish grinding of slag." *World Cement*, 24(10), 51-58.

Phoon, K.-K., and Kulhawy, F. H. (1999). "Characterization of geotechnical variability." *Canadian Geotechnical Journal*, 36(4), 612-624.

Phoon, K.-K., and Kulhawy, F. H. (2008). "Serviceability limit state reliability-based design." *Reliability-based design in geotechnical engineering: Computations and applications*, Taylor & Francis, New York, 344-383.

Pierce, M. E. "Stability analysis of paste back fill exposes at Brunswick mine." *Proc., Proceedings of the 2nd international FLAC symposium Lyon, France*, 147-156.

Pirapakaran, K. (2008). "Load-deformation characteristics of minefills with particular reference to arching and stress developments."PhD Thesis, James Cook University, Townsville.

Pirapakaran, K., Sivakugan, N., and Rankine, R. (2007). "Investigations into strength of Cannington paste fill mixed with blended cements."

Piratheepan, J., Gnanendran, C., and Arulrajah, A. (2012). "Determination of c and φ from IDT and Unconfined Compression Testing and Numerical Analysis." *Journal of Materials in Civil Engineering*.

Qiu, Y., and Sego, D. (2001). "Laboratory properties of mine tailings." *Canadian Geotechnical Journal*, 38(1), 183-190.

Rankine, R. M. (2004). "The geotechnical and static stability analysis of Cannington mine paste backfill."PhD Thesis, James Cook University, Townsville, Australia.

Rankine, R. M., Pacheco, M. N., and Sivakugan, N. (2007). "Underground Mining with Backfills." *Soils and Rocks*, 30(2), 9.

Rankine, R. M., and Sivakugan, N. (2007). "Geotechnical properties of cemented paste backfill from Cannington Mine, Australia." *Geotechnical and Geological Engineering*, 25(4), 383-393.

Sajedi, F., and Razak, H. A. (2011). "Comparison of different methods for activation of ordinary Portland cement-slag mortars." *Construction and Building Materials*, 25(1), 30-38.

Saw, H. A., and Villaescusa, E. (2013). "Geotechnical properties of mine fill." *Proc., 18th South East Asian Geotechnical & Inaugural AGSSEA Conference*, Research Publishing, Singapore.

Sivakugan, N. (2008). "Geotechnical Issues of Mining with Hydraulic Backfills." *Electronic Journal of Geotechnical Engineering*.

Sivakugan, N., Das, B., Lovisa, J., and Patra, C. (2014). "Determination of c and ϕ of rocks from indirect tensile strength and uniaxial compression tests." *International Journal of Geotechnical Engineering*, 8(1), 59-65.

Sivakugan, N., and Das, B. M. (2010). *Geotechnical engineering: a practical problem solving approach*, J. Ross Publishing, USA.

Sivakugan, N., Rankine, R. M., Rankine, K. J., and Rankine, K. S. (2006). "Geotechnical considerations in mine backfilling in Australia." *Journal of Cleaner Production*, 14(12-13), 1168-1175.

Sivakugan, N., Shukla, S. K., and Das, B. M. (2013). *Rock Mechanics: an introduction*, Crc Press.

Sivakugan, N., Veenstra, R., and Niroshan, N. (2015). "Underground Mine Backfilling in Australia Using Paste Fills and Hydraulic Fills." *Int. J. of Geosynth. and Ground Eng.*, 1(2), 1-7.

Sobhan, K., and Mashnad, M. (2002). "Tensile strength and toughness of soil–cement–fly-ash composite reinforced with recycled high-density polyethylene strips." *Journal of Materials in Civil Engineering*, 14(2), 177-184.

Stone, D. "The evolution of paste for backfill." *Proc., Proceedings of the 11th international symposium on mining with backfill: mine fill*, 31-38.

Thomas, E. G. (1979). *Fill technology in underground metalliferous mines*, University of British Columbia, Department of Mineral Enginnering.

Tokyay, M. (2016). *Cement and Concrete Mineral Admixtures*, CRC Press.

Verdolotti, L., Iannace, S., Lavorgna, M., and Lamanna, R. (2008). "Geopolymerization reaction to consolidate incoherent pozzolanic soil." *Journal of Materials Science*, 43(3), 865-873.

Volpe, R. (1979). "Physical and engineering properties of copper tailings." *Proceedings of Current Geotechnical Practice in Mine Waste Disposal. Edited by The Committee on Embankment Dams and Slopes of the Geotechnical Engineering Division. American Society of Civil Engineering, New York*, 242-260.

Waltham, T. (2009). *Foundations of engineering geology*, CRC Press.

Wang, Y., Zhao, T., and Cao, Z. (2015). "Site-specific probability distribution of geotechnical properties." *Computers and Geotechnics*, 70, 159-168.

White, G. (2006). "Laboratory characterisation of cementitiously stabilised pavement materials."

Wickland, B. E., and Wilson, G. W. (2005). "Self-weight consolidation of mixtures of mine waste rock and tailings." *Canadian Geotechnical Journal*, 42(2), 327-339.

Yilmaz, E., Belem, T., Benzaazoua, M., and Bussiere, B. (2010). "Assessment of the modified CUAPS apparatus to estimate in situ properties of cemented paste backfill." *Geotechnical Testing Journal*, 33(5), 1.

Yumlu, M. "Mining with paste fill." *Proc., AusIMM Cobar Mining Seminar, 26p*.